METAL ION COMPLEXING PROPERTIES OF THE HIGHLY PREORGANIZED LIGAND 1,10-PHENANTHROLINE-2,9-DICARBOXYLIC ACID

Nolan Edward Dean

A Thesis Submitted to the
University of North Carolina Wilmington in Partial Fulfillment
Of the Requirements for the Degree of
Master of Science

Department of Chemistry

University of North Carolina Wilmington

2007

Approved by

Advisory Committee

_____ _____

_____
Chair

Accepted by

_____
Dean, Graduate School

TABLE OF CONTENTS

ABSTRACT

Highly preorganized ligands have shown greater stability constants as well as increased metal-ion selectivities over their straight-chain analogs. These ligands show a promising future in the bioinorganic, nuclear and industrial fields as well as many others. The preorganized ligand 1,10-phenanthroline-2,9-dicarboxylic acid (PDA) was synthesized and subjected to purity verification for studies into its formation constants with various aqueous metal-ions as well as its metal-ligand complex crystal structure. Formation constants were determined from UV/Vis spectrophotometry detection methods using the absorbance spectra as a function of pH. Formation constants for the metal ions Al(III), Fe(III), Th(IV), Lu(III) and UO_2^{2+} are reported amongst others and crystal structures for the metal-PDA complexes of Ba(II),Th(IV) and UO_2^{2+} are also reported.

ACKNOWLEDGMENTS

I would like to thank my advisor Dr. Robert Hancock, for his help and support through all of my research objectives in addition to his furthering my knowledge of inorganic chemistry. I would also like to thank my committee members, Dr. John Tyrell and Dr. Sridhar Varadarajan as well as the faculty and staff of the UNCW Chemistry Department for all of their help both physically and intellectually.

Finally I would like to thank my friends and family for their love and support through all of my years both as student and as a person. Without their support I could not have accomplished all that I have.

LIST OF TABLES

LIST OF FIGURES

INTRODUCTION

Inorganic chemistry and ligand design have shown a large number of uses in the biomedical and industrial fields. For instance, ligands are used to remove harmful heavy metals such as Pb(II) and Hg(II) from the body,[1] Pu(IV) as well as other heavy metals must be reclaimed from nuclear wastes and other contaminated water supplies[2] and Gd(III)-ligand complexes are used almost exclusively as MRI contrasting agents.[1] In the case of Pu(IV), a ligand that can be found which binds selectively to the metal ion in solution while also having a simple means of removing the ion from the ligand solution would be invaluable in the nuclear waster industry.[2] Preorganised ligands such as PDA show a great degree of selectivity for particular metal ions making them ideal for use in certain circumstances such as possible heavy metal filters for contaminated water supplies. The concept of preorganization was first proposed by Donald J. Cram, who found that ligands which were more constrained to be in the conformation necessary to complex metal ions showed an increase in stability over their straight-chain analogs.[3]

Macrocycles, such as crown ethers[4,5] and cryptands[6,7], form very stable complexes due to their preorganized confirmations. This stability, termed the macrocyclic and cryptate effects, due to structural rigidity allows for the design of macrocycles that selectively complex particular metal ions over others.

Metal ion selectivity can be further improved by designing ligands with denticities to match the coordination number of the target metal ion. For example, Gd(III) is used medicinally as an MRI contrast agent.[1] However, as Gd(III) is toxic it must be administered in a ligand which binds Gd(III) selectively enough so as not to displace it for metals readily found in the body such as Zn(II) and Fe(III). Gd(III) has a coordination number of 9, which is why it forms a

complex of much greater stability with diethylenetetramine pentaacetic acid (DTPA) over ethylenediamine tetraacetic acid (EDTA) though the ligands exhibit the same types of donor atoms in a similar conformation. The reason for this is that DTPA has a denticity of 8, meaning it has 8 donor atoms available for complexation whereas EDTA only has a denticity of 6.

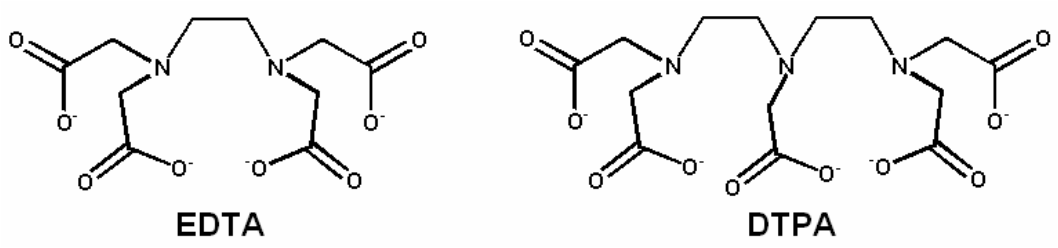

The term hemicyclic ligand, coined by the Hancock research group, exemplified by 1,10-phenanthroline-2,9-dicarboxylate (PDA), refers to non-macrocyclic ligands that derive their high levels of preorganization from an extended aromatic backbone. Hemicycles have the benefit of structurally rigid backbones which allow a fixed conformation of donor atoms while at the same time containing terminal donor atoms which make them acyclic.

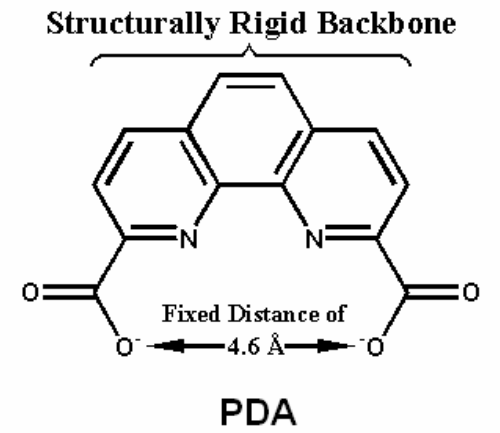

The rigid cleft selects for metal ions with an ionic radius of about 1.0 Å. However, this non-cyclic nature also allows for metal ions of with ionic radii greater than 1.0 Å to be complexed by being out of plane with the ligands itself. The complexes of hemicycles exhibit increased thermodynamic stability similar to macrocyclic ligands while also typically displaying

increased kinetic rates that allow for rapid metallation and demetallation. Hemicycles are also typically easier to synthesize and are less expensive than macrocycles.

METHODS

All chemicals and reagents used were of analytical grade and purchased commercially. Aqueous metal-ligand solutions were made using deionized water (Milli-Q, Waters Corp.) of > 18 $M\Omega.cm^{-1}$ resistivity.

Characterization of PDA from organic synthesis was performed using ^{1}H-NMR and FT-IR analysis. Organic synthesis products were prepared for ^{1}HNMR analysis in DMSO-d_6. ^{1}HNMR spectra were performed using a Bruker 400MHz NMR spectrometer. Organic synthesis products were prepared for FT-IR analysis as KBr pellets and were taken using a Nicolet 6700 FT-IR spectrometer with OMNIC32 Version 2.09 software.

UV/Vis absorbance spectra were recorded for aqueous metal-ligand titration experiments using a double beam Cary 1E UV/Vis spectrophotometer (Varian, Inc.) and WinUV Version 2.00(25) software and a double beam Cary 100sn UV/Vis spectrophotometer (Varian, Inc.) with WinUV Version 3.00(182) software. A 1.0 cm quartz flow cell, fitted with a variable flow peristaltic pump, was used to circulate the metal-ligand aqueous solution after each titrant addition was made to the sample. Figure 1 shows a diagram of the flow cell apparatus. The titrant solution was allowed to equilibrate for 6 to 7 minutes between each titrant addition depending on the metal ion being studied. Absorbance scan ranges were taken from 200 to 350 nm at a rate of 600.00 nm/min. Absorbance spectra were referenced using DI H_2O and a 1.0 cm quartz cell filled with DI H_2O was placed in the path of the reference beam.

All pH values for the titration experiments were recorded using a SympHony SR60IC pH meter (VWR Scientific, Inc.), which was either calibrated by titrating 0.010 M $HClO_4$ in 0.090 M $NaClO_4$ with 0.010 M NaOH in 0.090 M $NaClO_4$ and calculating E^0 to determine correlation between mV readings and calculated pH or calibrated using pH 4.00, 7.00, and 10.00 buffer solutions prior to each titration. Aqueous metal-ligand samples were of 0.10 *M* $NaClO_4$ for ionic strength and maintained at a constant 25.0 ± 0.1 °C throughout the experiment.

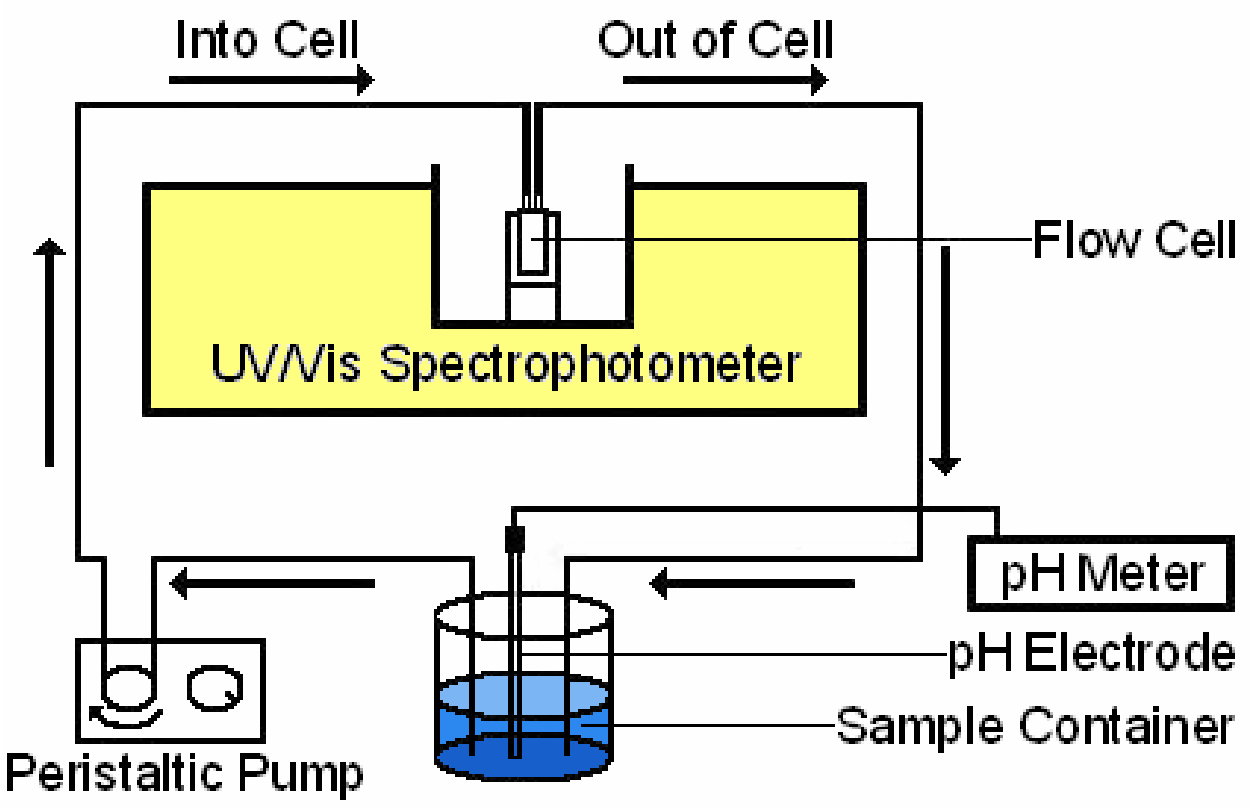

Figure 1: Diagram showing the flow cell apparatus used in the titration experiments.

Synthesis of PDA

The synthesis of PDA was carried out as described in the literature[8] with a few modifications. Characterization of the products was performed using FT-IR analysis and melting point analysis.

A mixture of 4.1232 g of 2,9-dimethyl-1,10-phenanthroline hemihydrate (18.98 mmol, Alfa Aesar, 98+%) and 11.0027 g of selenium dioxide (99.16 mmol, Alfa Aesar, 99.4%) was placed in 200 mL of 4% DI H_2O/p-dioxane (Alfa Aesar, 99+%) in a 500 mL round bottom flask. The mixture was stirred and allowed to reflux at 101 °C in a wax bath for 3 hours. The hot solution was immediately filtered and a yellow-orange product precipitated from the cold filtrate. The synthesis yielded 2.8091 g of impure 1,10-phenanthroline-2,9-dicarboxaldehyde (11.89 mmol, 62.60%), which was separated from the filtrate by vacuum filtration and allowed to dry. The dialdehyde product was not taken through further purification steps since the next step of the synthesis involved further oxidation.

A solution of 2.8091 g of non-purified 1,10-phenanthroline-2,9-dicarboxaldehyde (11.89 mmol) and 80 mL of 4:1 HNO_3 (15.8 N, Fisher Scientific)/H_2O was placed in a 200 mL round bottom flask. The mixture was stirred while refluxing at 122 °C for 10 hours. The solution was cooled to room temperature and then further cooled in a refrigerator. The precipitated 1,10-phenanthroline-2,9-dicarboxylic acid was filtered out by vacuum filtration and allowed to dry. This extended reaction time for the second step of the reaction yielded 2.2357 g (7.87 mmol, 66.19%) of crystalline 1,10-phenanthroline-2,9-dicarboxylic acid monohydrate.

Titrations Involving PDA

UV/Vis spectrophotometry was used to monitor acid-base titrations of aqueous metal-PDA solution. In the event that hydroxide ion was unable to displace the metal from PDA at high pH, another titration experiment was conducted with a competing ligand, either EDTA or DTPA, or another metal ion with a higher formation constant for PDA, such as thorium(IV). Stock solutions of 1.00×10^{-3} *M* PDA (0.0286 g into 100 mL of 0.0100 *M* NaOH), 1.00×10^{-3} *M* Na_2EDTA (0.0372 g in 100 mL H_2O), 1.00×10^{-3} *M* DTPA (0.1965 g into 500 mL H_2O), and 1.00×10^{-3} *M* triethylenetetramine hexaacetic aid, TTHA, (0.0494 g into 100 mL H_2O) were used in the titration experiments. A titrant solution of 1.00 *M* $HClO_4$ (6.00 mL of 69-72% $HClO_4$ in 100 mL H_2O, Fisher Scientific) was used to adjust the initial pH of the sample solutions used in the titrations to a value of approximately 2.00 and then titrant solutions of 0.0100 *M* NaOH (1.00 mL of 10 *N* NaOH into 100 mL of H_2O) and 1.00 *M* NaOH (10 mL of 10 *N* NaOH into 100 mL of H_2O) were used to titrate the metal-ligand solution to a pH of approximately 12.00. The ionic strength of each sample solution was held constant with 0.100 *M* $NaClO_4$ (1.2244 g into 100 mL H_2O, Aldrich, 99%)). The only exception to this case was the titration in order to determine the protonation constants for PDA.

Solution for titration of PDA

In order to determine the protonation constants for PDA, 100 mL of 2.00×10^{-5} *M* PDA (2.00 mL of 1.00×10^{-3} *M*) in 0.10 *M* $NaClO_4$ was prepared. A 50.00 ± 0.05 mL aliquot of this solution was placed in the flow cell setup described above and titrated with 0.100 $HClO_4$ (600 mL of 69-72% $HClO_4$ in 100 mL H_2O, Fisher Scientific) to a final pH of 2.08. The initial pH

was 9.02. Absorbance spectra and pH values were recorded for each titrant addition. The pH meter was calibrated using a 4,7,10 buffer system.

Solution for titration of PDA with Aluminum(III)

A stock solution of 1.00×10^{-3} *M* $Al(NO_3)_3$ (0.0220 g, Aldrich, 99%, in 100 mL of H_2O) was prepared for use in the titration. For the titration the concentrations for both the aluminum and PDA were 2.00×10^{-5} *M*. A 100 mL solution containing 2.00 mL of 1.00×10^{-3} *M* $Al(NO_3)_3$ and 2.00 mL of 1.00×10^{-3} *M* PDA was prepared. A 50.00 ± 0.05 mL portion of this solution was placed in the flow cell apparatus described above, acidified to pH 2.10 with 500 ± 0.05 μL of 1.00 *M* $HClO_4$ then titrated with NaOH. The pH meter was calibrated using a 4,7,10 buffer system.

Solution for titration of PDA with Bismuth(III)

Two separate titration experiments were performed. A stock solution of 1.00×10^{-3} *M* $Bi(NO_3)_3$·5H2O (0.0485 g, Aldrich, 99%, in 100 mL of H_2O) was prepared for use in each titration. For the first titration the concentrations for both the bismuth and PDA were 2.00×10^{-5} *M*. A 100 mL solution containing 2.00 mL of 1.00×10^{-3} *M* $Bi(NO_3)_3$·5H2O and 2.00 mL of 1.00×10^{-3} *M* PDA was prepared. A 50.00 ± 0.05 mL portion of this solution was placed in the flow cell apparatus described above, acidified to pH 1.74 with 500 ± 0.05 μL of 1.00 *M* $HClO_4$ then titrated with NaOH. The pH meter was calibrated using a 4,7,10 buffer system. For the second titration the concentrations for both the bismuth and PDA were 2.00×10^{-6} *M*. A 100 mL solution containing 200 μL of 1.00×10^{-3} *M* $Bi(NO_3)_3$·5H2O and 200 μL of 1.00×10^{-3} *M* PDA was prepared. A 50.00 ± 0.05 mL portion of this solution was placed in the flow cell apparatus

described above, acidified to pH 2.35 with 300 ± 0.05 μL of 1.00 *M* $HClO_4$ then titrated with NaOH. The pH meter was calibrated by using an acid-base titration.

Solution for titration of PDA with Cerium(IV)

A stock solution of 1.00×10^{-3} *M* $(NH_4)_2Ce(NO_3)_6$ (0.0548 g, Fischer Scientific, 99%, in 100 mL of H_2O) was prepared for use in the titration. For the titration the concentrations for both the cerium and PDA were 2.00×10^{-5} *M*. A 100 mL solution containing 2.00 mL of 1.00×10^{-3} *M* $(NH_4)_2Ce(NO_3)_6$ and 2.00 mL of 1.00×10^{-3} *M* PDA was prepared. A 50.00 ± 0.05 mL portion of this solution was placed in the flow cell apparatus described above, acidified to pH 2.11 with 250 ± 0.05 μL of 1.00 *M* $HClO_4$ then titrated with NaOH. The pH meter was calibrated using a 4,7,10 buffer system.

Solution for titration of PDA with Gallium(III)

A stock solution of 1.00×10^{-3} *M* $Ga(NO_3)_3\cdot5H_2O$ (0.0346 g, Aldrich, 99%, in 100 mL of H_2O) was prepared for use in the titration. For the titration the concentrations for both the gallium and PDA were 2.00×10^{-5} *M*. A 100 mL solution containing 2.00 mL of 1.00×10^{-3} *M* $Ga(NO_3)_3\cdot5H_2O$ and 2.00 mL of 1.00×10^{-3} *M* PDA was prepared. A 50.00 ± 0.05 mL portion of this solution was placed in the flow cell apparatus described above, acidified to pH 1.95 with 500 ± 0.05 μL of 1.00 *M* $HClO_4$ then titrated with NaOH. The pH meter was calibrated using a 4,7,10 buffer system.

Solution for titration of PDA with Indium(III)

A stock solution of 1.00×10^{-3} *M* $In(ClO_4)_3\cdot8H_2O$ (0.0413 g, Aldrich, 99%, in 100 mL of H_2O) was prepared for use in the titration. For the titration the concentrations for both the indium and PDA were 2.00×10^{-5} *M*. A 100 mL solution containing 2.00 mL of 1.00×10^{-3} *M* $In(ClO_4)_3\cdot8H_2O$ and 2.00 mL of 1.00×10^{-3} *M* PDA was prepared. A 50.00 ± 0.05 mL portion of this solution was placed in the flow cell apparatus described above, acidified to pH 1.74 with 300 ± 0.05 μL of 1.00 *M* $HClO_4$ then titrated with NaOH. The pH meter was calibrated using a 4,7,10 buffer system.

Solutions for titrations of PDA with Iron(III)

Three separate titration experiments were performed. A stock solution of 1.00×10^{-3} *M* $Fe(ClO_4)_3\cdot H_2O$ (0.0354 g, Aldrich, 99%, in 100 mL of H_2O) was prepared for use in each titration. For the titration of iron(III) and PDA the concentrations for both the cerium and PDA were 2.00×10^{-5} *M*. A 100 mL solution containing 2.00 mL of 1.00×10^{-3} *M* $Fe(ClO_4)_3\cdot H_2O$ and 2.00 mL of 1.00×10^{-3} *M* PDA was prepared. A 50.00 ± 0.05 mL portion of this solution was placed in the flow cell apparatus described above, acidified to pH 2.28 with 500 ± 0.05 μL of 1.00 *M* $HClO_4$ then titrated with NaOH. For the titration of iron(III), PDA and EDTA at 1:1:1 the concentrations for all components were 2.00×10^{-5} *M*. A 100 mL solution containing 2.00 mL of 1.00×10^{-3} *M* $Fe(ClO_4)_3\cdot H_2O$, 2.00 mL of 1.00×10^{-3} *M* Na_2EDTA and 2.00 mL of 1.00×10^{-3} *M* PDA was prepared. A 50.00 ± 0.05 mL portion of this solution was placed in the flow cell apparatus described above, acidified to pH 2.28 with 500 ± 0.05 μL of 1.00 *M* $HClO_4$ then titrated with NaOH. For the titration of iron(III), PDA and EDTA at 1:1:10 the concentrations for both iron and PDA were 2.00×10^{-5} *M* and the concentration of EDTA was 2.00×10^{-4} *M*. A

100 mL solution containing 2.00 mL of 1.00×10^{-3} *M* $Fe(ClO_4)_3\cdot H_2O$, 20.0 mL of 1.00×10^{-3} *M* Na_2EDTA and 2.00 mL of 1.00×10^{-3} *M* PDA was prepared. A 50.00 ± 0.05 mL portion of this solution was placed in the flow cell apparatus described above, acidified to pH 2.32 with 500 ± 0.05 μL of 1.00 *M* $HClO_4$ then titrated with NaOH. For all of the titrations, the pH meter was calibrated using a 4,7,10 buffer system.

Solution for titration of PDA with Lutetium(III)

A stock solution of 1.00×10^{-3} *M* $Lu(ClO_4)_3\cdot6H_2O$ (0.1162 g of 50% w/w aqueous solution, Alfa Aesar, 99%, in 100 mL of H_2O) was prepared for use in the titration. For the titration the concentrations for lutetium and PDA were 2.00×10^{-5} *M*. A 100 mL solution containing 2.00 mL of 1.00×10^{-3} *M* $Lu(ClO_4)_3\cdot6H_2O$ and 2.00 mL of 1.00×10^{-3} *M* PDA was prepared. A 50.00 ± 0.05 mL portion of this solution was placed in the flow cell apparatus described above, acidified to pH 1.34 with 1.00 ± 0.05 mL of 1.00 *M* $HClO_4$ then titrated with NaOH. The pH meter was calibrated using a 4,7,10 buffer system.

Solution for titration of PDA with Manganese(II)

A stock solution of 1.00×10^{-3} *M* $Mn(ClO_4)_2\cdot6H_2O$ (0.0362 g, Aldrich, 99%, in 100 mL of H_2O) was prepared for use in the titration. For the titration the concentrations for both the manganese and PDA were 2.00×10^{-5} *M*. A 100 mL solution containing 2.00 mL of 1.00×10^{-3} *M* $Mn(ClO_4)_2\cdot6H_2O$ and 2.00 mL of 1.00×10^{-3} *M* PDA was prepared. A 50.00 ± 0.05 mL portion of this solution was placed in the flow cell apparatus described above, acidified to pH 2.01 with 500 ± 0.05 μL of 1.00 *M* $HClO_4$ then titrated with NaOH. The pH meter was calibrated using a 4,7,10 buffer system.

Solutions for titrations of PDA with Thorium(IV)

Numerous titrations were performed with PDA and thorium in an attempt to fully comprehend the nature of the metal-ligand aqueous complex. A stock solution of 1.00×10^{-3} *M* $Th(NO_3)_4\cdot4H_2O$ (0.0552 g, Aldrich, 99%, in 100 mL of H_2O) was prepared for use in the titration. For the first titration of 1:1 PDA with thorium the concentrations for both the thorium and PDA were 2.00×10^{-5} *M*. A 100 mL solution containing 2.00 mL of 1.00×10^{-3} *M* $Th(NO_3)_4\cdot4H_2O$ and 2.00 mL of 1.00×10^{-3} *M* PDA was prepared. A 50.00 ± 0.05 mL portion of this solution was placed in the flow cell apparatus described above, acidified to pH 2.14 with 500 ± 0.05 μL of 1.00 *M* $HClO_4$ then titrated with NaOH. The pH meter was calibrated using a 4,7,10 buffer system. For the second titration of 1:1 PDA with thorium the concentrations for both the thorium and PDA were 4.00×10^{-6} *M*. A 100 mL solution containing 0.40 mL of 1.00×10^{-3} *M* $Th(NO_3)_4\cdot4H_2O$ and 0.40 mL of 1.00×10^{-3} *M* PDA was prepared. A 50.00 ± 0.05 mL portion of this solution was placed in the flow cell apparatus described above, acidified to pH 2.14 with 500 ± 0.05 μL of 1.00 *M* $HClO_4$ then titrated with NaOH. The pH meter was calibrated using an acid-base titration. For the titration of 2:1 PDA with thorium the concentration for the PDA was 4.00×10^{-5} *M* and the concentration for thorium was 2.00×10^{-5} *M*. A 100 mL solution containing 2.00 mL of 1.00×10^{-3} *M* $Th(NO_3)_4\cdot4H_2O$ and 4.00 mL of 1.00×10^{-3} *M* PDA was prepared. A 50.00 ± 0.05 mL portion of this solution was placed in the flow cell apparatus described above, acidified to pH 2.11 with 500 ± 0.05 μL of 1.00 *M* $HClO_4$ then titrated with NaOH. The pH meter was calibrated using a 4,7,10 buffer system. For the titration of 1:1:1 PDA, thorium and DTPA the concentration all components was 2.00×10^{-5} *M*. A 100 mL solution containing 2.00 mL of 1.00×10^{-3} *M* $Th(NO_3)_4\cdot4H_2O$, 2.00 mL of 1.00×10^{-3} *M* PDA and 2.00 mL of 1.00×10^{-3} *M* DTPA was prepared. A 50.00 ± 0.05 mL portion of this solution was

placed in the flow cell apparatus described above, acidified to pH 2.25 with 420 ± 0.05 μL of 1.00 *M* $HClO_4$ then titrated with NaOH. The pH meter was calibrated using a 4,7,10 buffer system. For the titration of 1:1:10 PDA, thorium and DTPA the concentrations of PDA and thorium were 2.00×10^{-5} *M* and the concentration of DTPA was 2.00×10^{-4} *M*. A 100 mL solution containing 2.00 mL of 1.00×10^{-3} *M* $Th(NO_3)_4\cdot4H_2O$, 2.00 mL of 1.00×10^{-3} *M* PDA and 20.00 mL of 1.00×10^{-3} *M* DTPA was prepared. A 50.00 ± 0.05 mL portion of this solution was placed in the flow cell apparatus described above, acidified to pH 2.28 with 500 ± 0.05 μL of 1.00 *M* $HClO_4$ then titrated with NaOH. The pH meter was calibrated using a 4,7,10 buffer system. For the titration of 1:1:100 PDA, thorium and DTPA the concentrations of PDA and thorium were 2.00×10^{-5} *M* and the concentration of DTPA was 2.00×10^{-3} *M*. A 100 mL solution containing 2.00 mL of 1.00×10^{-3} *M* $Th(NO_3)_4\cdot4H_2O$, 2.00 mL of 1.00×10^{-3} *M* PDA and 200.0 mL of 1.00×10^{-3} *M* DTPA was prepared. A 50.00 ± 0.05 mL portion of this solution was placed in the flow cell apparatus described above, acidified to pH 2.10 with 420 ± 0.05 μL of 1.00 *M* $HClO_4$ then titrated with NaOH. The pH meter was calibrated using a 4,7,10 buffer system. For the titration of 1:1:1 PDA, thorium and TTHA the concentrations of all components were 2.00×10^{-5} *M*. A 100 mL solution containing 2.00 mL of 1.00×10^{-3} *M* $Th(NO_3)_4\cdot4H_2O$, 2.00 mL of 1.00×10^{-3} *M* PDA and 2.00 mL of 1.00×10^{-3} *M* TTHA was prepared. A 50.00 ± 0.05 mL portion of this solution was placed in the flow cell apparatus described above, acidified to pH 1.79 with 500 ± 0.05 μL of 1.00 *M* $HClO_4$ then titrated with NaOH. The pH meter was calibrated using a 4,7,10 buffer system. For the titration of 1:1:10 PDA, thorium and TTHA the concentrations of PDA and thorium were 2.00×10^{-5} *M* and the concentration of TTHA was 2.00×10^{-4} *M*. A 100 mL solution containing 2.00 mL of 1.00×10^{-3} *M* $Th(NO_3)_4\cdot4H_2O$, 2.00 mL of 1.00×10^{-3} *M* PDA and 20.00 mL of 1.00×10^{-3} *M* TTHA was prepared. A 50.00 ± 0.05 mL portion of this solution was

placed in the flow cell apparatus described above, acidified to pH 1.88 with 1.50 ± 0.01 mL of 1.00 *M* $HClO_4$ then titrated with NaOH. The pH meter was calibrated using a 4,7,10 buffer system. For the titration of thorium and DTPA the concentrations of thorium and DTPA were 2.00×10^{-5} *M*. A 100 mL solution containing 2.00 mL of 1.00×10^{-3} *M* $Th(NO_3)_4\cdot4H_2O$, 2.00 mL of 1.00×10^{-3} *M* DTPA was prepared. A 50.00 ± 0.05 mL portion of this solution was placed in the flow cell apparatus described above, acidified to pH 2.00 with 0.500 ± 0.01 mL of 1.00 *M* $HClO_4$ then titrated with NaOH. The pH meter was calibrated using a 4,7,10 buffer system.

Solutions for titrations of PDA with Uranyl(VI)

Two titration experiments were performed. A stock solution of 1.00×10^{-3} *M* $UO_2(NO_3)_2\cdot6H_2O$ (0.0502 g, Fischer Scientific, 99%, in 100 mL of H_2O) was prepared for use in the titration. For the first titration the concentrations for both the uranyl ion and PDA were 2.00×10^{-5} *M*. A 100 mL solution containing 2.00 mL of 1.00×10^{-3} *M* $UO_2(NO_3)_2\cdot6H_2O$ and 2.00 mL of 1.00×10^{-3} *M* PDA was prepared. A 50.00 ± 0.05 mL portion of this solution was placed in the flow cell apparatus described above, acidified to pH 2.41 with 275 ± 0.05 μL of 1.00 *M* $HClO_4$ then titrated with NaOH. The pH meter was calibrated using a 4,7,10 buffer system. For the second titration the concentrations for both the uranyl ion and PDA were 2.00×10^{-6} *M*. A 100 mL solution containing 0.20 mL of 1.00×10^{-3} *M* $UO_2(NO_3)_2\cdot6H_2O$ and 0.20 mL of 1.00×10^{-3} *M* PDA was prepared. A 50.00 ± 0.05 mL portion of this solution was placed in the flow cell apparatus described above, acidified to pH 2.32 with 500 ± 0.05 μL of 1.00 *M* $HClO_4$ then titrated with NaOH. The pH meter was calibrated using an acid-base titration.

Synthesis and crystal preparation of the complex [Ba(PDAH)$(H_2O)_2(NO_3)$].

A solution of 1.00×10^{-3} *M* $Ba(ClO_4)_2$ (0.0336 g, Aldrich, 97%, in 100 mL of H_2O) and a solution of 1.00×10^{-3} *M* PDA (0.0286 g into 100 mL of n-butanol) was prepared. A 15mL aliquot of the aqueous barium solution was placed in the bottom of a 1×12" test tube. A layer of approximately 60 mL of n-butanol was placed atop the aqueous layer and a 15 mL aliquot of the PDA in n-butanol solution was placed atop the pure n-butanol layer with care taken to not disturb the n-butanol layer. A piece of Parafilm was placed atop the test tube and the tube was allowed to sit undisturbed for 5 months until crystals formed at the interface between the n-butanol and aqueous layers. The crystals were gathered through vacuum filtration and were sent off to Clemson University, SC for analysis by Dr. Donald VanDerVeer. These crystals have yet to have an elemental analysis performed on them.

Synthesis and crystal growth of the complex [Th$(PDA)_2(H_2O)_2$].H_2O.

The solution of 1.00×10^{-3} *M* $Th(NO_3)_4\cdot4H_2O$ used in the titration experiment and the solution of 1.00×10^{-3} *M* PDA in n-butanol used in the barium crystal growing experiment were used to attempt a similar crystal growing procedure as the barium crystal experiment. A 15mL aliquot of the aqueous thorium solution was placed in the bottom of a 1×12" test tube. A layer of approximately 60 mL of n-butanol was placed atop the aqueous layer and a 15 mL aliquot of the PDA in n-butanol solution was placed atop the pure n-butanol layer with care taken to not disturb the n-butanol layer. A piece of Parafilm was placed atop the test tube and the tube was allowed to sit undisturbed for 5 months. Crystals never formed, and instead an insoluble powder formed

at the interface. Instead of a conventional approach to growing crystals of the Th(IV)/PDA complex, crystals of $[Th(PDA)_2(H_2O)_2].H_2O$ were obtained for us by Drs. C. Cahill and M. Frisch (George Washington University) from a hydrothermal reaction mixture that contained 81 mg (0.167 mmol) $Th(NO_3)_4.4H_2O$, 44 mg (0.167 mmol) PDA and 1.69 g deionized H_2O (93.6 mmol). These reagents were combined in a 23 mL Teflon-lined stainless steel reaction vessel (initial pH = 1.23) and heated to 180 ºC for 1 day. The reaction mixture was then allowed to cool to room temperature. The clear colorless mother liquor (final pH = 0.95) was extracted and the remaining clear colorless crystals were subsequently washed with both distilled water and ethanol and allowed to air dry at room temperature. An elemental analysis calculation for $C_{28}H_{18}N_4O_{11}Th$: C, 41.08, H, 2.20, N, 6.85 %, found: C, 40.46; H, 2.08; N, 6.81 %.

Synthesis and crystal preparation of the complex $[UO_2(PDA)]$.

The solution of 1.00×10^{-3} *M* $UO_2(NO_3)_2\cdot6H_2O$ and the solution of 1.00×10^{-3} *M* PDA in n-butanol were used to attempt a similar crystal growing procedure as the barium crystal experiment. A 15mL aliquot of the aqueous uranyl solution was placed in the bottom of a 1×12" test tube. A layer of approximately 60 mL of n-butanol was placed atop the aqueous layer and a 15 mL aliquot of the PDA in n-butanol solution was placed atop the pure n-butanol layer with care taken to not disturb the n-butanol layer. A piece of Parafilm was placed atop the test tube and the tube was allowed to sit undisturbed for 7 months. Crystals never formed, and instead an insoluble powder formed at the interface. Crystals of $[(UO_2)(PDA)]$ were obtained for us by Drs. C. Cahill and M. Frisch (George Washington University) from a hydrothermal reaction mixture that contained 84 mg (0.167 mmol) $UO_2(NO_3)_2.6H_2O$, 53 mg (0.198 mmol) PDA and 1.67 g

deionized H_2O (92.5 mmol). These reagents were combined in a 23 mL Teflon-lined stainless steel reaction vessel (initial pH = 1.36) and heated to 180 ºC for 1 day. The reaction mixture was then allowed to cool to room temperature. The yellow mother liquor (final pH = 1.03) was extracted and the remaining yellow crystals were subsequently washed with both distilled water and ethanol then allowed to air dry at room temperature. An elemental analysis calculation for $C_{14}H_6N_2O_6U$: C, 31.34, H, 1.12, N, 5.22 %, found: C, 31.76; H, 1.06; N, 5.35 %.

X-ray structure determination.

The crystal structures of $(UO_2)(C_{14}H_6N_2O_4)$ (**1**) and $Th(C_{14}H_6N_2O_4)_2(H_2O)_2 \cdot H_2O$ (**2**) and [Ba(PDAH)$(H_2O)_2(NO_3)$] were determined via single crystal X-ray diffraction. A representative crystal of each compound was mounted on a glass fiber using epoxy gel. Intensity data were collected on a Bruker SMART diffractometer equipped with an APEX II CCD detector. Data processing was performed using SAINT[9]. The structures were solved using direct methods while the refinement was carried out using SHELXL-97[10] within the WINGX software suite[11]. Powder X-ray diffraction data were collected on a Rigaku MiniFlex II Desktop X-ray Diffractometer (Cu-Kα, 3-60˚, 0.05˚ step, 1.0 s step^{-1}) and manipulated utilizing the JADE[12] software package. The observed and calculated powder diffraction patterns for both 1 and 2 were in excellent agreement. The structures of **1** and **2** are shown in Figs. 4 and 5. Details of the structure determinations are given in Table 1, and coordinates for **1** and **2** have been deposited with the Cambridge Structural Database (CSD)[13]. A selection of bond lengths and angles for **1** and **2** are given in Tables 2 and 3.

RESULTS AND DISCUSSION

Synthesis of PDA

The synthesis of 1,10-phenanthroline-2,9-dicarboxaldehyde (PDALD) resulted in an impure mixture. The synthesis yielded 2.8091 g of PDALD for a percent yield of 62.60%. The product was obtained as a purple-tinted powder with some small crystals also present. The IR spectrum in Figure 2 shows a major product of PDALD with a peak at 1726cm^{-1} for the C=O stretch. The aldehyde also contained evidence of a C-OH stretch at 3012cm^{-1}, which is indicative that much of the aldehyde had been at least partially oxidized into PDA. This is not a concern since the aldehyde product is further oxidized into PDA during step two of the synthesis. Further purification of PDALD was not performed as another oxidation step was needed to produce the desired final product.

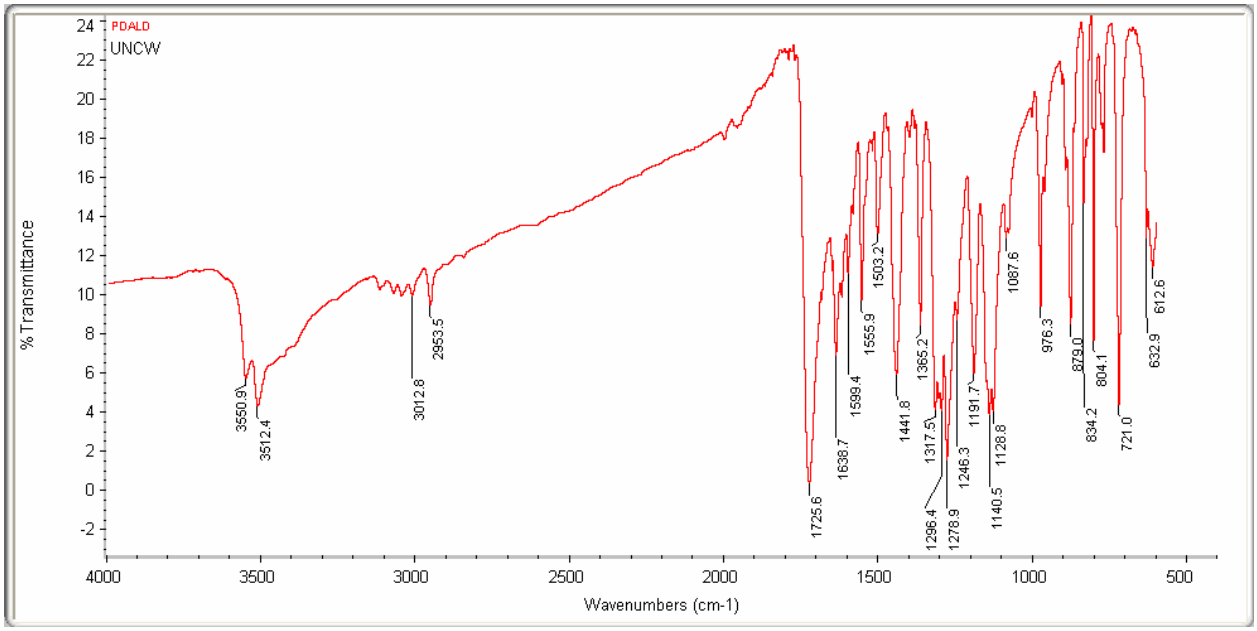

Figure 2. IR spectrum of 1,10-phenanthroline-2,9-dicarboxaldehyde (PDALD) product as a KBr pellet.

The PDALD product was used to synthesize 1,10-phenanthroline-2,9-dicarboxylic acid (PDA). The PDA product was not taken through further purification techniques due to the very pure nature of the crystalline product as a result of the increased reaction time. The reaction yielded 2.2357 g of PDA for a percent yield of 66.19% and an overall synthesis yield of 62.03%. The melting point for the crystalline product was 229-232°C was measured which compares very favorably with the literature value[11] of 231-232°C. An IR analysis was also conducted and the spectrum is shown in Figure 3. The spectrum shows a clean carboxylic acid with a peak at 1724cm^{-1} for the C=O stretch and a peak at 3012cm^{-1} for the C-OH stretch. The spectrum also revealed a peak at 3551cm^{-1} resulting from a water molecule in the crystal lattice. The melting point analysis and IR spectrum showed a clean product of PDA from the synthesis using PDALD. Further evidence of the purity of our product was later obtained through crystallographic study of PDA with various metal ions. All solutions used in the titration experiments and all crystallographic studies were made up or conducted using these crystals.

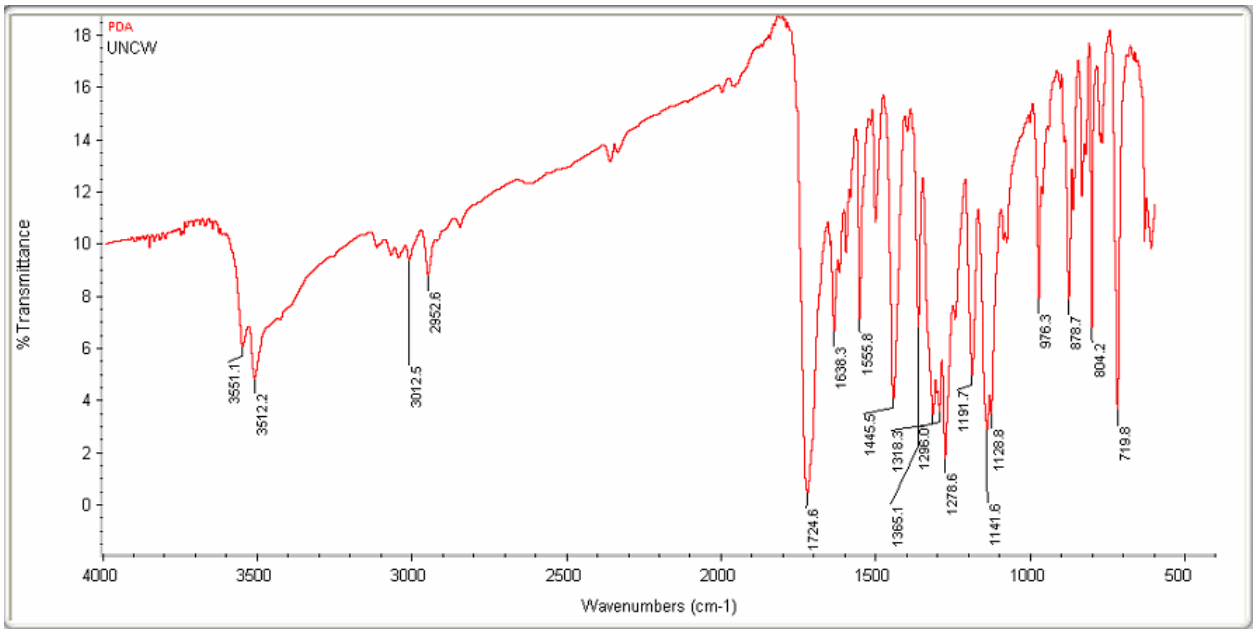

Figure 3. IR spectrum of 1,10-phenanthroline-2,9-dicarboxylic acid (PDA) product as a KBr pellet.

Titrations Involving PDA

The titration experiments were performed utilizing UV/Vis spectroscopy as an analytical tool to detect metal complex formation involving PDA. Absorbance scans were performed from 200 to 350 nm for each titrant addition of NaOH. Absorbance data were taken at selected wavelengths of approximately 236, 248, 262, 282, and 294 nm. Absorbance maxima were shown at approximately 236 and 283 nm for the free PDA. Upon complexation of PDA with a metal ion, a new peak at approximately 248 nm was observed, as well as a peak shift from 280 to 294 nm. The presence of the 248 nm peak came to be regarded as diagnostic of the metal-ligand complex formation.

In order to determine the protonation constants for the ligand, PDA, a titration experiment was performed at 25.0 ± 0.1 °C in 0.10 *M* $NaClO_4$ for ionic strength. Figure 4 shows absorbance versus wavelength (nm) for the titration of PDA. Absorbance data for various wavelengths were used to generate the plot of absorbance versus pH. This plot is shown in Figure 5. The points drawn in are experimental values and the solid lines are theoretical curves of absorbance versus pH calculated for the constants corresponding to the observed protonation equilibria. The theoretical curves of absorbance versus pH in Figure 5 were fitted to the experimental points using the SOLVER module of the program EXCEL[14]. The standard deviations of these protonation constants were calculated using the SOLVSTAT macro provided with reference 14. The set of data obtained at 246 nm for the absorbance spectra was the best indication of complex formation. The protonation constants for PDA were calculated using the absorbance data and pH values from this plot. The corrected protonation constants of pK_1 and pK_2 for PDA were 4.71 and 2.53, respectively. An illustration of the protonation equilibria for PDA is shown in Figure 6.

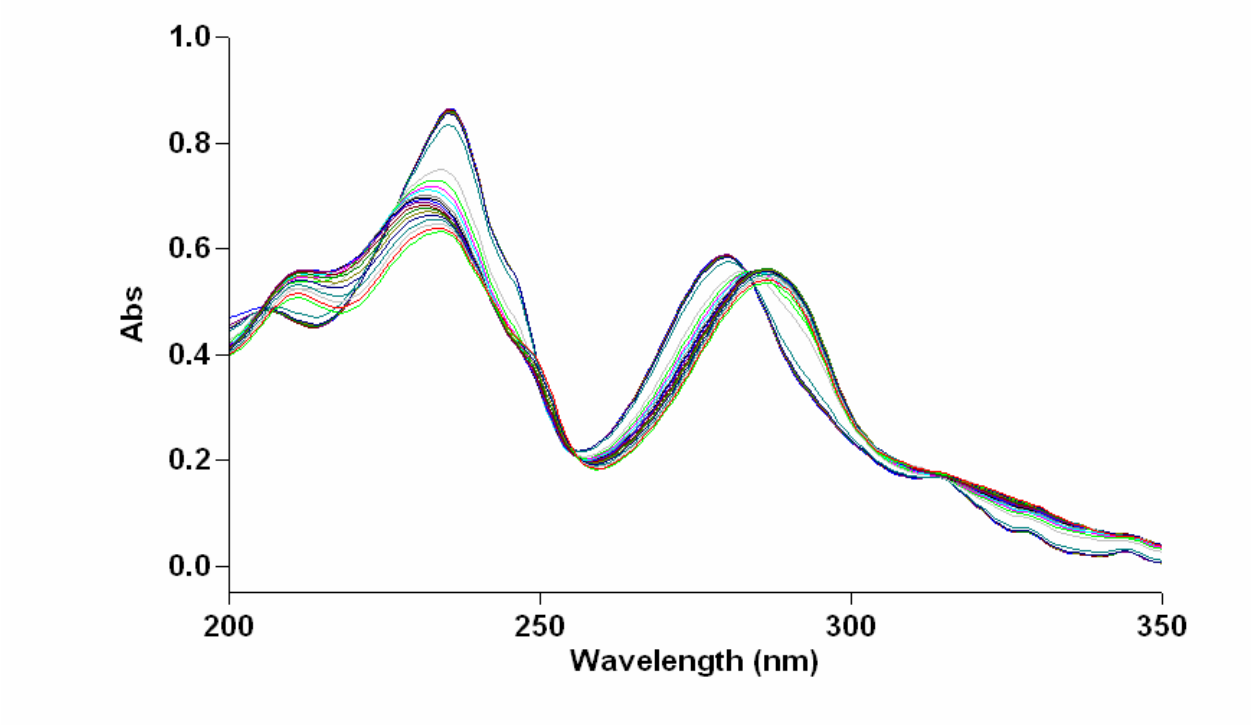

Figure 4. UV-Vis absorbance spectrum of the titration of PDA at 2.00×10^{-5} *M*.

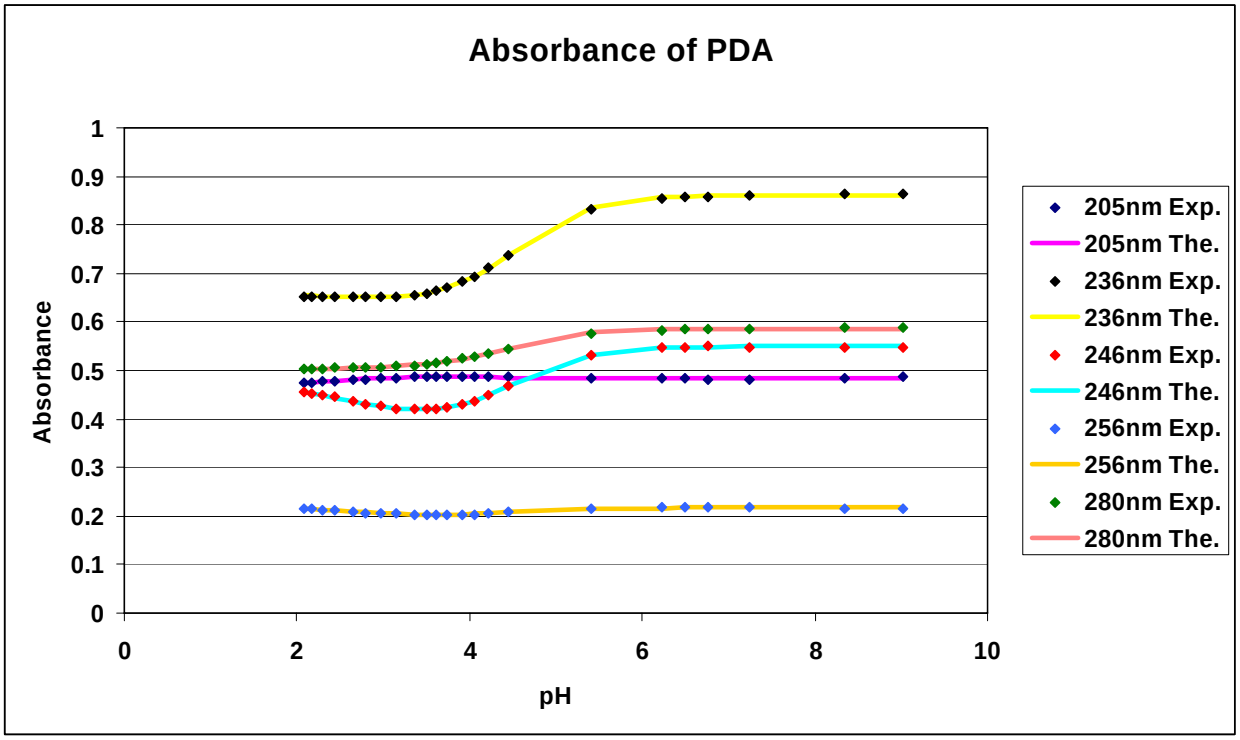

Figure 5. Experimental absorbance data (Exp.) fitted with calculated values (The.) to determine the protonation constants of PDA at 2.00×10^{-5} *M*.

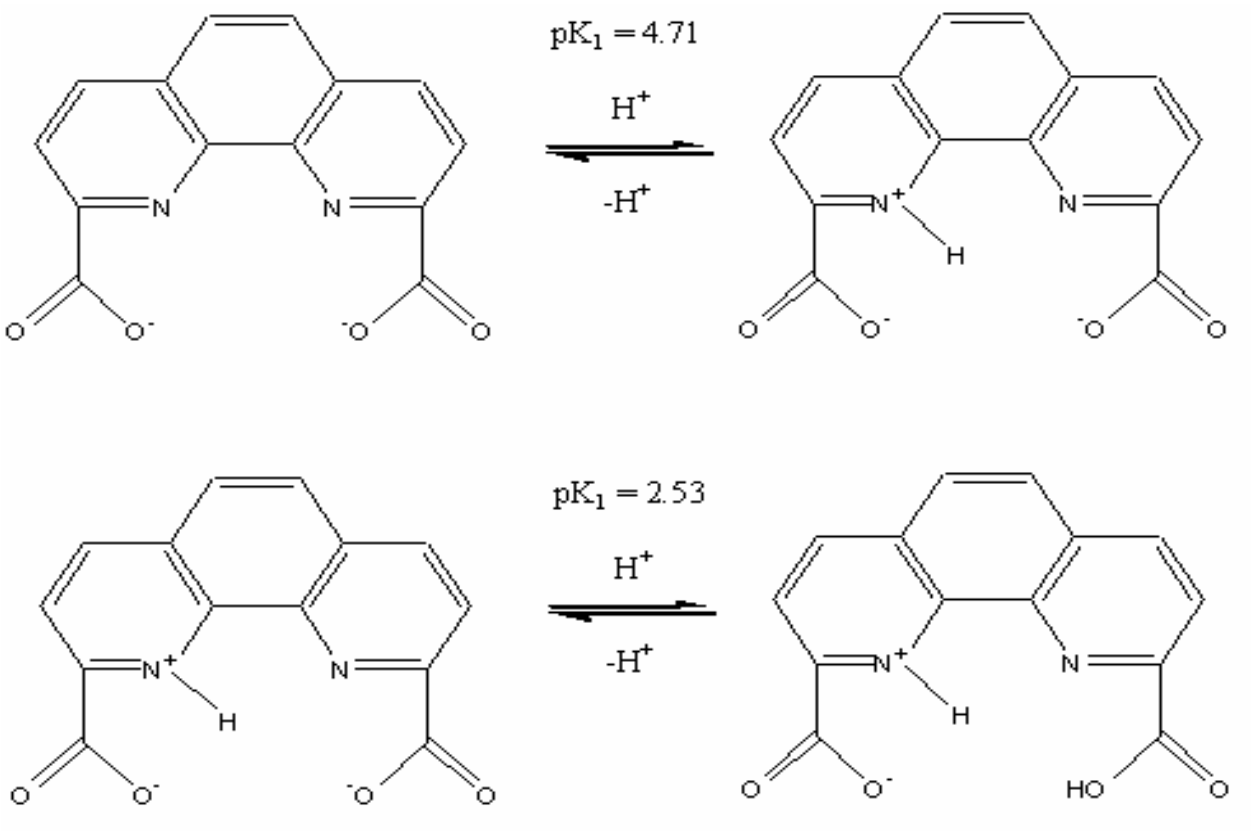

Figure 6. Protonation equilibria for 1,10-phenanthroline-2,9-dicarboxylic acid (PDA).

Titrations Involving Metal Ion Complexation with PDA

As PDA has low protonation constants, it would be difficult to displace the metal ion from the ligand by titrating with $HClO_4$. Instead solutions were acidified to an approximate pH of 2, then NaOH was titrated into the solution. This was found to be an acceptable method of removing the metals from PDA as the free-ligand absorbance spectrum began to be generated around pH of 7 to 12, depending upon the metal ion being studied, and the metals were fully removed from PDA by pH 12 in most cases. The equilibrium being studied is shown in Equation (1).

$$M^{n+}(PDA)^{2-} + 4\ OH^- \leftrightarrows M^{n+}(OH)_4^- + PDA^{2-} \quad (1)$$

As the pH of the solution was increased this equilibrium moves from left to right forcing the metal out of PDA into a hydroxide complex. From a knowledge of the log $K_n(OH^-)$[15] values for various metals it is possible[16] to calculate log K_1(PDA) for the metal ions. Absorbance values were modeled as a function of pH for each titration experiment. Using Equation (2), absorbance values were corrected for dilution.

$$\text{Corrected Absorbance} = \frac{\text{Absorbance} \cdot V_{total}}{V_{initial}} \quad (2)$$

Values of corrected absorbance versus pH were plotted using EXCEL. The points drawn in are experimental values of absorbance. From this plot a series of isosbestic or inflection points are seen over a range of pH values. The points represent specific protonation equilibria which are used to plot theoretical curves of absorbance versus pH, which incorporate the fitted extinction coefficients of the L, ML, and $ML(OH)_n$ species present in solution. The theoretical curves of absorbance versus pH were fitted to the experimental points using the SOLVER module of the program EXCEL. The standard deviations of these protonation constants were calculated using the SOLVSTAT macro. Using the experimentally determined protonation equilibria values and

the ionization constant of water[15] log K_w = 13.78 along with the log of the concentration of free ligand, a log K_1 value for PDA can be calculated.

As ethylenediamine dicarboxylic acid (EDDA) is a less preorganized analog of PDA, log K_1 values for metals with PDA are reported with log K_1 values for the metal with EDDA[17] along with Δ log K_1 values between PDA and EDDA. However, EDDA is not an ideal analog for PDA since EDDA has sp^3 hybridized N-donors where those on PDA are sp^2 hybridized, but this fact should favor EDDA, since sp^3 hybridized N-donors (e.g. ammonia) are[15] generally much stronger bases in aqueous solution than sp^2 hybridized N-donor bases such as pyridine. Thus, if anything, the effect of the high levels of preorganization of PDA on its log K_1 values should be understated by using EDDA complexes for comparison with PDA.

Aluminum(III)-PDA results

Aluminum(III) has an ionic radius of 0.54 Å which is much smaller than the ideal 1.0 Å favored by PDA. The UV absorbance spectrum for aluminum(III) and PDA is shown in Figure 7. A plot of the corrected absorbance values versus pH is shown in Figure 8 and a plot of the theoretical absorbance values calculated to determine the protonation constants of the complex is shown alongside the experimental data in Figure 9(a). From the selected wavelengths of 208, 233, 249, 260 and 283 nm, 4 successive pH-dependent equilibria were observed. The equilibria are described below at the pH at which they occurred.

$$Al(PDA) + H^+ \leftrightarrows Al(PDA)H^+ \qquad (pH = 2.83)$$

$$Al(PDA) + OH^- \leftrightarrows Al(PDA)OH \qquad (pH = 4.07)$$

$$Al(PDA)(OH) + OH^- \leftrightarrows Al(PDA)(OH)_2 \qquad (pH = 5.92)$$

$$Al(PDA)(OH)_2 + 2\ OH^- \leftrightarrows Al(OH)_4^- + PDA^{2-} \qquad (pH = 8.41)$$

Figure 9(b) shows a species distribution diagram for these protonation equilibria. Using log K_w = 13.78[15], the equilibria for the Al-PDA complex with hydroxide can be described as follows.

$$Al(PDA) + OH^- \leftrightarrows Al(PDA)OH^- \qquad (\log K_1\,[OH^-] = 9.73)$$

$$Al(PDA)(OH) + OH^- \leftrightarrows Al(PDA)(OH)_2 \qquad (\log K_1\,[OH^-] = 7.88)$$

$$Al(PDA)(OH)_2 + 2\,OH^- \leftrightarrows Al(OH)_4^- + PDA^{2-} \qquad (\log K_3K_4\,[OH^-] = 10.78)$$

The log β_4 $[OH^-]$ for aluminum is 31.5 and from this value[15] log K_1 for PDA with aluminum of 8.11 was calculated as follows,

$$\log K_1 = 31.5 - (10.78) + 7.88 + 9.73) + 5.0 \qquad (3)$$

where the 5.0 takes into account the amount of free ligand at the midpoint of the equilibrium where Al(III) is displaced from PDA. This midpoint is called the isosbestic point. There was no reported[15] formation constant for EDDA with aluminum(III). However, the affinity of the very small Al(III) ion for PDA is remarkably low when compared to other trivalent metal ions, which would be expected from the preference of PDA for larger metal ions.

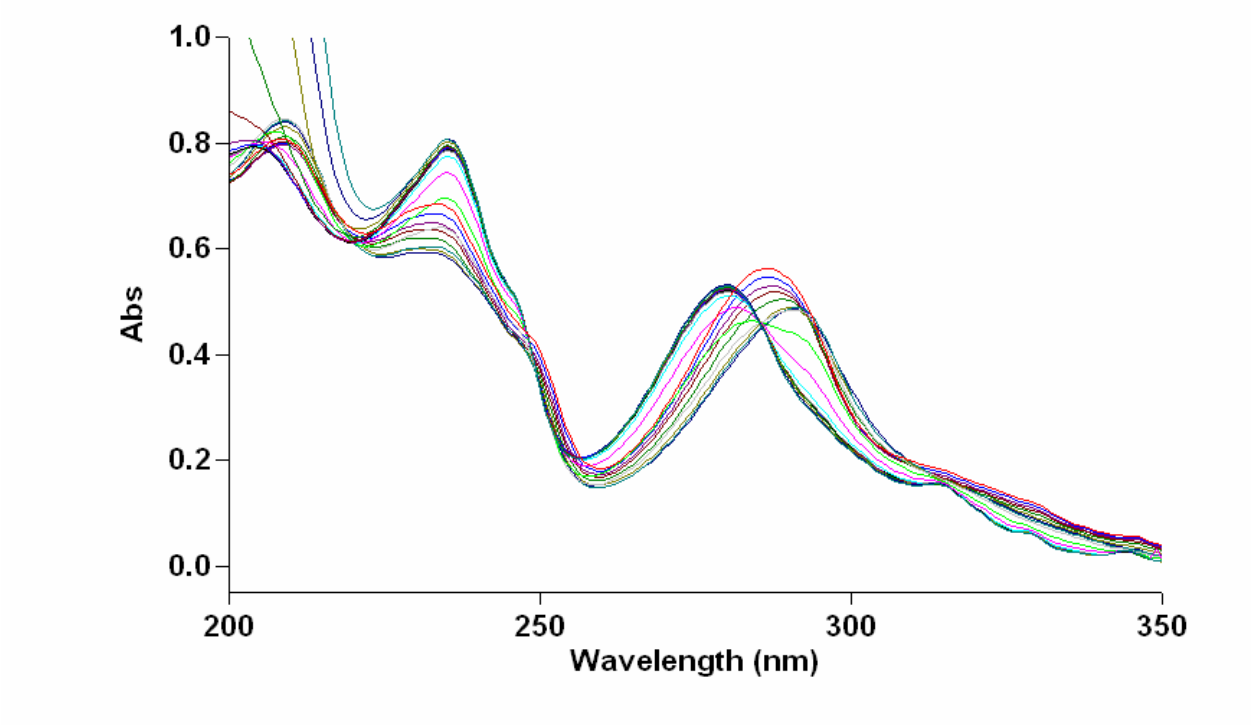

Figure 7. UV-Vis absorbance spectrum of the titration of aluminum(III) and PDA both at 2.00×10^{-5} *M*, in 0.10 *M* $NaClO_4$ at 25.0 ºC.

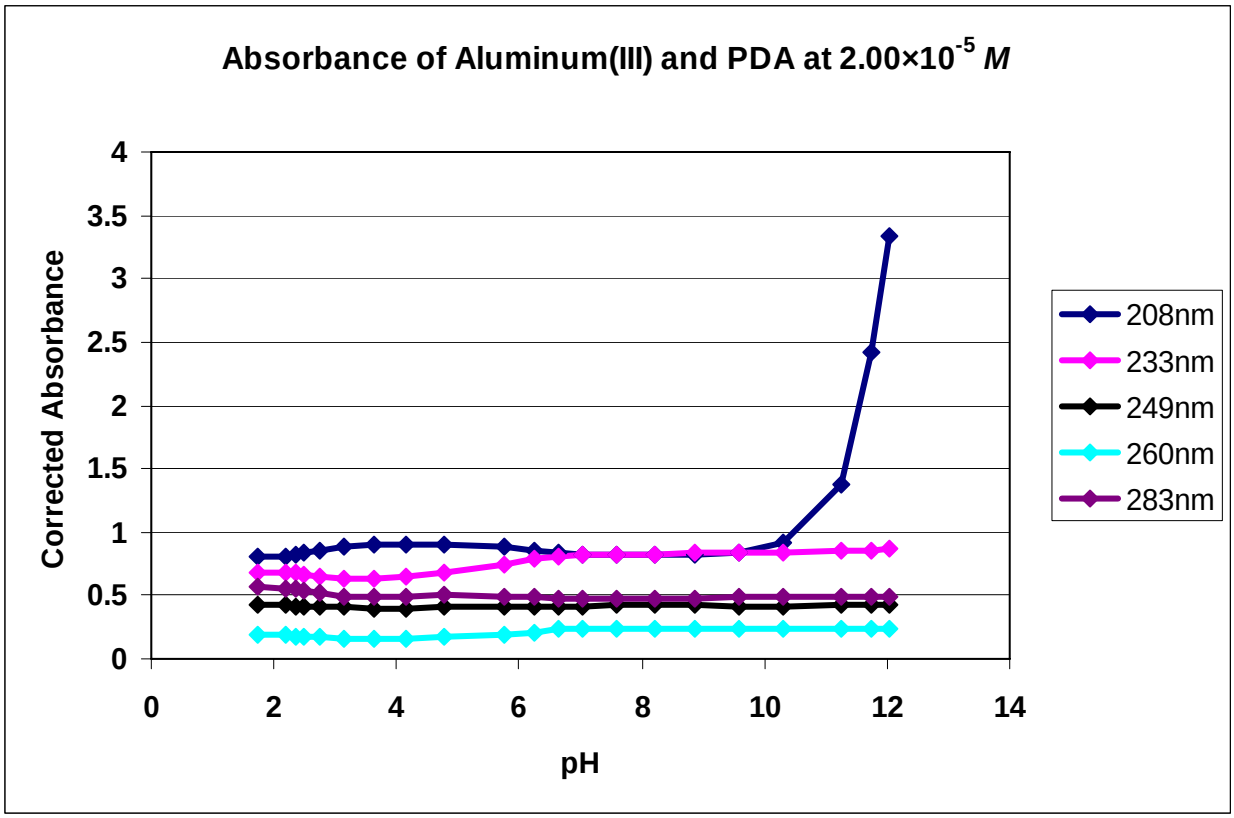

Figure 8. Plot of absorbance values corrected for dilution of the titration of aluminum(III) and PDA at 2.00×10^{-5} *M*, in 0.10 *M* $NaClO_4$ at 25.0 ºC.

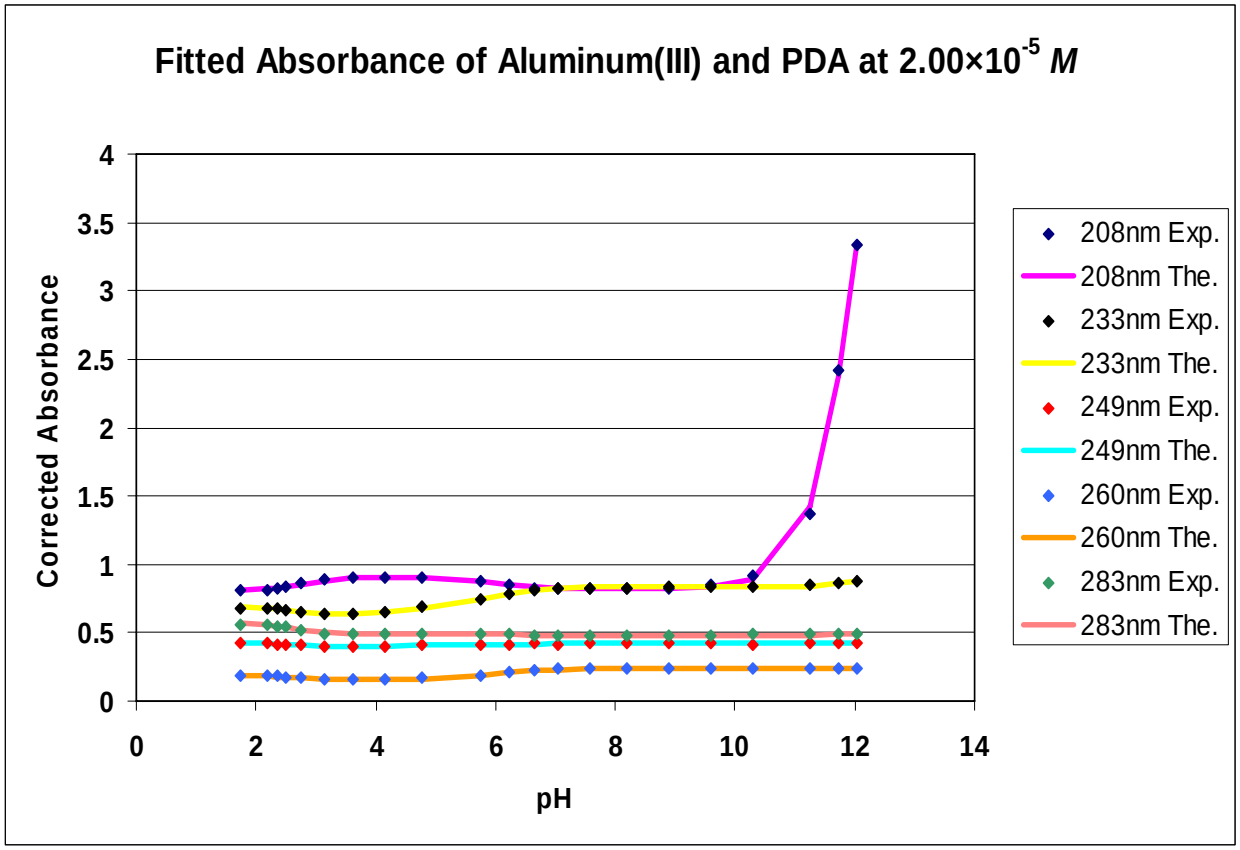

Figure 9(a). Experimental absorbance data (Exp.) fitted with calculated values (The.) to determine the protonation equilibria of the titration of aluminum(III) and PDA at 2.00×10^{-5} *M*, in 0.10 *M* $NaClO_4$ at 25.0 ºC.

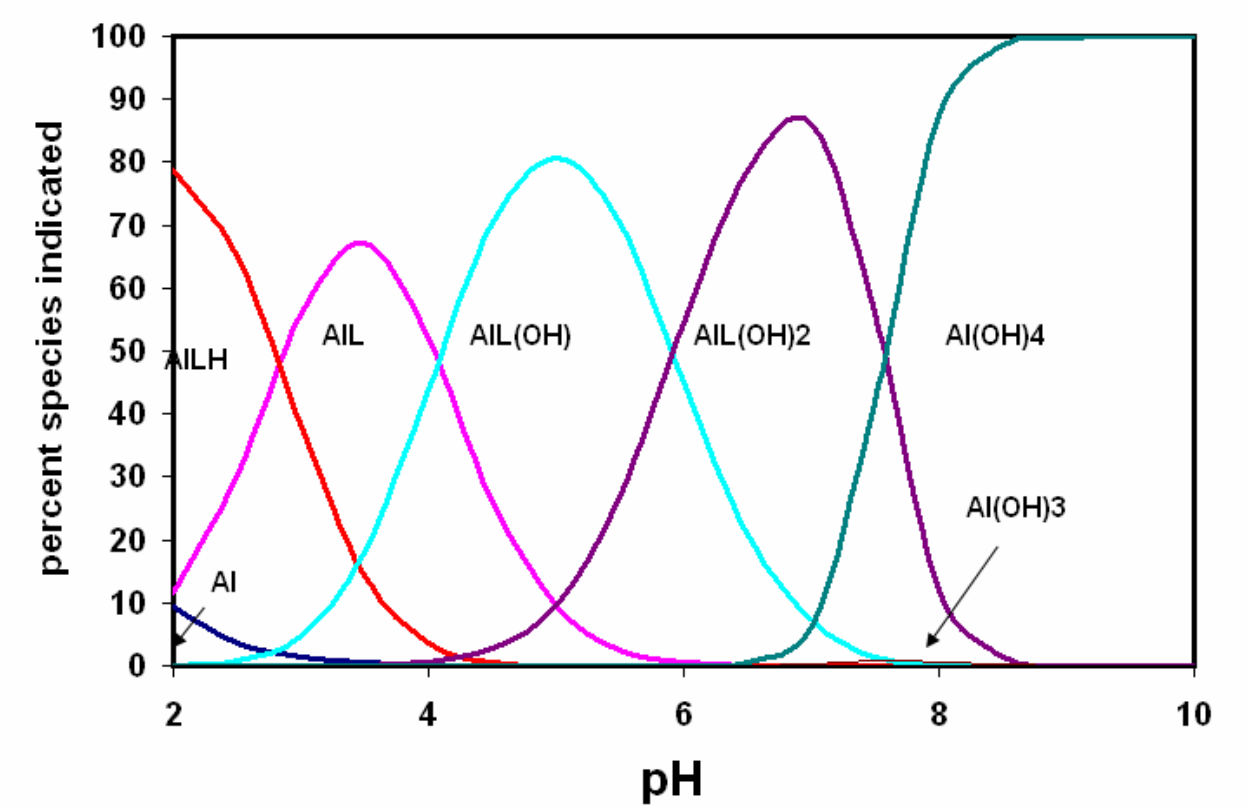

Figure 9(b). Species distribution diagram for the Al(III)/PDA system at 2.00×10^{-5} M calculated using log K values determined here for Al(III) and PDA. Diagram calculated using EXCEL. Abbreviation: L = PDA. Charges on species omitted for simplicity.

Bismuth(III)-PDA results

Bismuth(III) has an ionic radius of 1.03 Å which is very close to the ideal 1.0 Å favored by PDA. The UV absorbance spectrum for bismuth(III) and PDA at 2.00×10^{-5} *M* is shown in Figure 10. A plot of the corrected absorbance values versus pH is shown in Figure 11 and a plot of the theoretical absorbance values calculated to determine the protonation constants of the complex is shown alongside the experimental data in Figure 12(a). From the selected wavelengths of 233, 250, 263, 280 and 294 nm, 5 successive pH-dependent equilibria were observed. The equilibria are described below at the pH at which they occurred.

$$Bi(PDA) + H^+ \leftrightarrows Bi(PDA)H \qquad (pH = 1.85)$$

$$Bi(PDA) + OH^- \leftrightarrows Bi(PDA)OH \qquad (pH = 6.26)$$

$$Bi(PDA)(OH) + OH^- \leftrightarrows Bi(PDA)(OH)_2 \qquad (pH = 9.67)$$

$$Bi(PDA)(OH)_2 + 2\ OH^- \leftrightarrows [Bi(OH)_4]^- + PDA \qquad (pH = 11.07)$$

Figure 12(b) shows a species distribution diagram for these protonation equilibria. Using $\log K_w = 13.78$, the $\log K_1 [OH^-]$ of the Bi-PDA complex can be described as follows.

$$Bi(PDA) + OH^- \leftrightarrows Bi(PDA)OH \qquad (\log K_1 [OH^-] = 7.52)$$

$$Bi(PDA)(OH) + OH^- \leftrightarrows Bi(PDA)(OH)_2 \qquad (\log K_2 [OH^-] = 4.11)$$

$$Bi(PDA)(OH)_2 + 2\ OH^- \leftrightarrows [Bi(OH)_4]^- + PDA \qquad (\log K_3K_4 [OH^-] = 2.71)$$

The $\log \beta_4 [OH^-]$ for bismuth is 33.6 and from this value[15] a $\log K_1$ for PDA with bismuth of 21.6 was calculated using Equation (4),

$$\log K_1 = 33.6–(2\times(2.71)+4.11+7.52)+5.0 \qquad (4)$$

where the 5.0 takes into account the amount of free ligand at the isosbestic point. The UV absorbance spectrum for bismuth(III) and PDA at 2.00×10^{-6} *M* is shown in Figure 13. A plot of

the correlation between E (mV) and the calculated pH, which was used to calculate E^0, is shown in Figure 14. A plot of the corrected absorbance values versus calculated pH is shown in Figure 15 and a plot of the theoretical absorbance values calculated to determine the protonation constants of the complex is shown alongside the experimental data in Figure 16. This scan was conducted to show that at a dilution of 10, there was no significant change on the observed values for the protonation equilibria which reveals that the bismuth-PDA complex does not form any dimers. There was no reported[15] formation constant for EDDA with bismuth(III).

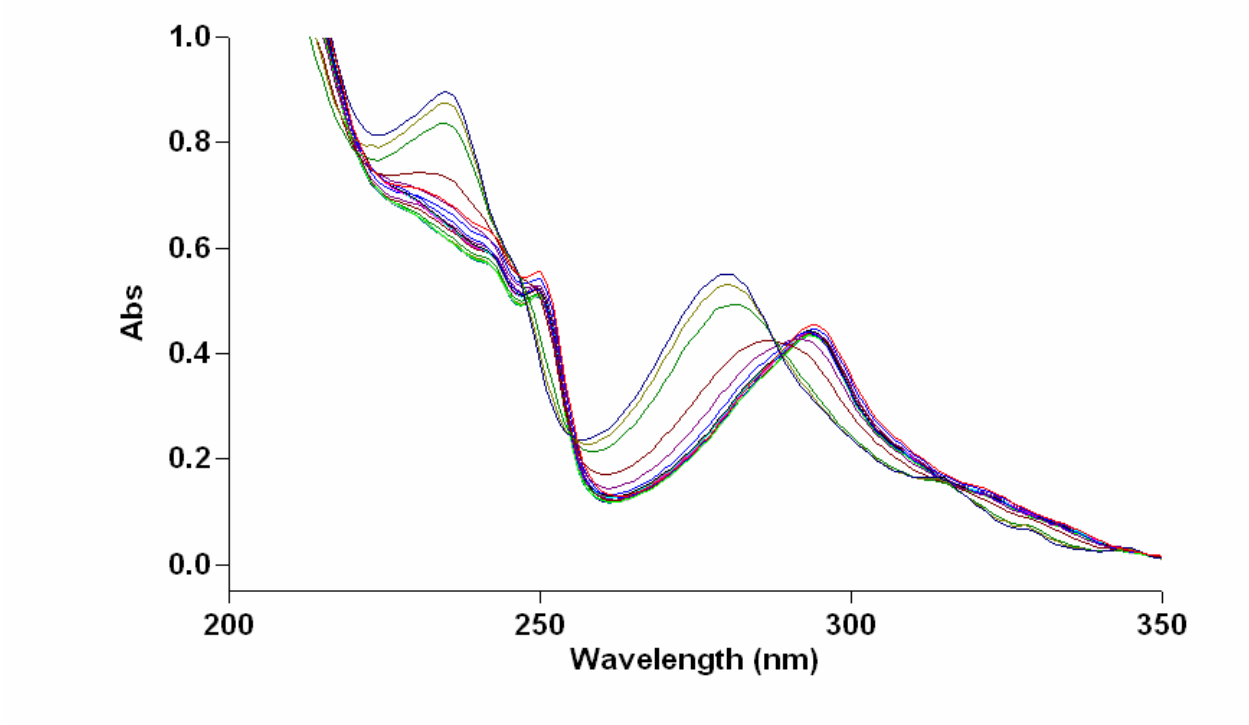

Figure 10. UV-Vis absorbance spectrum of the titration of bismuth(III) and PDA at 2.00×10^{-5} *M*, in 0.10 *M* $NaClO_4$ at 25.0 ºC.

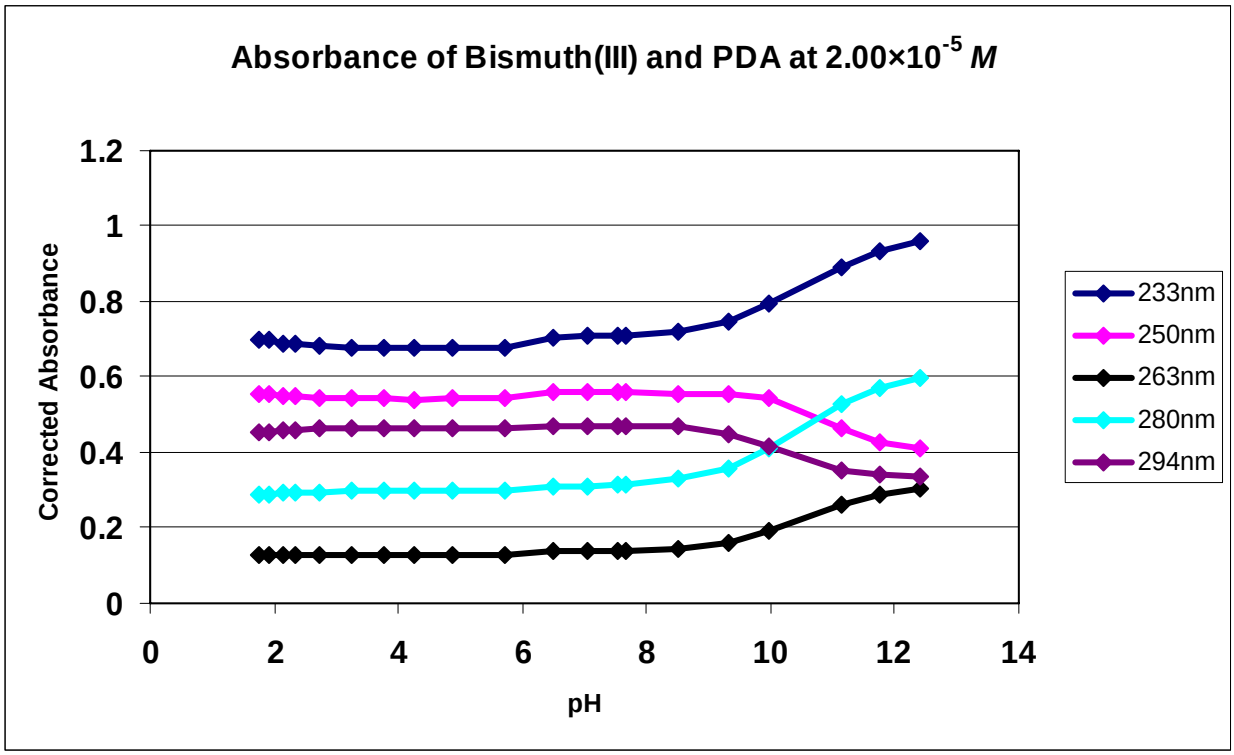

Figure 11. Plot of absorbance values corrected for dilution of the titration of bismuth(III) and PDA at 2.00×10^{-5} *M*, in 0.10 *M* $NaClO_4$ at 25.0 ºC.

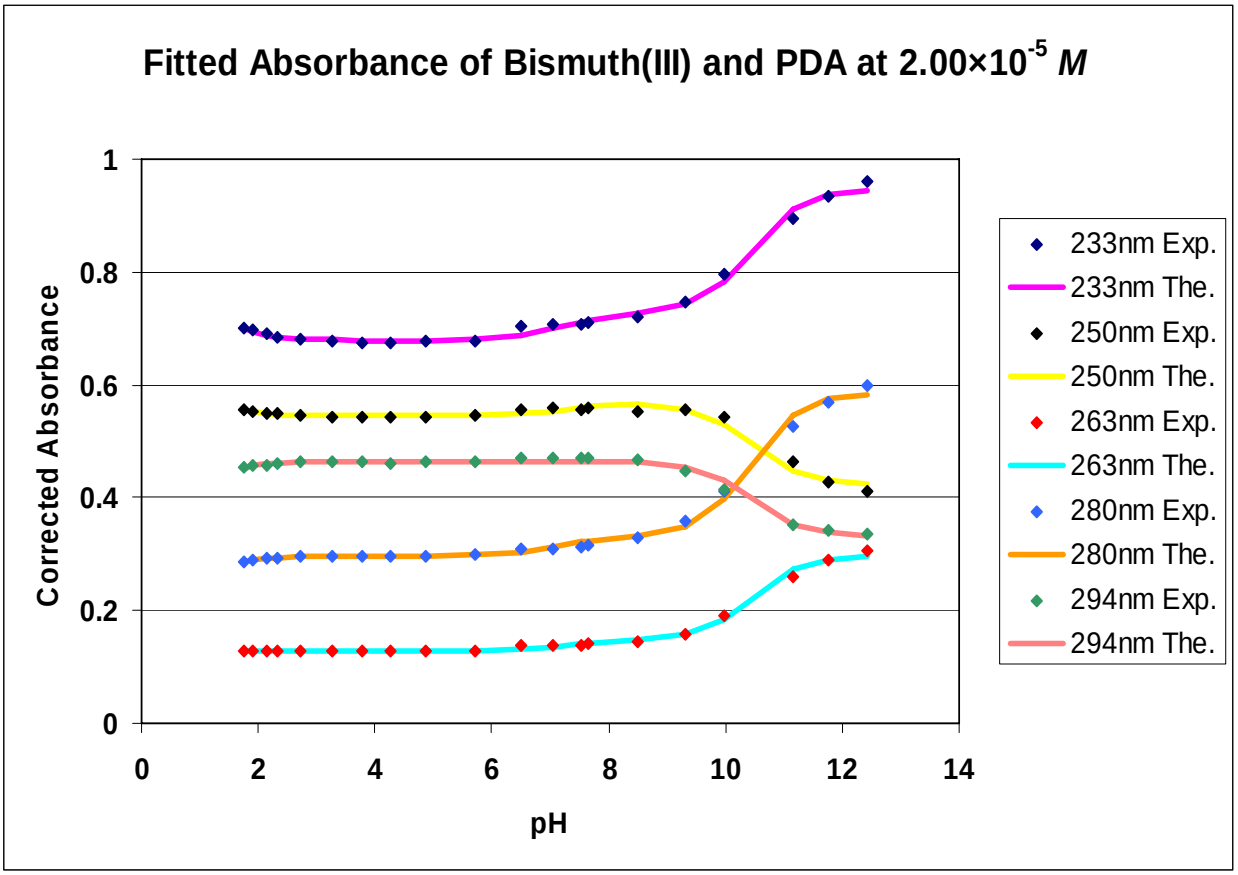

Figure 12(a). Experimental absorbance data (Exp.) fitted with calculated values (The.) to determine the protonation equilibria of the titration of bismuth(III) and PDA at 2.00×10^{-5} *M*, in 0.10 *M* $NaClO_4$ at 25.0 ºC.

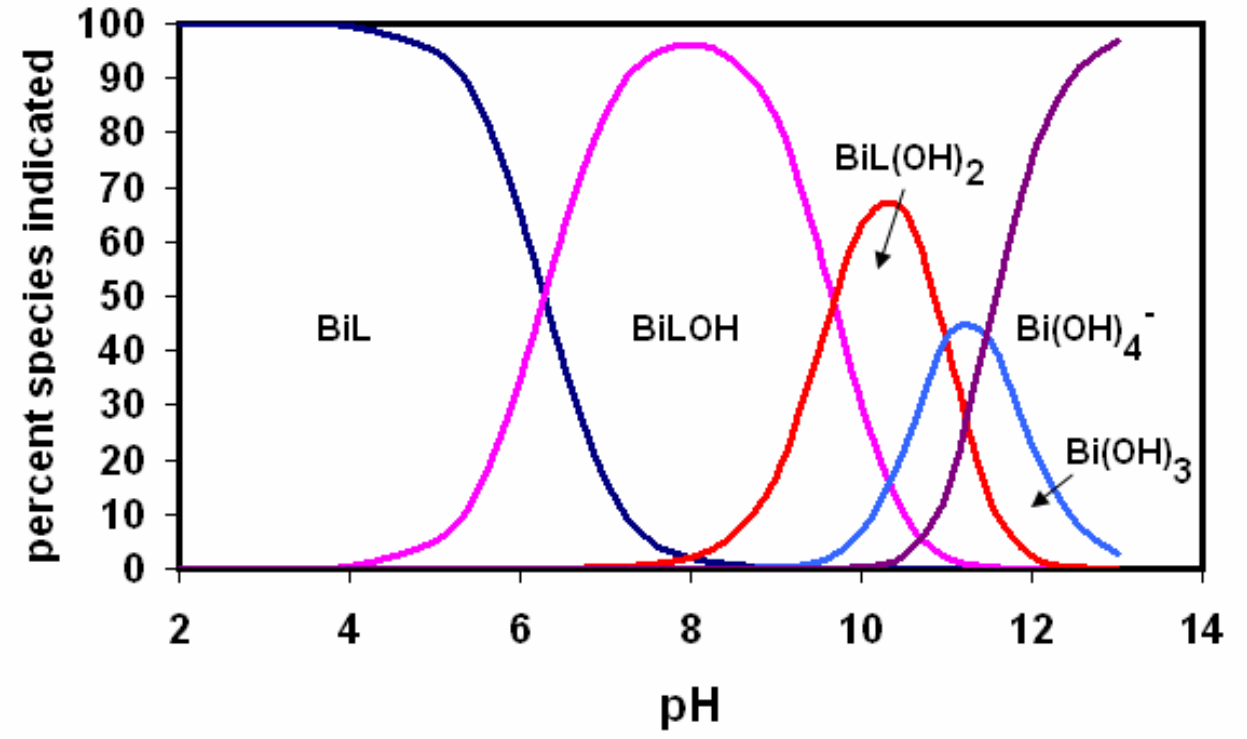

Figure 12(b). Species distribution diagram for the Bi(III)/PDA system at 2.00×10^{-5} *M* calculated using log K values determined here for Bi(III) and PDA. Diagram calculated using EXCEL. Abbreviation: L = PDA. Charges on species omitted for simplicity.

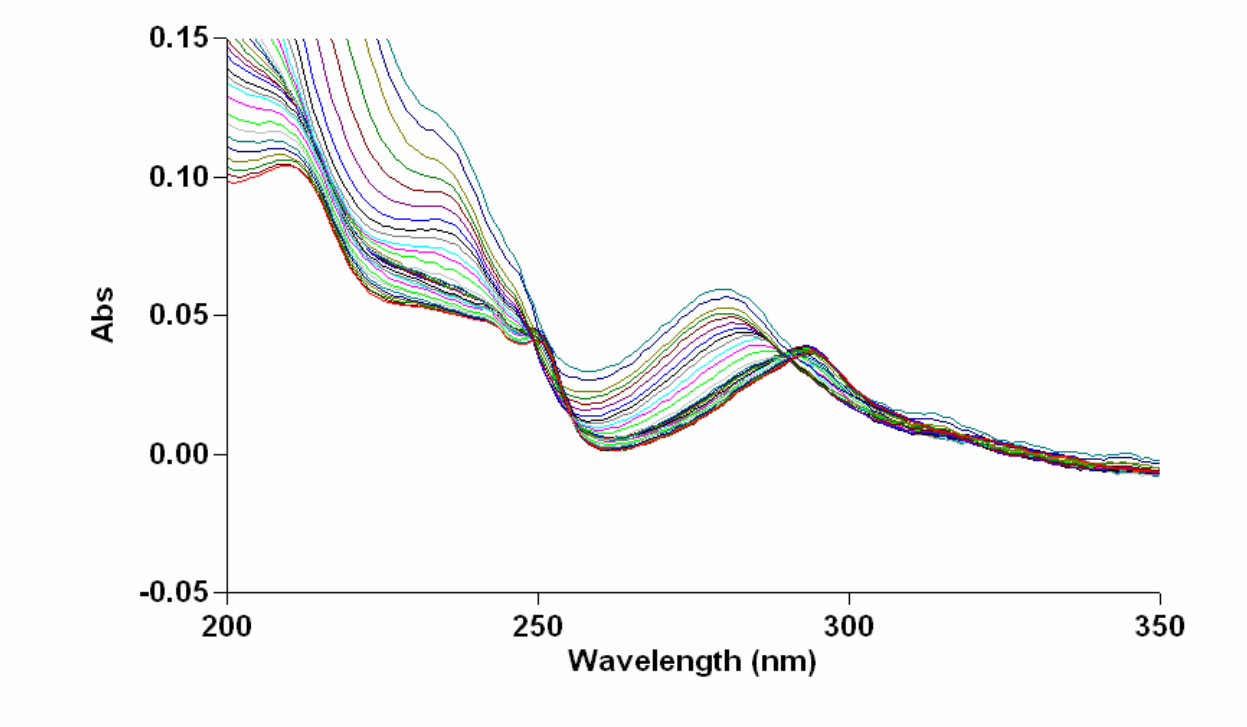

Figure 13. UV-Vis absorbance spectrum of the titration of bismuth(III) and PDA at 2.00×10^{-6} *M*, in 0.10 *M* $NaClO_4$ at 25.0 ºC.

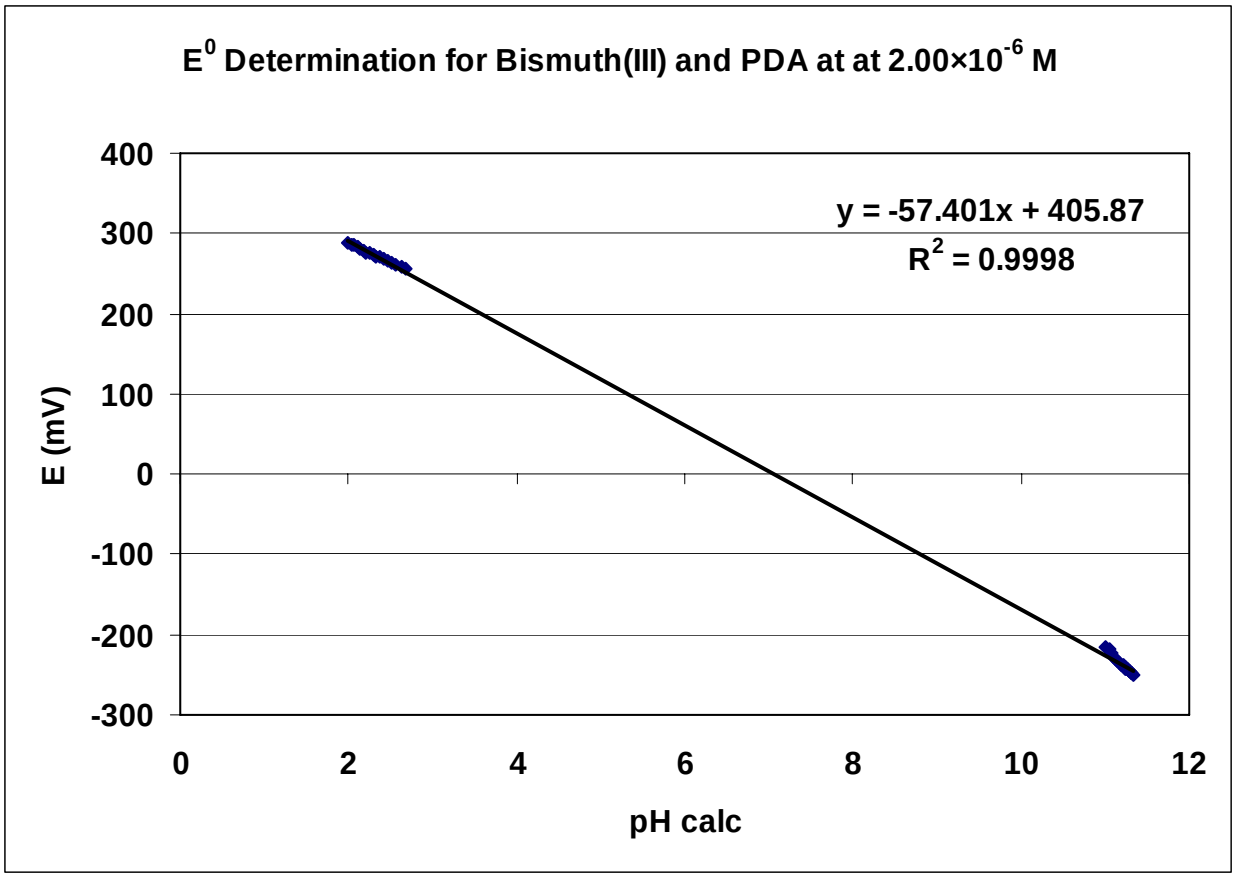

Figure 14. Plot of the correlation between E (mV) and the calculated pH used to calculate E^0 for the titration of bismuth(III) and PDA at 2.00×10^{-6} *M*, in 0.10 *M* $NaClO_4$ at 25.0 ºC.

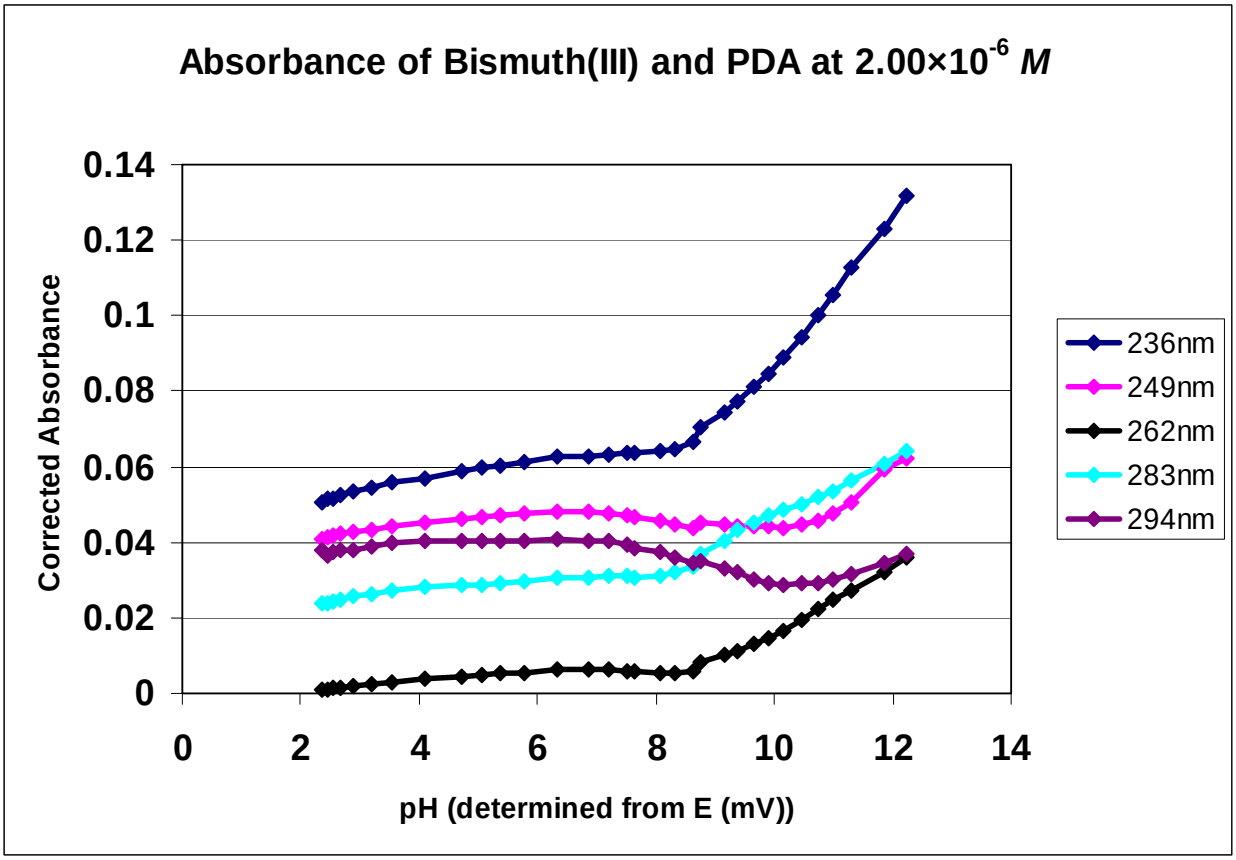

Figure 15. Plot of absorbance values corrected for dilution of the titration of bismuth(III) and PDA at 2.00×10^{-6} *M*, in 0.10 *M* $NaClO_4$ at 25.0 ºC.

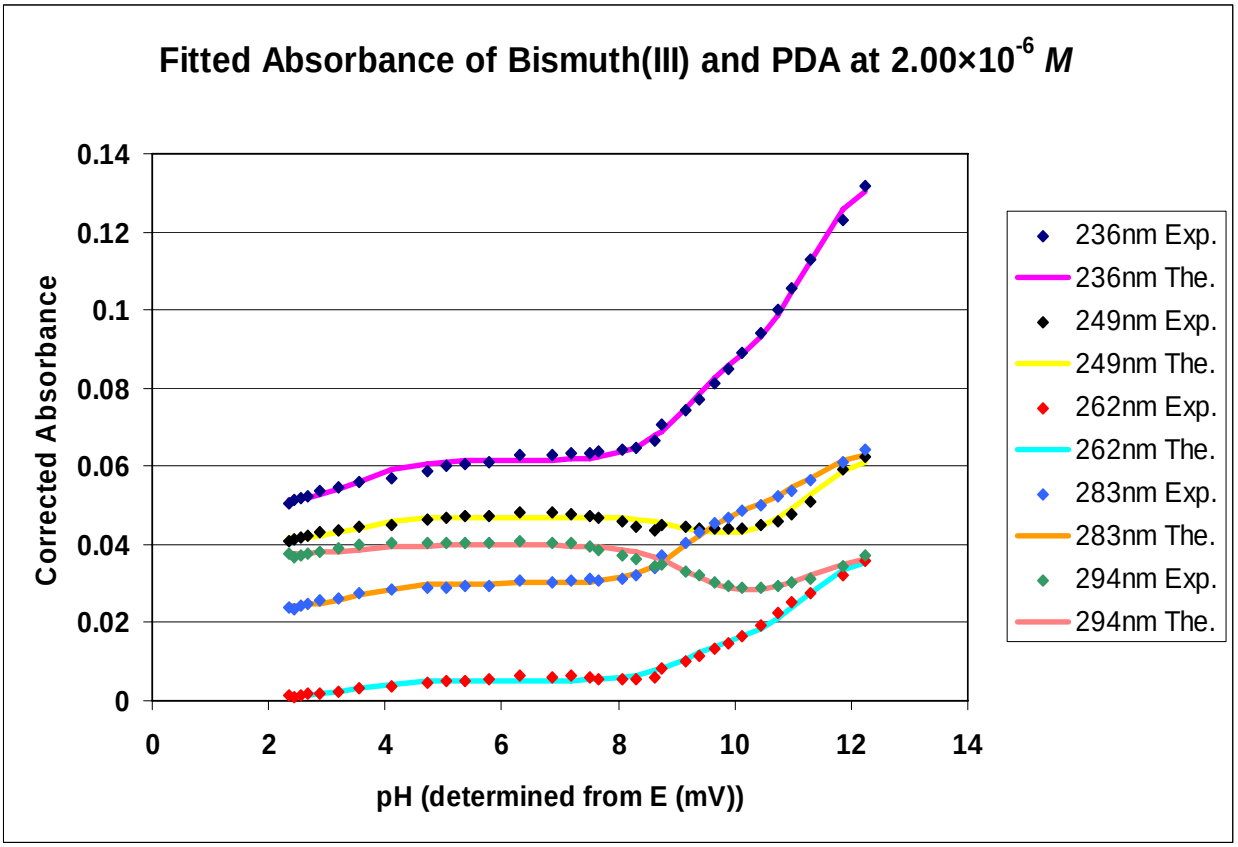

Figure 16. Experimental absorbance data (Exp.) fitted with calculated values (The.) to determine the protonation equilibria of the titration of bismuth(III) and PDA at 2.00×10^{-6} *M*, in 0.10 *M* $NaClO_4$ at 25.0 ºC.

Cerium(IV)-PDA results

Cerium(IV) has an ionic radius of 0.87 Å which is somewhat less than the ideal value of 1.0 Å favored by PDA. The UV absorbance spectrum for cerium(IV) and PDA at 2.00×10^{-5} *M* is shown in Figure 17. A plot of the corrected absorbance values versus pH is shown in Figure 18 and a plot of the theoretical absorbance values calculated to determine the protonation constants of the complex is shown alongside the experimental data in Figure 19. From the selected wavelengths of 236, 251, 262, 283 and 294 nm, 5 successive pH-dependent equilibria were observed. The equilibria are described below at the pH at which they occurred.

$$Ce(PDA) + H^{+} \leftrightarrows Ce(PDA)H \qquad (pH = 2.30)$$

$$Ce(PDA) + OH^{-} \leftrightarrows Ce(PDA)OH \qquad (pH = 3.95)$$

$$Ce(PDA)(OH) + OH^{-} \leftrightarrows Ce(PDA)(OH)_2 \qquad (pH = 6.43)$$

$$Ce(PDA)(OH)_2 + OH^{-} \leftrightarrows Ce(PDA)(OH)_3 \qquad (pH = 8.48)$$

$$Ce(PDA)(OH)_3 + OH^{-} \leftrightarrows Ce(OH)_4 + PDA^{2-} \qquad (pH = 11.47)$$

Using log K_w = 13.78, the log K_1 [OH^-] of the Ce-PDA complex can be described as follows.

$$Ce(PDA) + OH^{-} \leftrightarrows Ce(PDA)OH \qquad (\log K_1 [OH^-] = 9.83)$$

$$Ce(PDA)(OH) + OH^{-} \leftrightarrows Ce(PDA)(OH)_2 \qquad (\log K_2 [OH^-] = 7.35)$$

$$Ce(PDA)(OH)_2 + OH^{-} \leftrightarrows Ce(PDA)(OH)_3 \qquad (\log K_3 [OH^-] = 5.30)$$

$$Ce(PDA)(OH)_3 + OH^{-} \leftrightarrows Ce(OH)_4 + PDA^{2-} \qquad (\log K_4 [OH^-] = 2.31)$$

However, there has been no log β_4 [OH^-] for cerium(IV) reported[15] so another titration experiment was performed. The UV absorbance spectrum for cerium(IV) and PDA at 2.00×10^{-5} *M*, at initial pH 1.25, titrated with 0.01 *M* Th(IV), acidified to pH 1.29, is shown in Figure 20. A plot of the corrected absorbance values versus [Th(IV)] is shown in Figure 21. The selected

wavelengths of 283, 293, 303, 313 and 323 nm were plotted in an attempt to calculate a log K_1 value. The higher wavelengths used were selected for analysis because Th(IV) absorbs UV light between 200 and 250 nm. However, an overall increase in absorbance is still seen for most wavelengths as the [Th(IV)] increases. The wavelengths at 283 nm is especially useful in this case because it still exhibits characteristic decrease in absorbance indicating displacement of Ce(IV) from PDA by Th(IV). This absorbance spectrum is shown in Figure 22.

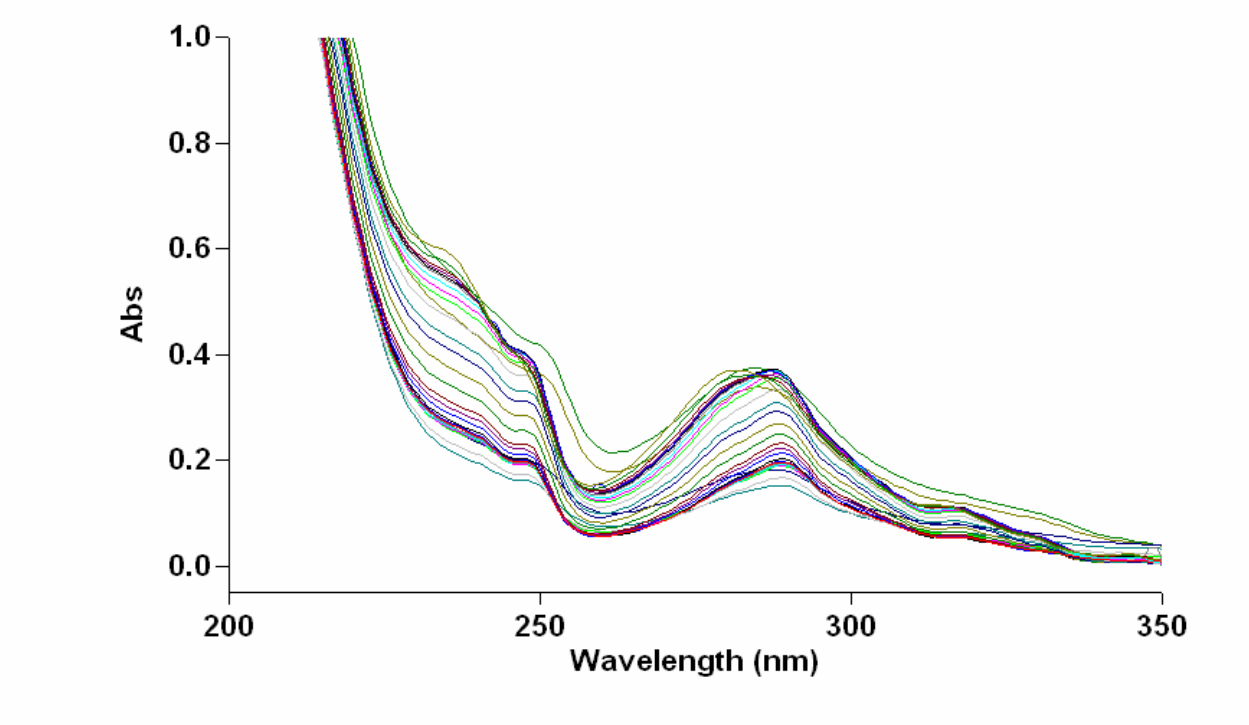

Figure 17. UV-Vis absorbance spectrum of the titration of cerium(IV) and PDA at 2.00×10^{-5} *M*, in 0.10 *M* $NaClO_4$ at 25.0 ºC.

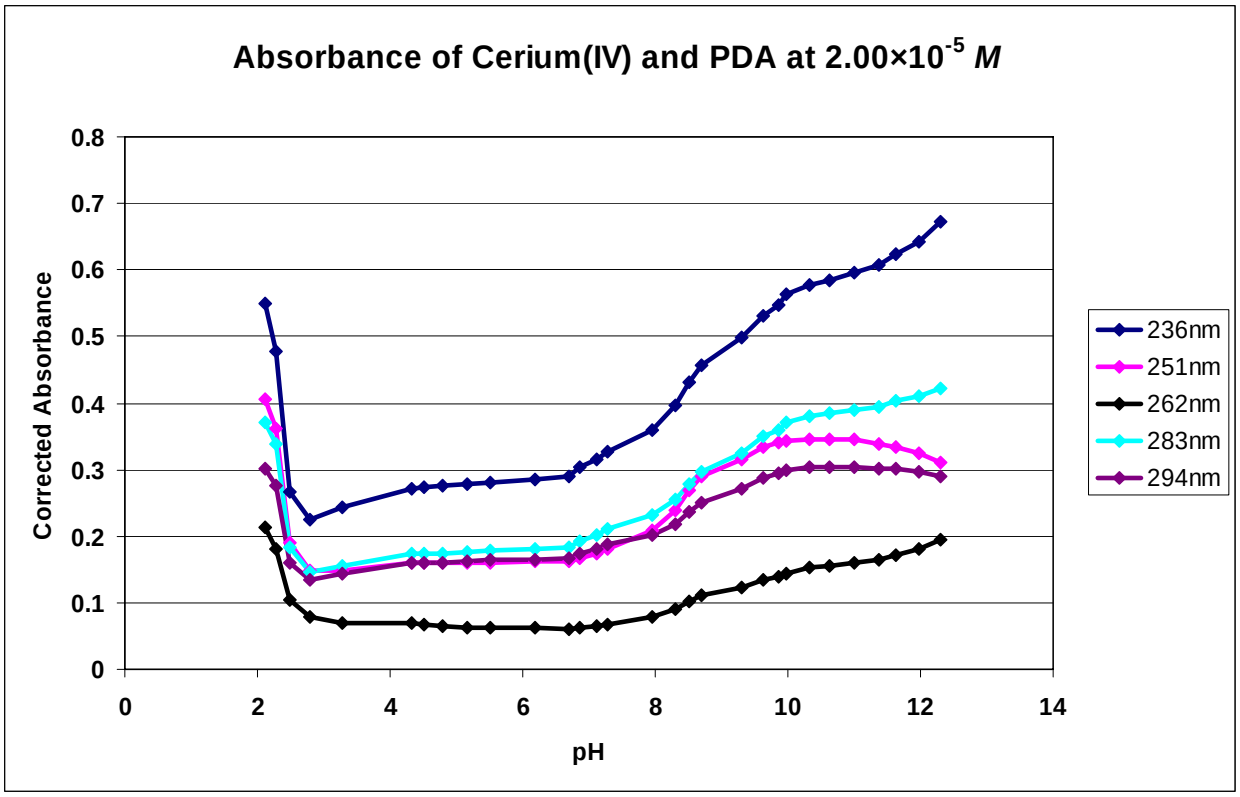

Figure 18. Plot of absorbance values corrected for dilution of the titration of cerium(IV) and PDA at 2.00×10^{-5} *M*, in 0.10 *M* $NaClO_4$ at 25.0 ºC.

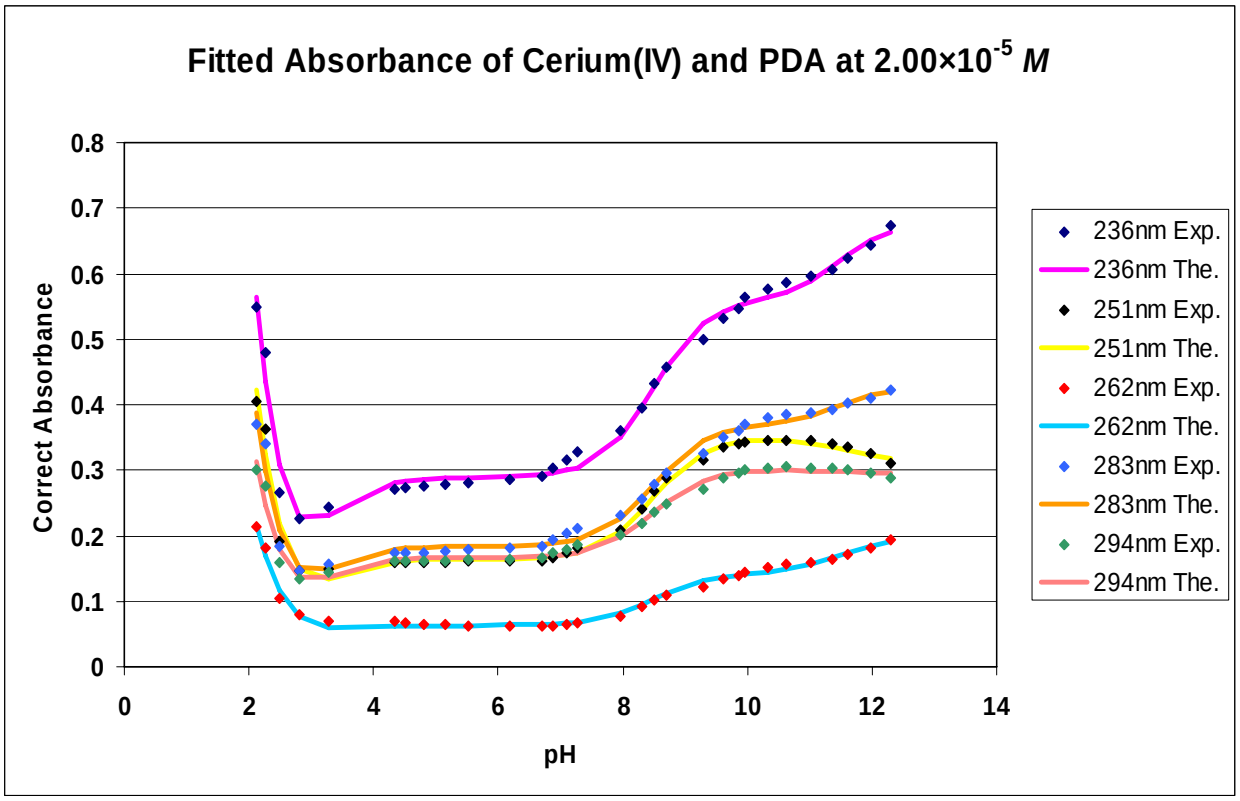

Figure 19. Experimental absorbance data (Exp.) fitted with calculated values (The.) to determine the protonation equilibria of the titration of cerium(IV) and PDA at 2.00×10^{-5} *M*, in 0.10 *M* $NaClO_4$ at 25.0 ºC.

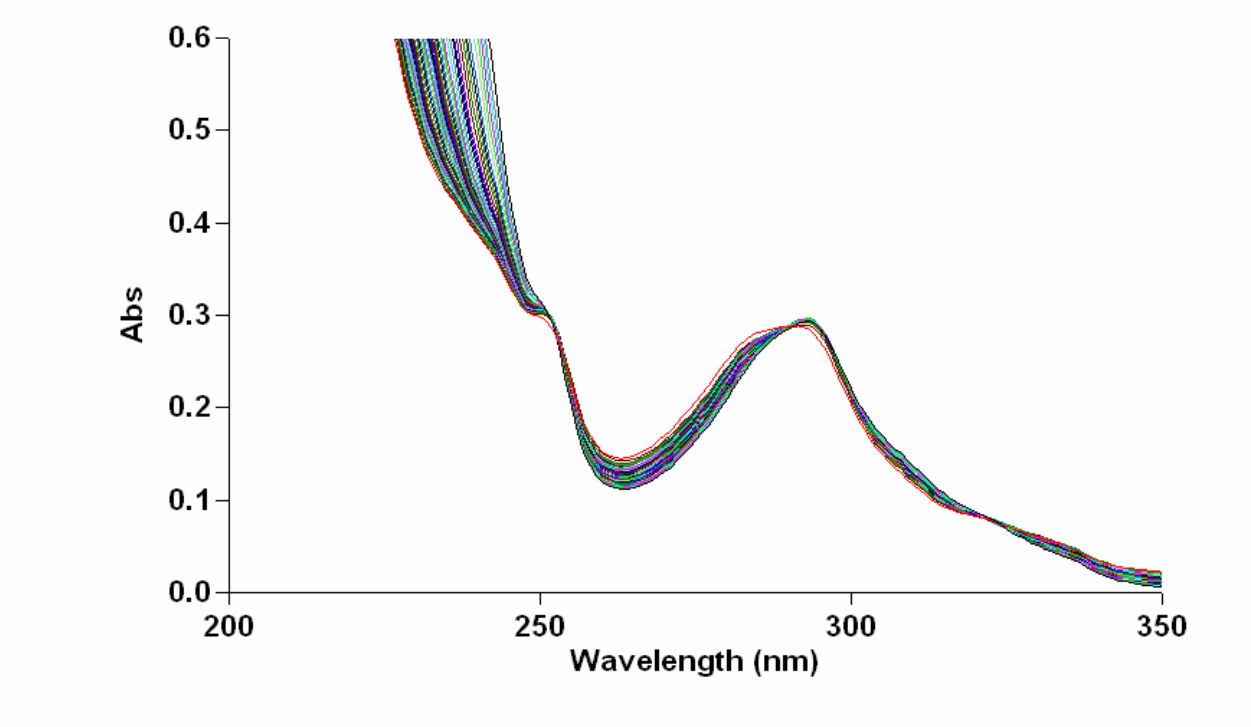

Figure 20. UV-Vis absorbance spectrum of the titration of cerium(IV) and PDA at 2.00×10^{-5} *M*, initial pH 1.25, titrated with 0.01 *M* Th(IV), acidified to pH 1.29.

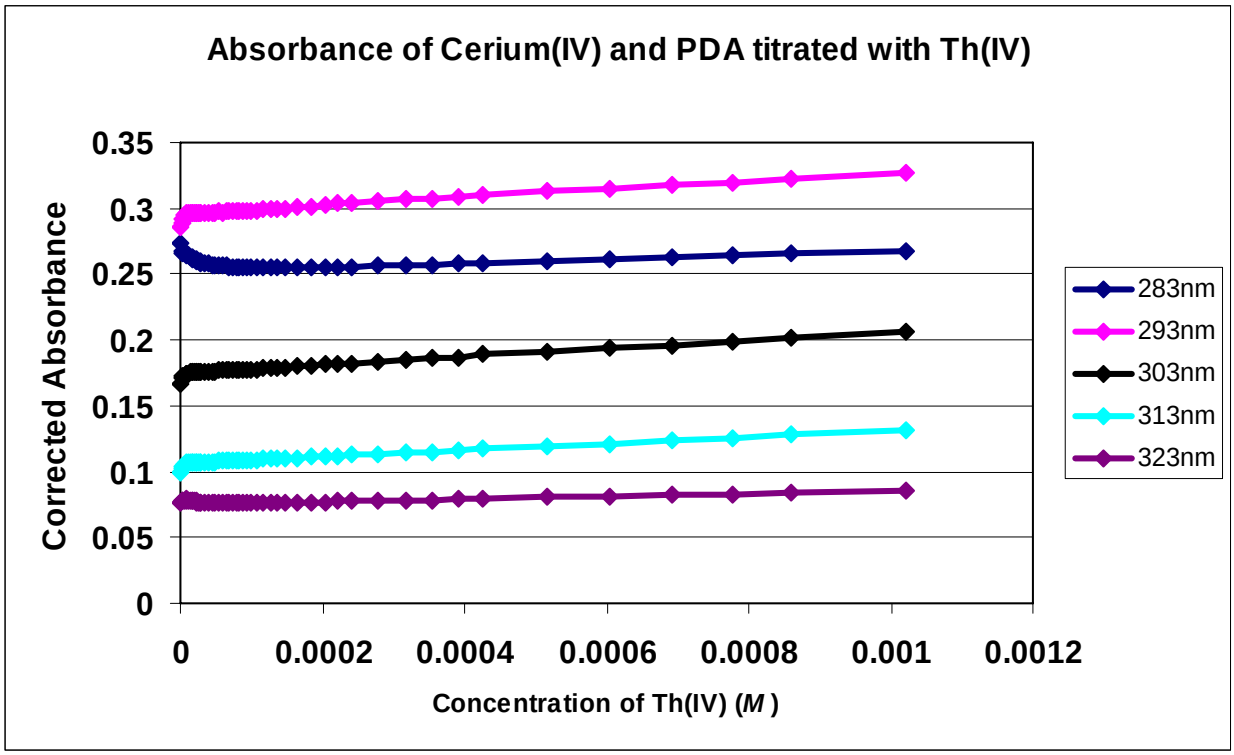

Figure 21. Plot of absorbance values corrected for dilution of the titration of cerium(IV) and PDA at 2.00×10^{-5} *M*, initial pH 1.25, titrated with 0.01 *M* Th(IV), acidified to pH 1.29.

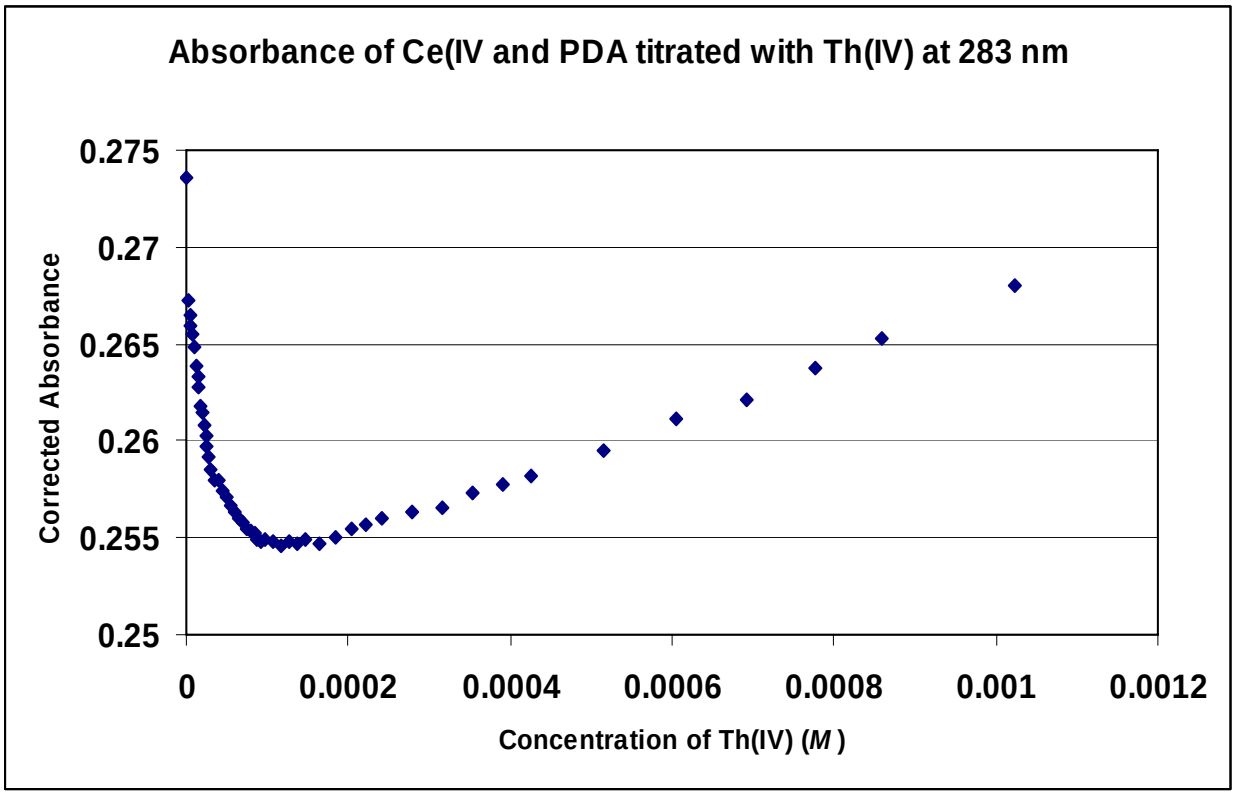

Figure 22. Plot of absorbance values corrected for dilution at 283 nm of the titration of cerium(IV) and PDA at 2.00×10^{-5} *M*, initial pH 1.25, titrated with 0.01 *M* Th(IV), acidified to pH 1.29.

Gallium(III)-PDA results

Gallium(III) has an ionic radius of 0.62 Å which is much smaller than the ideal 1.0 Å favored by PDA. The UV absorbance spectrum for the gallium(III) and PDA complex at 2.00×10^{-5} *M* is shown in Figure 23. A plot of the corrected absorbance values versus pH is shown in Figure 24 and a plot of the theoretical absorbance values calculated to determine the protonation constants of the complex is shown alongside the experimental data in Figure 25. From the selected wavelengths of 208, 236, 249, 263 and 286 nm, 4 successive pH-dependent equilibria were observed. The equilibria are described below at the pH at which they occurred.

$$Ga(PDA) + H^+ \leftrightarrows Ga(PDA)H^+ \qquad (pH = 1.57)$$

$$Ga(PDA) + OH^- \leftrightarrows Ga(PDA)OH^- \qquad (pH = 4.34)$$

$$Ga(PDA)(OH) + OH^- \leftrightarrows Ga(PDA)(OH)_2 \qquad (pH = 9.58)$$

$$Ga(PDA)(OH)_2 + 2\ OH^- \leftrightarrows [Ga(OH)_4]^- + PDA^{2-} \qquad (pH = 12.37)$$

Using log K_w = 13.78, the log K_1 [OH^-] of the Ga-PDA complex can be described as follows.

$$Ga(PDA) + OH^- \leftrightarrows Ga(PDA)OH^- \qquad (\log K_1\ [OH^-] = 9.44)$$

$$Ga(PDA)(OH) + OH^- \leftrightarrows Ga(PDA)(OH)_2 \qquad (\log K_2\ [OH^-] = 4.20)$$

$$Ga(PDA)(OH)_2 + 2\ OH^- \leftrightarrows [Ga(OH)_4]^- + PDA^{2-} \qquad (\log K_3K_4\ [OH^-] = 1.41)$$

The log β_4 [OH^-] for gallium(III) is 37.6 and from this value[15] a log K_1 for PDA with gallium(III) of 22.3 was calculated using Equation (5),

$$\log K_1 = 37.6 - (2\times(1.41) + 4.20 + 9.44) + 5.0 \qquad (5)$$

where the 5.0 takes into account the amount of free ligand at the isosbestic point. The reported formation constant for EDDA with gallium(III)[15] was 19.12, which was weaker when compared to the log K_1 for that of PDA with gallium(III). A Δ log K_1 of 3.18 between the log K_1 values of

PDA and EDDA with gallium(III) was calculated and showed a slight increase in stability of the PDA complex of gallium(III) relative to the EDDA complex of gallium(III).

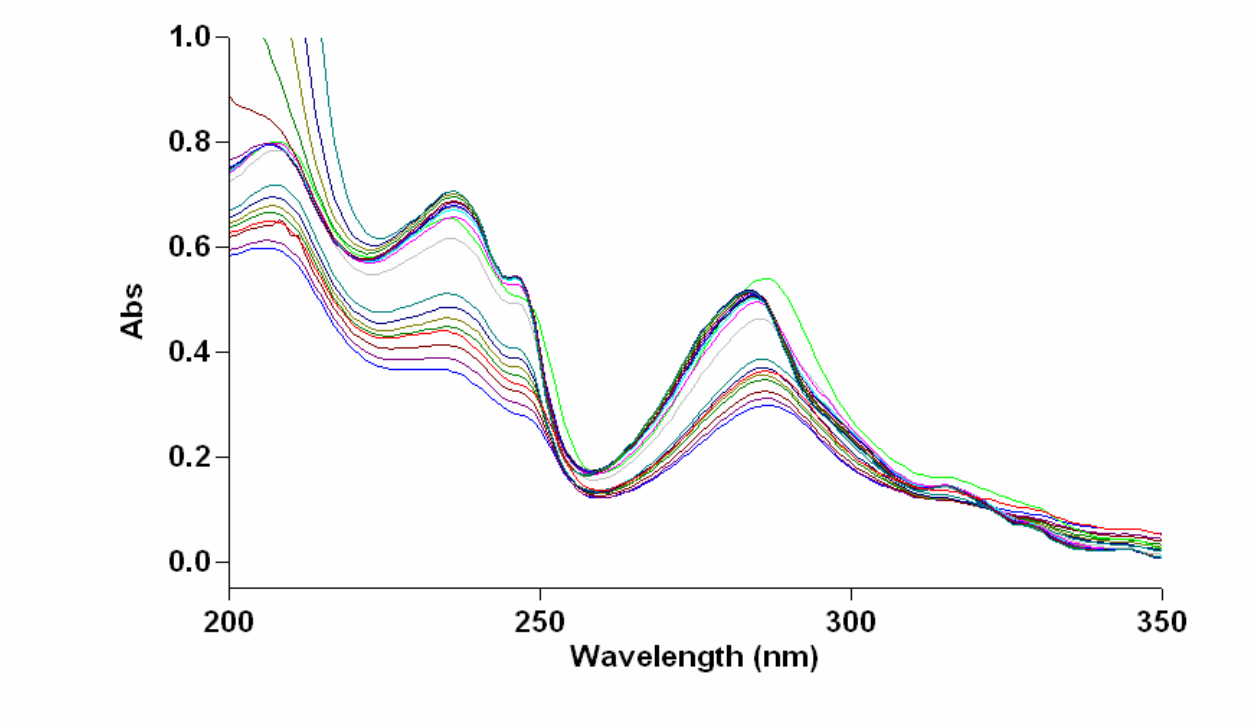

Figure 23. UV-Vis absorbance spectrum of the titration of gallium(III) and PDA at 2.00×10^{-5} *M*, in 0.10 *M* $NaClO_4$ at 25.0 ºC.

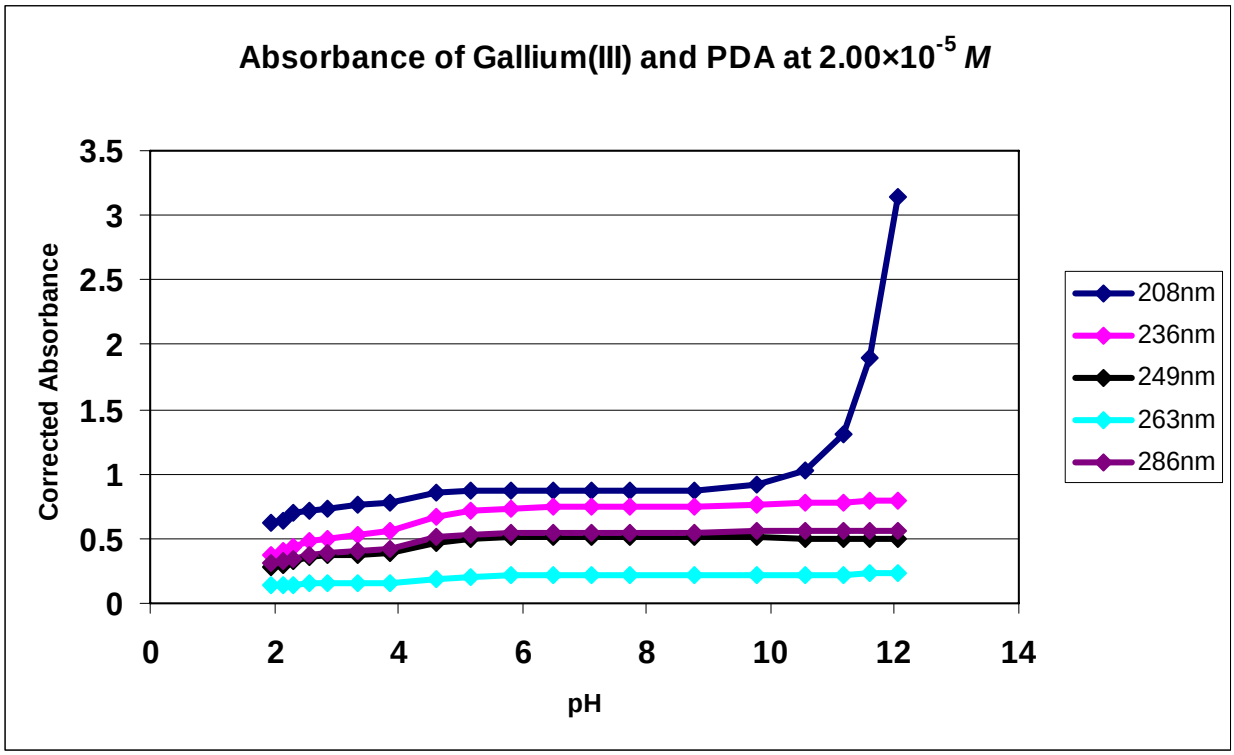

Figure 24. Plot of absorbance values corrected for dilution of the titration of gallium(III) and PDA at 2.00×10^{-5} *M*, in 0.10 *M* $NaClO_4$ at 25.0 ºC.

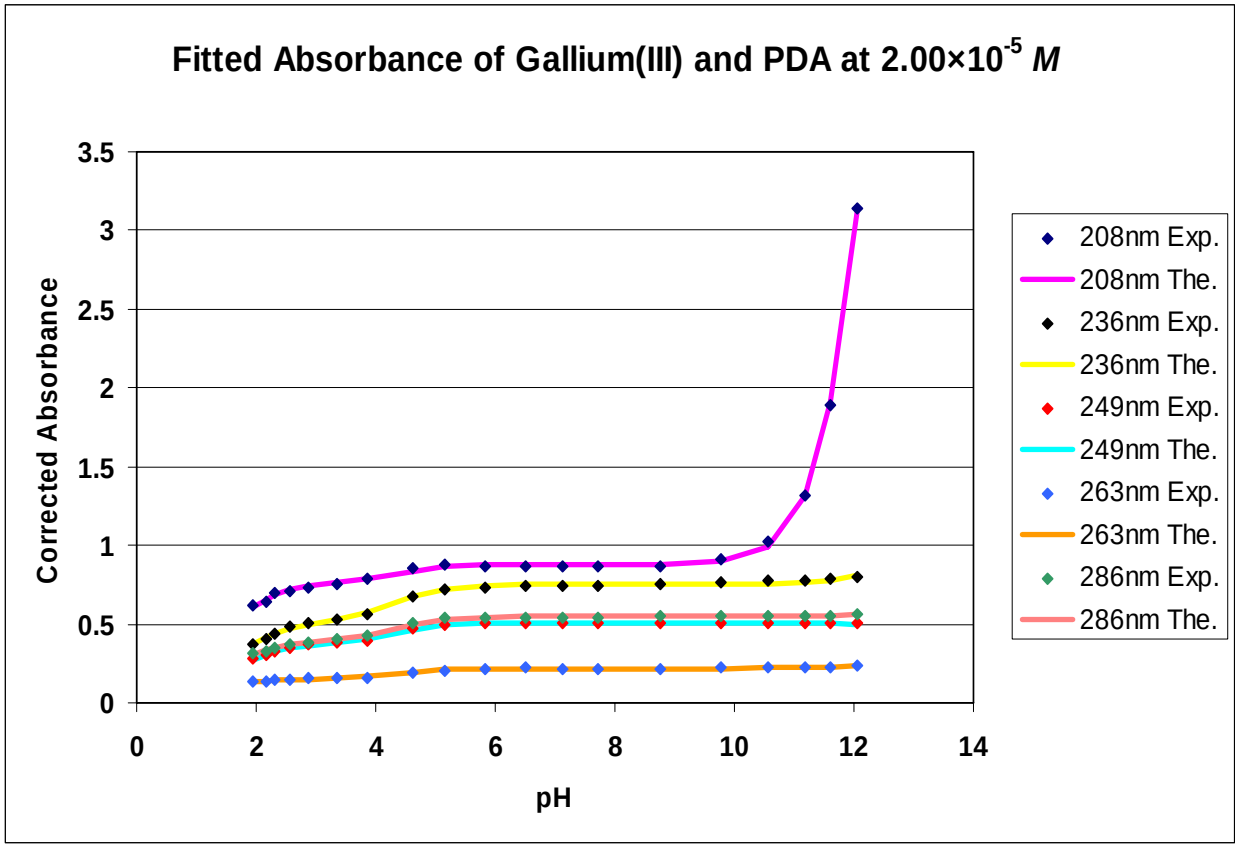

Figure 25. Experimental absorbance data (Exp.) fitted with calculated values (The.) to determine the protonation equilibria of the titration of gallium(III) and PDA at 2.00×10^{-5} *M*, in 0.10 *M* $NaClO_4$ at 25.0 ºC.

Indium(III)-PDA results

Indium(III) has an ionic radius of 0.80 Å which is slightly smaller than the ideal 1.0 Å favored by PDA. The UV absorbance spectrum for indium(III) and PDA complex at 2.00×10^{-5} *M* is shown in Figure 26. A plot of the corrected absorbance values versus pH is shown in Figure 27 and a plot of the theoretical absorbance values calculated to determine the protonation constants of the complex is shown alongside the experimental data in Figure 28. From the selected wavelengths of 236, 248, 259, 283 and 290 nm, 4 successive pH-dependent equilibria were observed. The equilibria are described below at the pH at which they occurred.

$$In(PDA) + H^+ \leftrightarrows In(PDA)H \qquad (pH = 2.61)$$

$$In(PDA) + OH^- \leftrightarrows In(PDA)OH \qquad (pH = 5.78)$$

$$In(PDA)(OH) + OH^- \leftrightarrows In(PDA)(OH)_2 \qquad (pH = 8.43)$$

$$In(PDA)(OH)_2 + 2\ OH^- \leftrightarrows [In(OH)_4]^- + PDA^{2-} \qquad (pH = 10.85)$$

Using log K_w = 13.78, the log K_1 [OH^-] of the In-PDA complex can be described as follows.

$$In(PDA) + OH^- \leftrightarrows In(PDA)OH \qquad (\log K_1\ [OH^-] = 8.00)$$

$$In(PDA)(OH) + OH^- \leftrightarrows In(PDA)(OH)_2 \qquad (\log K_2\ [OH^-] = 5.35)$$

$$In(PDA)(OH)_2 + 2\ OH^- \leftrightarrows [In(OH)_4]^- + PDA^{2-} \qquad (\log K_3K_4\ [OH^-] = 2.93)$$

The log β_4 [OH^-] for indium(III) is 33.9 and from this value[15] a log K_1 for PDA with indium(III) of 19.7 was calculated using Equation (6),

$$\log K_1 = 33.9–(2\times(2.93)+5.35+8.00)+5.0 \qquad (6)$$

where the 5.0 takes into account the amount of free ligand at the isosbestic point. There was no reported[15] formation constant for EDDA with indium(III).

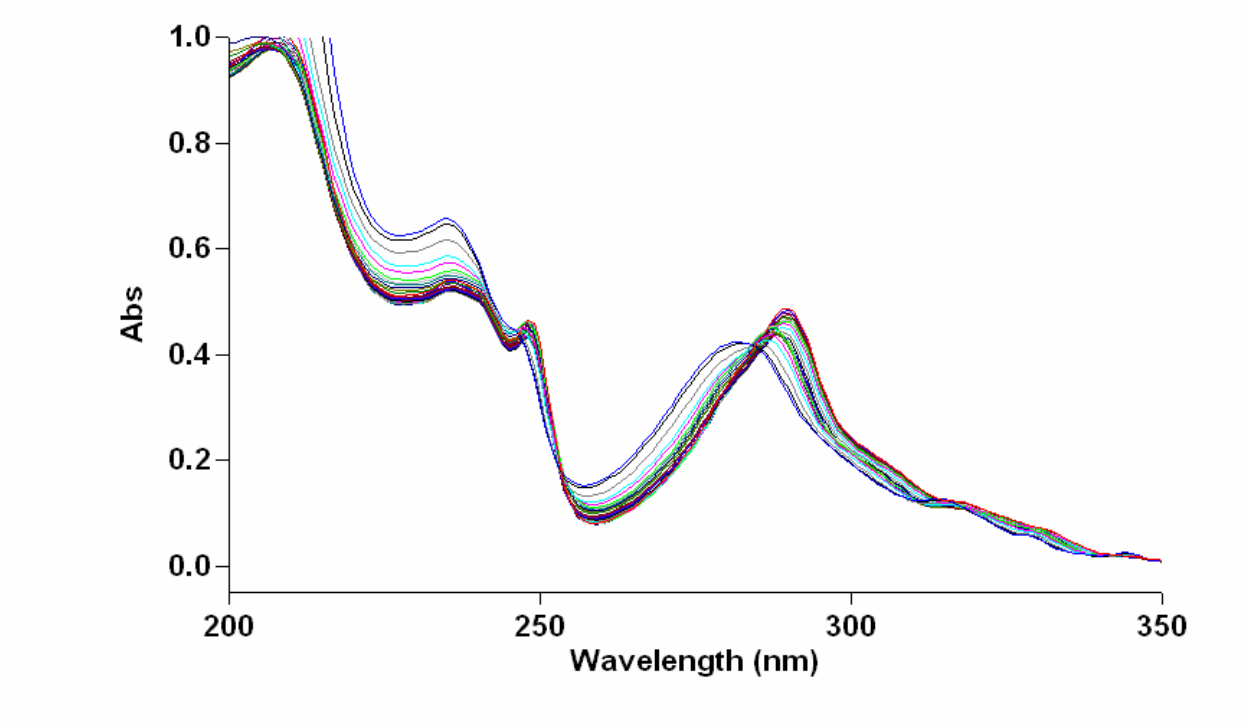

Figure 26. UV-Vis absorbance spectrum of the titration of indium(III) and PDA at 2.00×10^{-5} *M*, in 0.10 *M* $NaClO_4$ at 25.0 ºC.

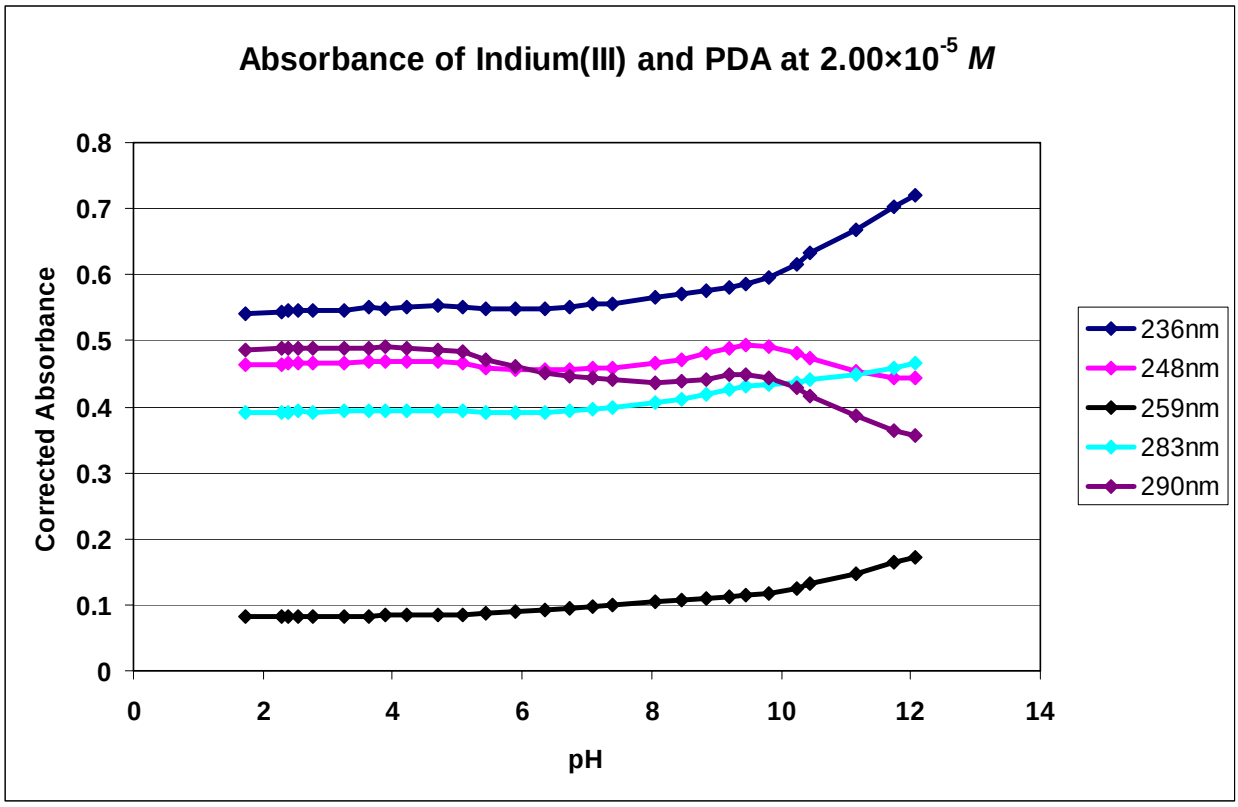

Figure 27. Plot of absorbance values corrected for dilution of the titration of indium(III) and PDA at 2.00×10^{-5} *M*, in 0.10 *M* $NaClO_4$ at 25.0 ºC.

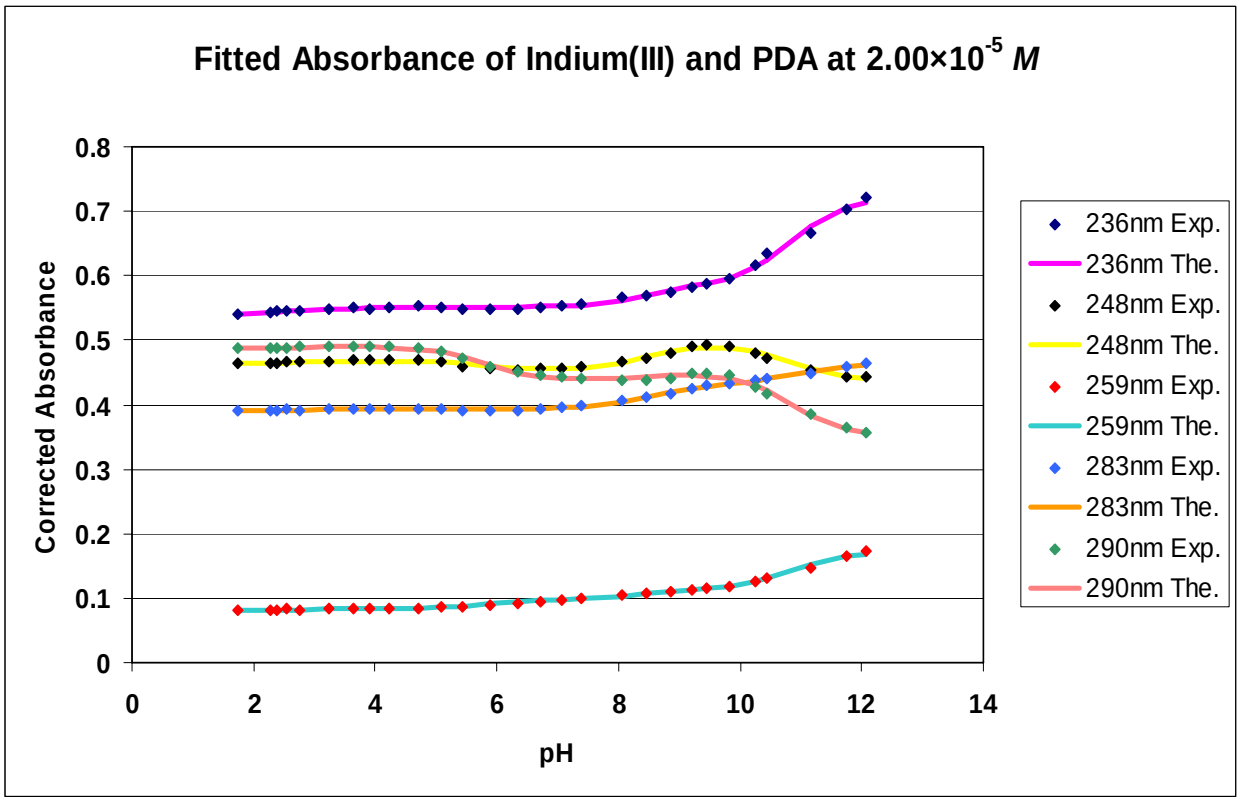

Figure 28. Experimental absorbance data (Exp.) fitted with calculated values (The.) to determine the protonation equilibria of the titration of indium(III) and PDA at 2.00×10^{-5} *M*, in 0.10 *M* $NaClO_4$ at 25.0 ºC.

Iron(III)-PDA results

Iron(III) has an ionic radius of 0.55 Å which is much smaller than the ideal 1.0 Å favored by PDA. Many titration experiments were performed with iron and PDA. The UV absorbance spectrum for iron(III) and PDA complex at 2.00×10^{-5} *M* is shown in Figure 29. A plot of the corrected absorbance values versus pH is shown in Figure 30 and a plot of the theoretical absorbance values calculated to determine the protonation constants of the complex is shown alongside the experimental data in Figure 31. From the selected wavelengths of 236, 249, 260, 270and 283 nm, 4 successive pH-dependent equilibria were observed. The equilibria are described below at the pH they occured.

$$Fe(PDA) + H^+ \leftrightarrows Fe(PDA)H \qquad (pH = 2.51)$$

$$Fe(PDA) + OH^- \leftrightarrows Fe(PDA)OH \qquad (pH = 6.37)$$

$$Fe(PDA)(OH) + OH^- \leftrightarrows Fe(PDA)(OH)_2 \qquad (pH = 8.24)$$

$$Fe(PDA)(OH)_2 + 2\ OH^- \leftrightarrows [Fe(OH)_4]^- + PDA^{2-} \qquad (pH = 10.48)$$

Using log K_w = 13.78, the log K_1 [OH^-] of the Fe-PDA complex can be described as follows.

$$Fe(PDA) + OH^- \leftrightarrows Fe(PDA)OH \qquad (\log K_1\ [OH^-]= 7.41)$$

$$Fe(PDA)(OH) + OH^- \leftrightarrows Fe(PDA)(OH)_2 \qquad (\log K_2\ [OH^-]= 5.54)$$

$$Fe(PDA)(OH)_2 + 2\ OH^- \leftrightarrows [Fe(OH)_4]^- + PDA^{2-} \qquad (\log K_3K_4\ [OH^-]= 3.30)$$

The log β_4 [OH^-] for iron(III) is 34.4 and from this value[15] a log K_1 for PDA with iron(III) of 19.85 was calculated using Equation (7),

$$\log K_1 = 34.4–(2\times(3.30)+5.54+7.41)+5.0 \qquad (7)$$

where the 5.0 takes into account the amount of free ligand at the isosbestic point. To further test the validity of this result other titrations were conducted with the competing ligand EDTA. The

UV absorbance spectrum for 1:1:1 iron(III), PDA and EDTA at 2.00×10^{-5} *M* is shown in Figure 32. A plot of the corrected absorbance values versus pH is shown in Figure 33 and a plot of the theoretical absorbance values calculated to determine the protonation constants of the complex is shown alongside the experimental data in Figure 34. The UV absorbance spectrum for 1:1:10 with iron(III) and PDA at 2.00×10^{-5} *M* and EDTA at 2.00×10^{-4} *M* is shown in Figure 35. A plot of the corrected absorbance values versus pH is shown in Figure 36 and a plot of the theoretical absorbance values calculated to determine the protonation constants of the complex is shown alongside the experimental data in Figure 37. The EDTA was unable to remove the iron from the PDA even at low pH and 10 fold excess. The free-ligand spectrum was only observed once the pH had risen to 9.5 in each scan showing that hydroxide was still the competing ligand responsible for the removal of the iron. There was no reported[15] formation constant for EDDA with iron(III).

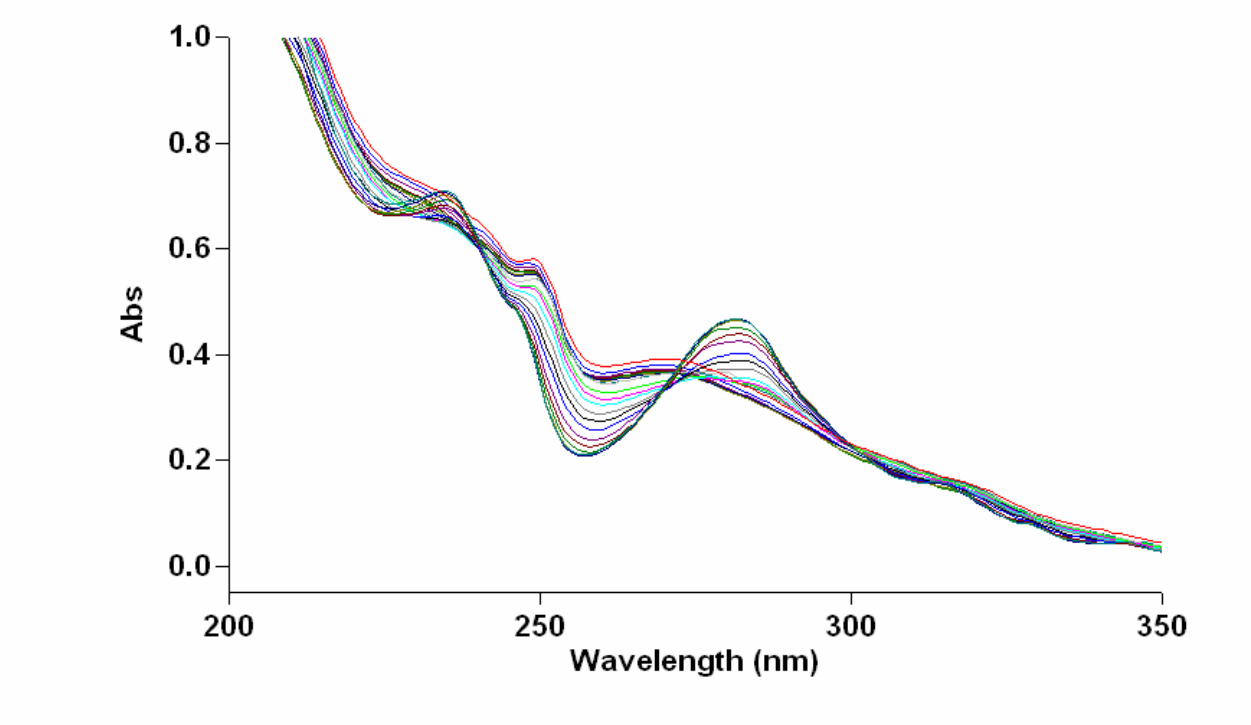

Figure 29. UV-Vis absorbance spectrum of the titration of iron(III) and PDA at 2.00×10^{-5} *M*, in 0.10 *M* $NaClO_4$ at 25.0 ºC.

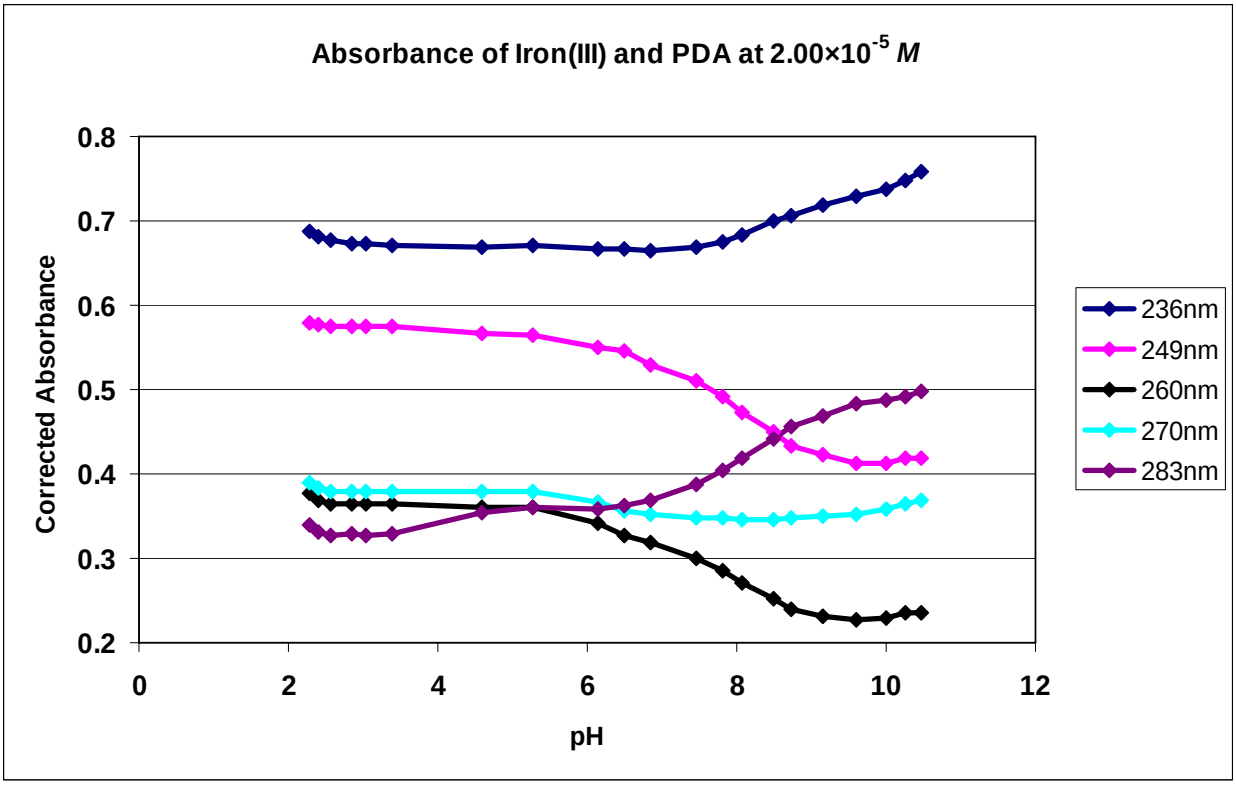

Figure 30. Plot of absorbance values corrected for dilution of the titration of iron(III) and PDA at 2.00×10^{-5} *M*, in 0.10 *M* $NaClO_4$ at 25.0 ºC.

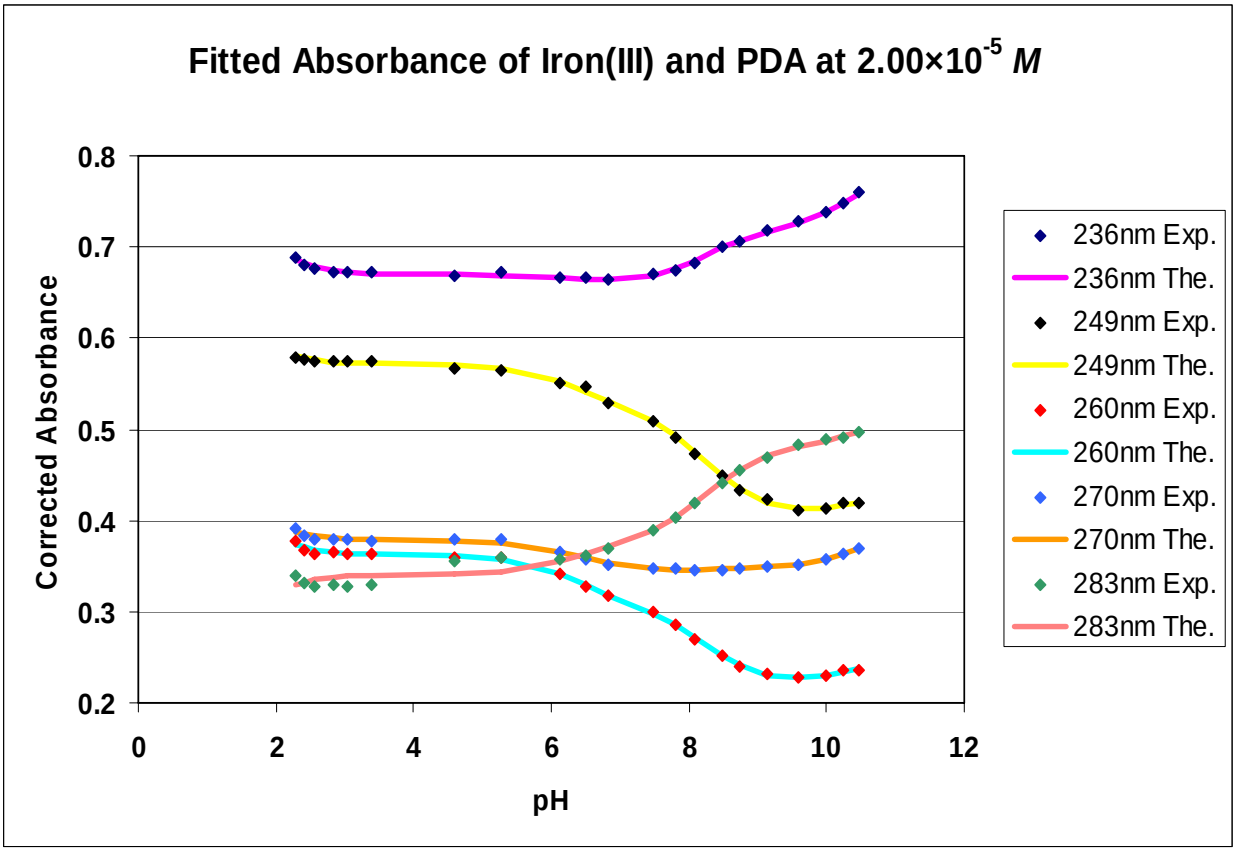

Figure 31. Experimental absorbance data (Exp.) fitted with calculated values (The.) to determine the protonation equilibria of the titration of iron(III) and PDA at 2.00×10^{-5} *M*, in 0.10 *M* $NaClO_4$ at 25.0 ºC.

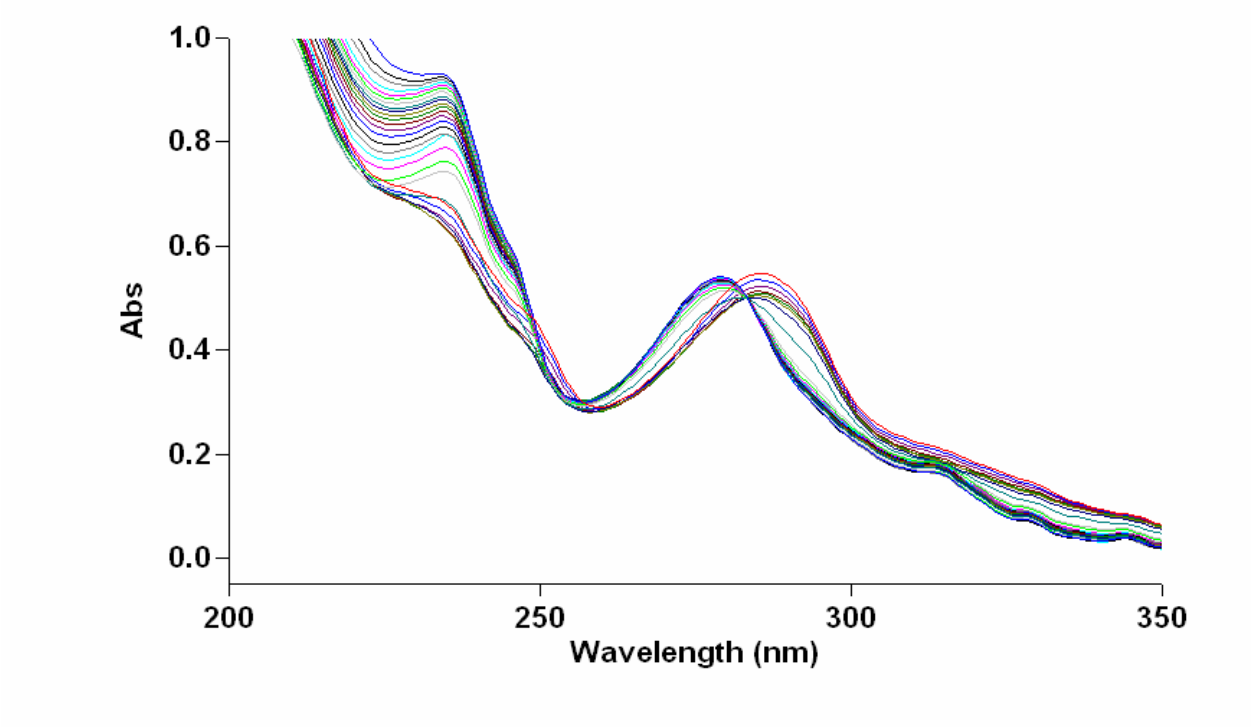

Figure 32. UV-Vis absorbance spectrum of the titration of 1:1:1 iron(III), PDA and EDTA at 2.00×10^{-5} *M*, in 0.10 *M* $NaClO_4$ at 25.0 ºC.

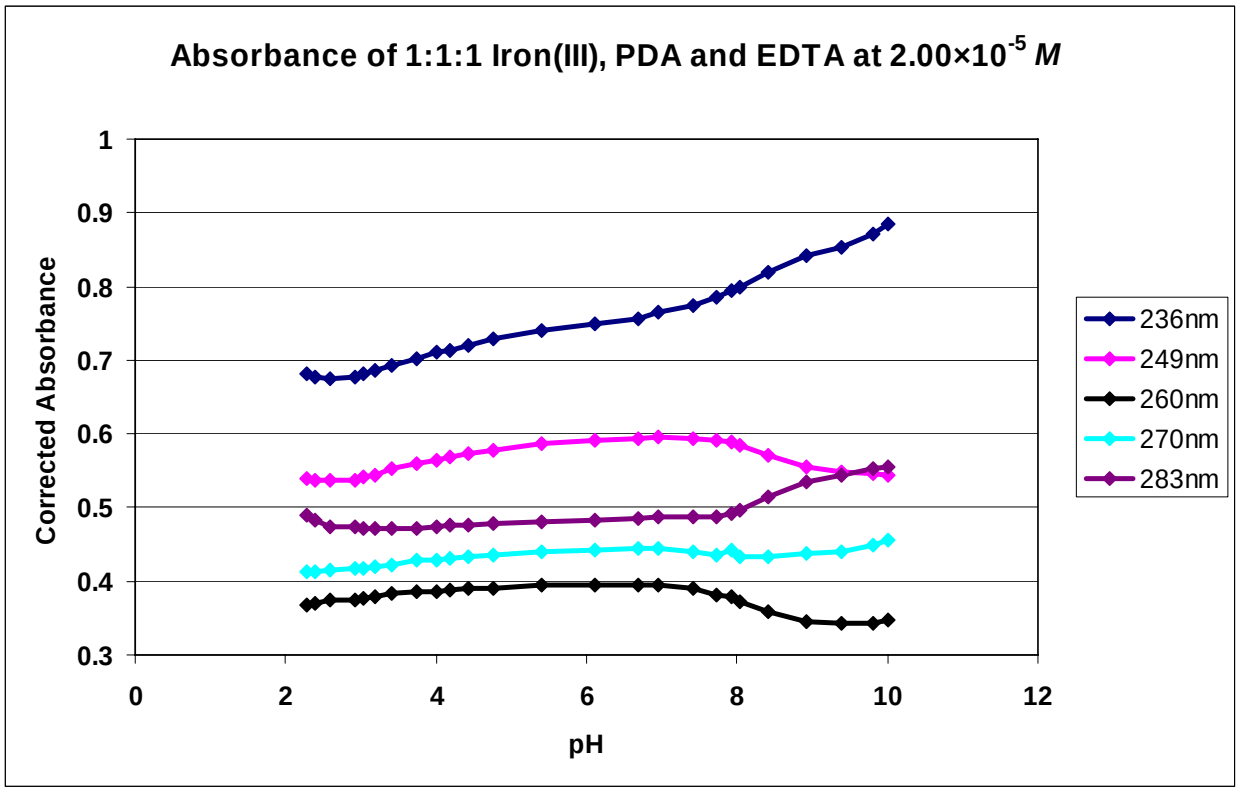

Figure 33. Plot of absorbance values corrected for dilution of the titration of 1:1:1 iron(III), PDA and EDTA at 2.00×10^{-5} *M*, in 0.10 *M* $NaClO_4$ at 25.0 ºC.

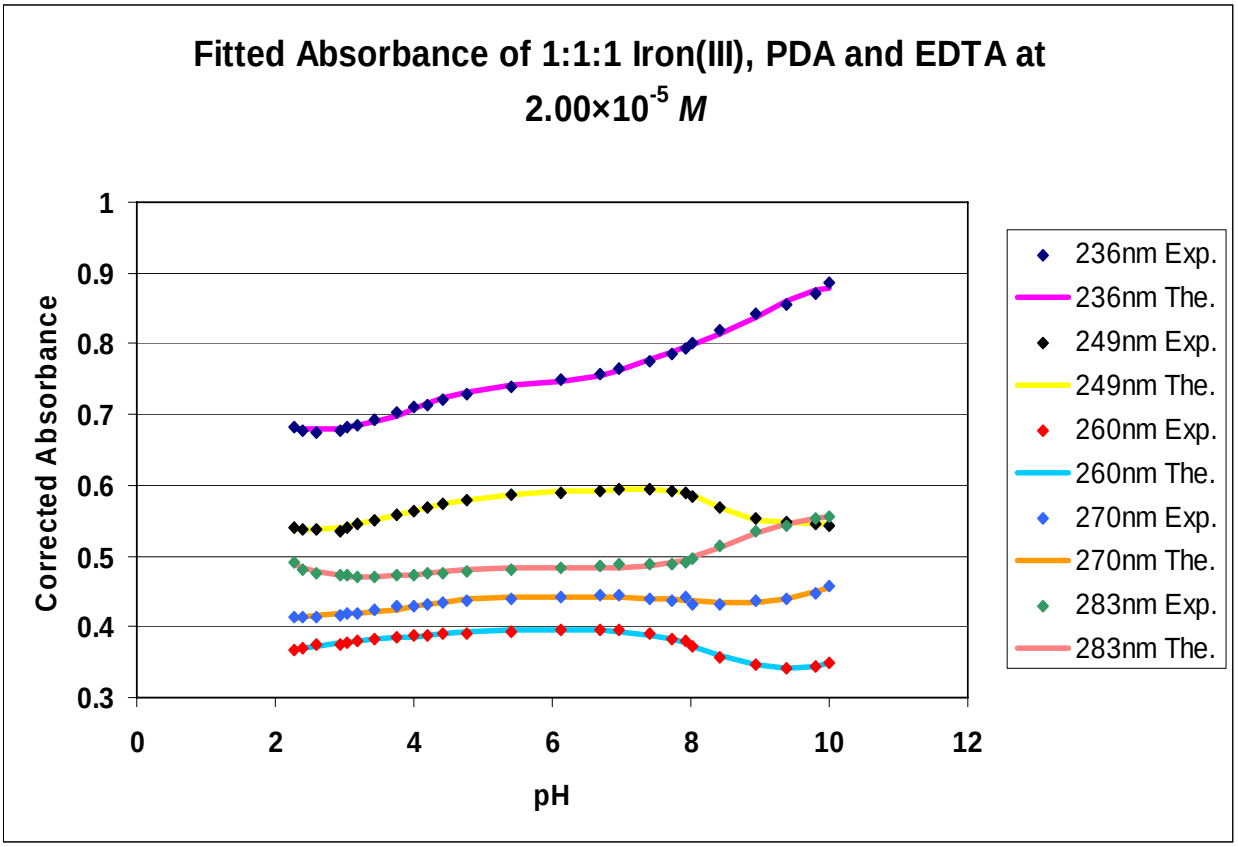

Figure 34. Experimental absorbance data (Exp.) fitted with calculated values (The.) to determine the protonation equilibria of the titration of 1:1:1 iron(III), PDA and EDTA at 2.00×10^{-5} *M*, in 0.10 *M* $NaClO_4$ at 25.0 ºC.

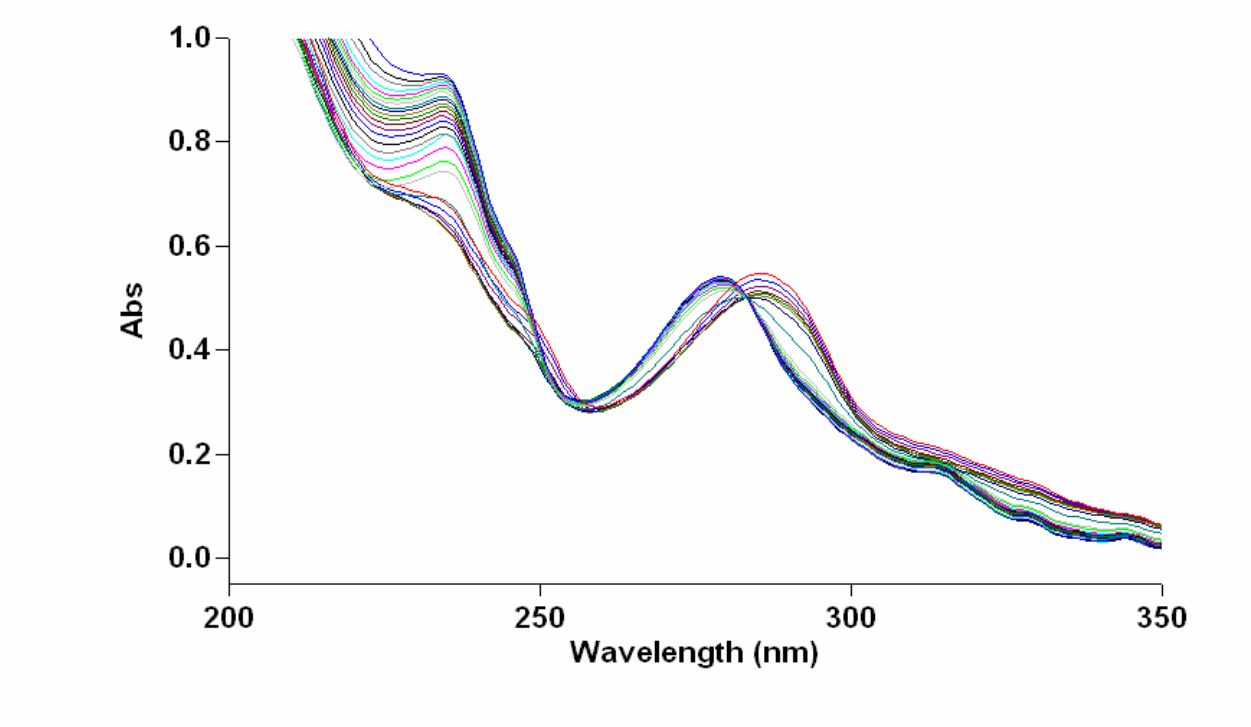

Figure 35. UV-Vis absorbance spectrum of the titration of 1:1:10 iron(III), PDA and EDTA with iron(III) and PDA at 2.00×10^{-5} *M* and EDTA at 2.00×10^{-4} *M*, in 0.10 *M* $NaClO_4$ at 25.0 ºC.

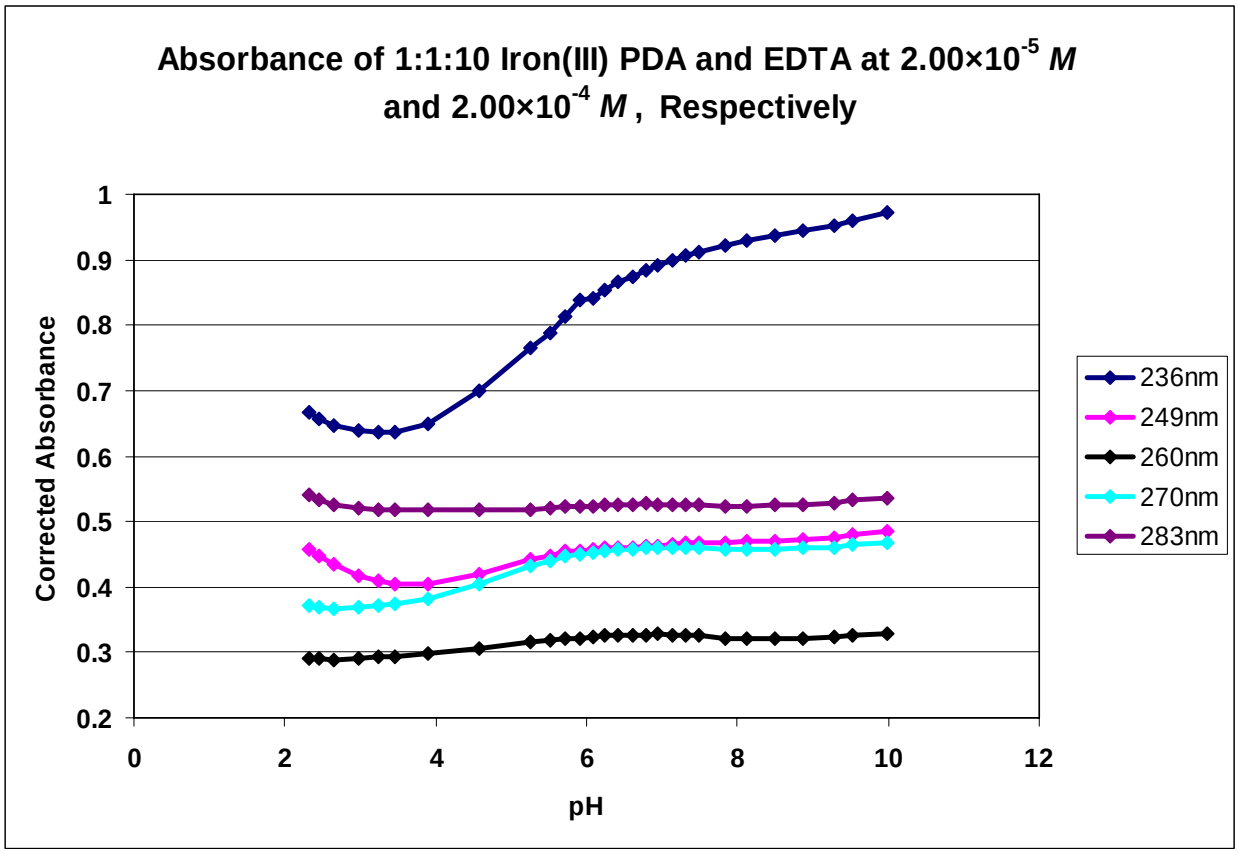

Figure 36. Plot of absorbance values corrected for dilution of the titration of 1:1:10 iron(III), PDA and EDTA with iron(III) and PDA at 2.00×10^{-5} *M* and EDTA at 2.00×10^{-4} *M*, in 0.10 *M* $NaClO_4$ at 25.0 ºC.

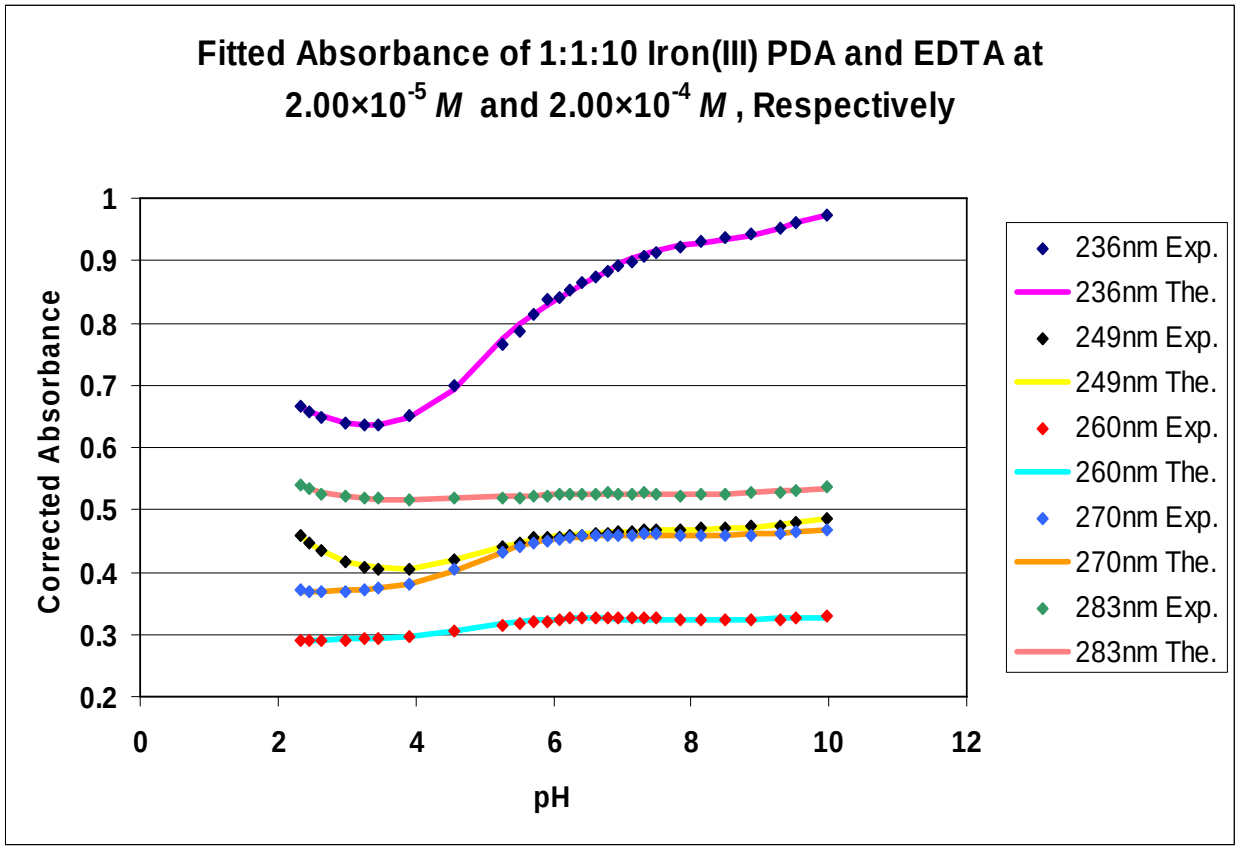

Figure 37. Experimental absorbance data (Exp.) fitted with calculated values (The.) to determine the protonation equilibria of the titration of 1:1:10 iron(III), PDA and EDTA with iron(III) and PDA at 2.00×10^{-5} *M* and EDTA at 2.00×10^{-4} *M*, in 0.10 *M* $NaClO_4$ at 25.0 ºC.

Lutetium(III)-PDA results

Lutetium(III) has an ionic radius of 0.86 Å which is slightly smaller than the ideal 1.0 Å favored by PDA. The UV absorbance spectrum for lutetium(III) and PDA at 2.00×10^{-5} *M* is shown in Figure 38. A plot of the corrected absorbance values versus pH is shown in Figure 39 and a plot of the theoretical absorbance values calculated to determine the protonation constants of the complex is shown alongside the experimental data in Figure 40. From the selected wavelengths of 233, 250, 263, 280 and 294 nm, 3 successive pH-dependent equilibria were observed. The equilibria are described below at the pH at which they occurred.

$$Lu(PDA) + OH^- \leftrightarrows Lu(PDA)OH \qquad (pH = 6.26)$$

$$Lu(PDA)(OH) + OH^- \leftrightarrows Lu(PDA)(OH)_2 \qquad (pH = 9.67)$$

$$Lu(PDA)(OH)_2 + 2\ OH^- \leftrightarrows [Lu(OH)_4]^- + PDA \qquad (pH = 11.07)$$

Figure 12(b) shows a species distribution diagram for these protonation equilibria. Using log K_w = 13.78, the log K_1 [OH^-] of the Lu-PDA complex can be described as follows.

$$Lu(PDA) + OH^- \leftrightarrows Lu(PDA)OH \qquad (\log K_1\,[OH^-] = 7.52)$$

$$Lu(PDA)(OH) + OH^- \leftrightarrows Lu(PDA)(OH)_2 \qquad (\log K_2\,[OH^-] = 4.11)$$

$$Lu(PDA)(OH)_2 + 2\ OH^- \leftrightarrows [Lu(OH)_4]^- + PDA \qquad (\log K_3K_4\,[OH^-] = 2.71)$$

The log β_4 [OH^-] for indium(III) is 31.65 and from this value[15] a log K_1 for PDA with lutetium(III) of 19.6 was calculated using Equation (8),

$$\log K_1 = 31.65–(2\times(2.71)+4.11+7.52)+5.0 \qquad (8)$$

where the 5.0 takes into account the amount of free ligand at the isosbestic point. The reported[15] formation constant for EDDA with lutetium(III) was 9.09, which was weaker when compared to the log K_1 for that of PDA with lutetium(III). A Δ log K_1 of 10.3 between the log K_1 values of

PDA and EDDA with lutetium(III) was calculated and showed a large increase in stability of the PDA complex of lutetium(III) relative to the EDDA complex of lutetium(III).

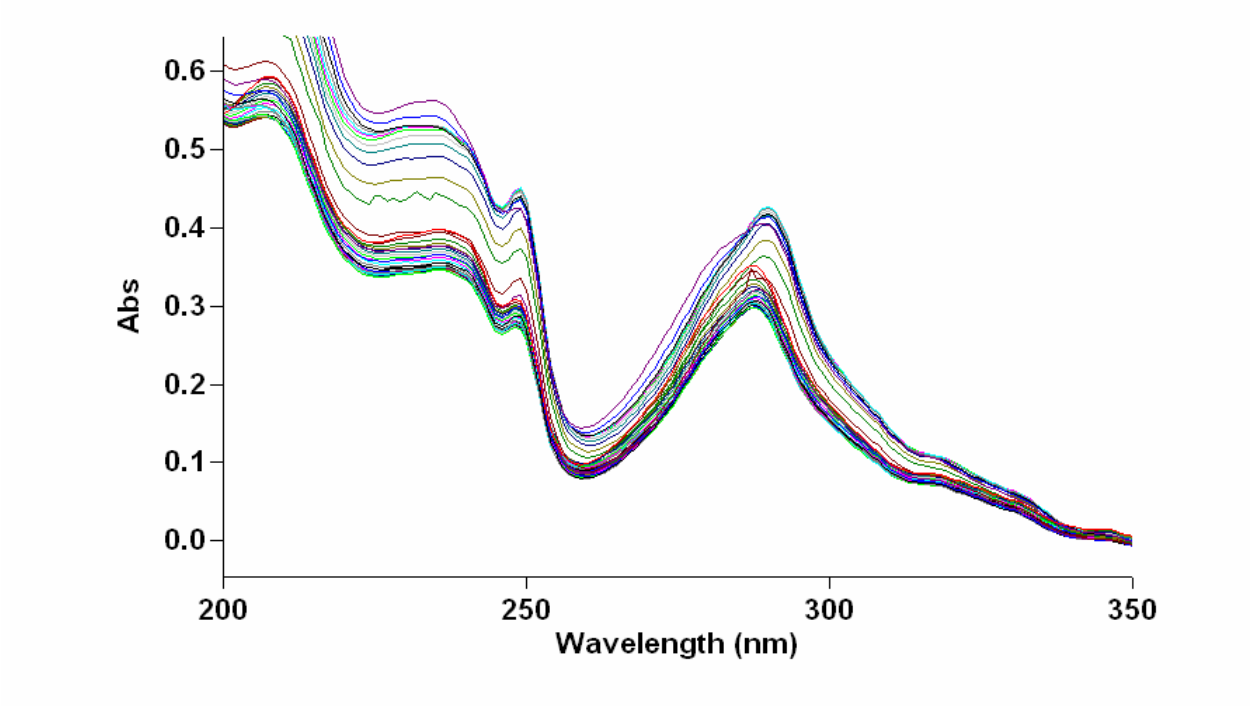

Figure 38. UV-Vis absorbance spectrum of the titration of lutetium(III) and PDA at 2.00×10^{-5} *M*, in 0.10 *M* $NaClO_4$ at 25.0 ºC.

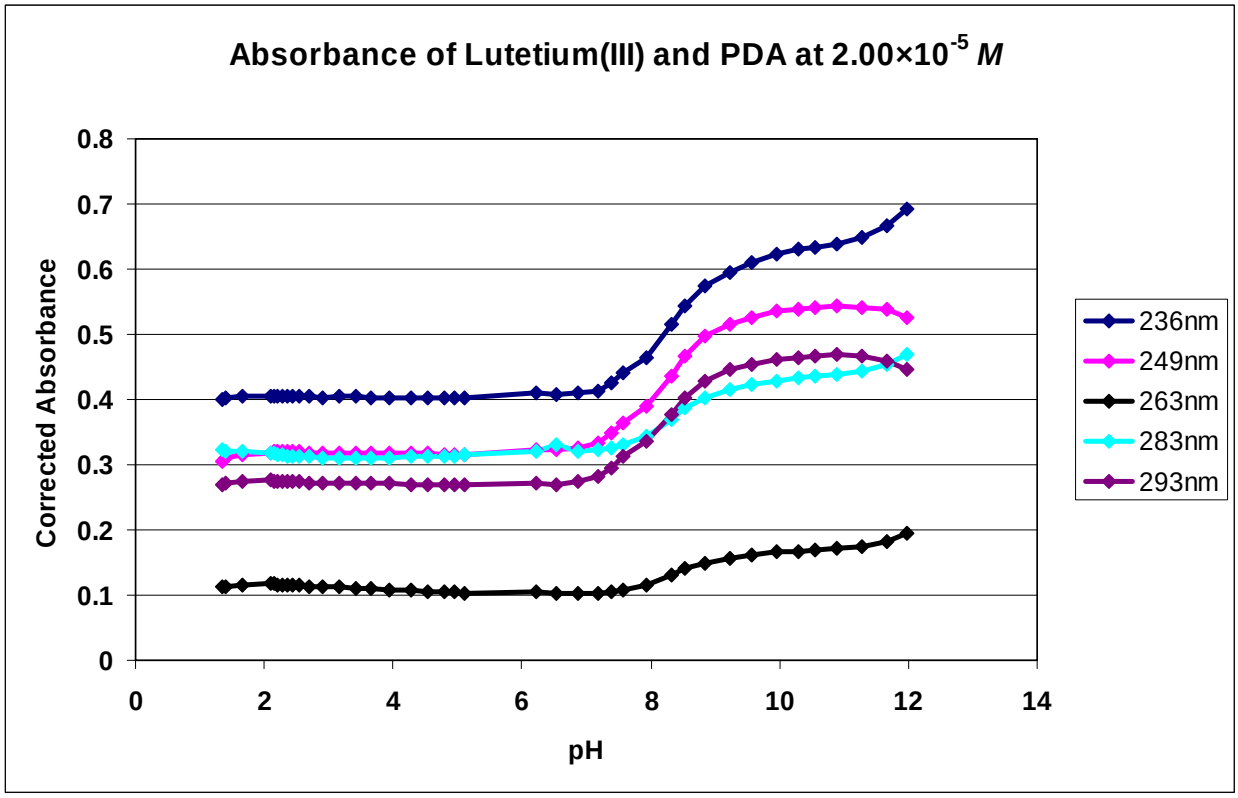

Figure 39. Plot of absorbance values corrected for dilution of the titration of lutetium(III) and PDA at 2.00×10^{-5} *M*, in 0.10 *M* $NaClO_4$ at 25.0 ºC.

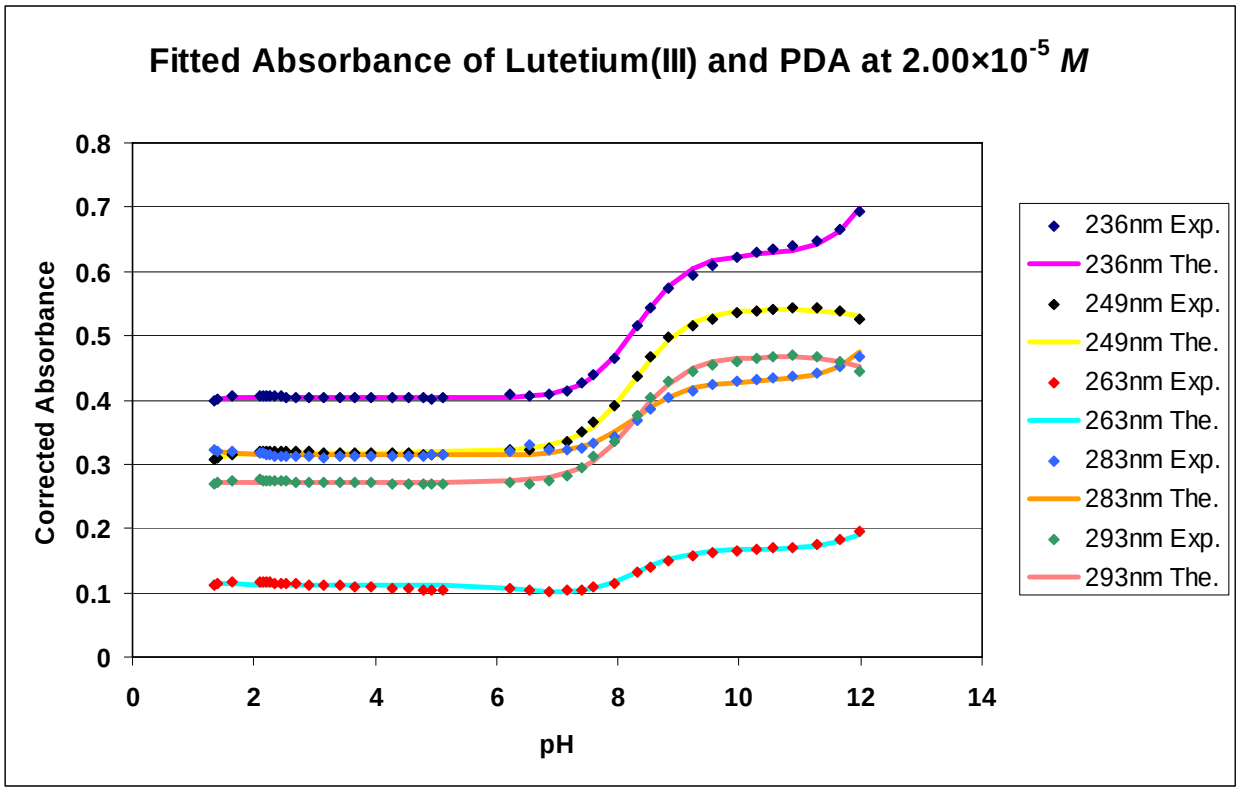

Figure 40. Experimental absorbance data (Exp.) fitted with calculated values (The.) to determine the protonation equilibria of the titration of lutetium(III) and PDA at 2.00×10^{-5} *M*, in 0.10 *M* $NaClO_4$ at 25.0 ºC.

Manganese(II)-PDA results

Manganese(II) has an ionic radius of 0.74 Å which is smaller than the ideal 1.0 Å favored by PDA. The UV absorbance spectrum for manganese(II) and PDA at 2.00×10^{-5} *M* is shown in Figure 41. A plot of the corrected absorbance values versus pH is shown in Figure 42 and a plot of the theoretical absorbance values calculated to determine the protonation constants of the complex is shown alongside the experimental data in Figure 43. This data does not appear as expected for such a small metal ion of low charge. It is hypothesized that the negative oxygen donors on the carboxylate groups of PDA had oxidized the manganese(II) metal ion into manganese(III), which prevents analysis of the manganese data attained. Additional titrations and crystallography would have to be done to determine whether this hypothesis is correct.

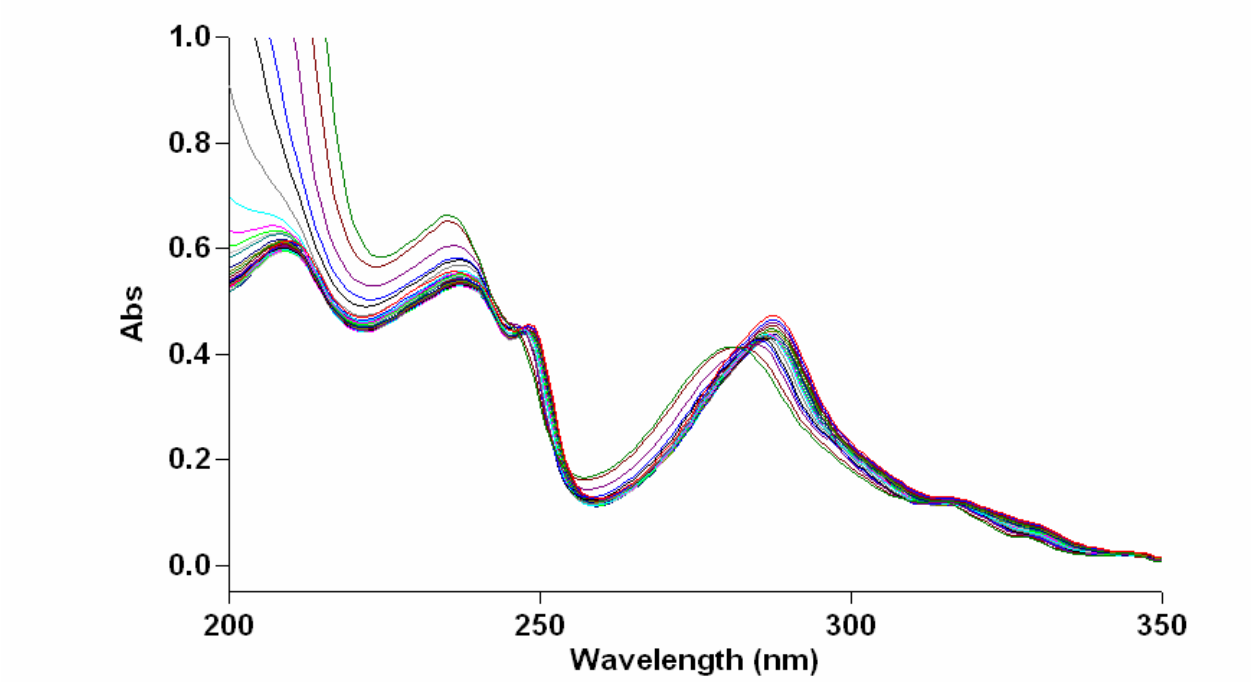

Figure 41. UV-Vis absorbance spectrum of the titration of manganese(II) and PDA at 2.00×10^{-5} *M*, in 0.10 *M* $NaClO_4$ at 25.0 ºC.

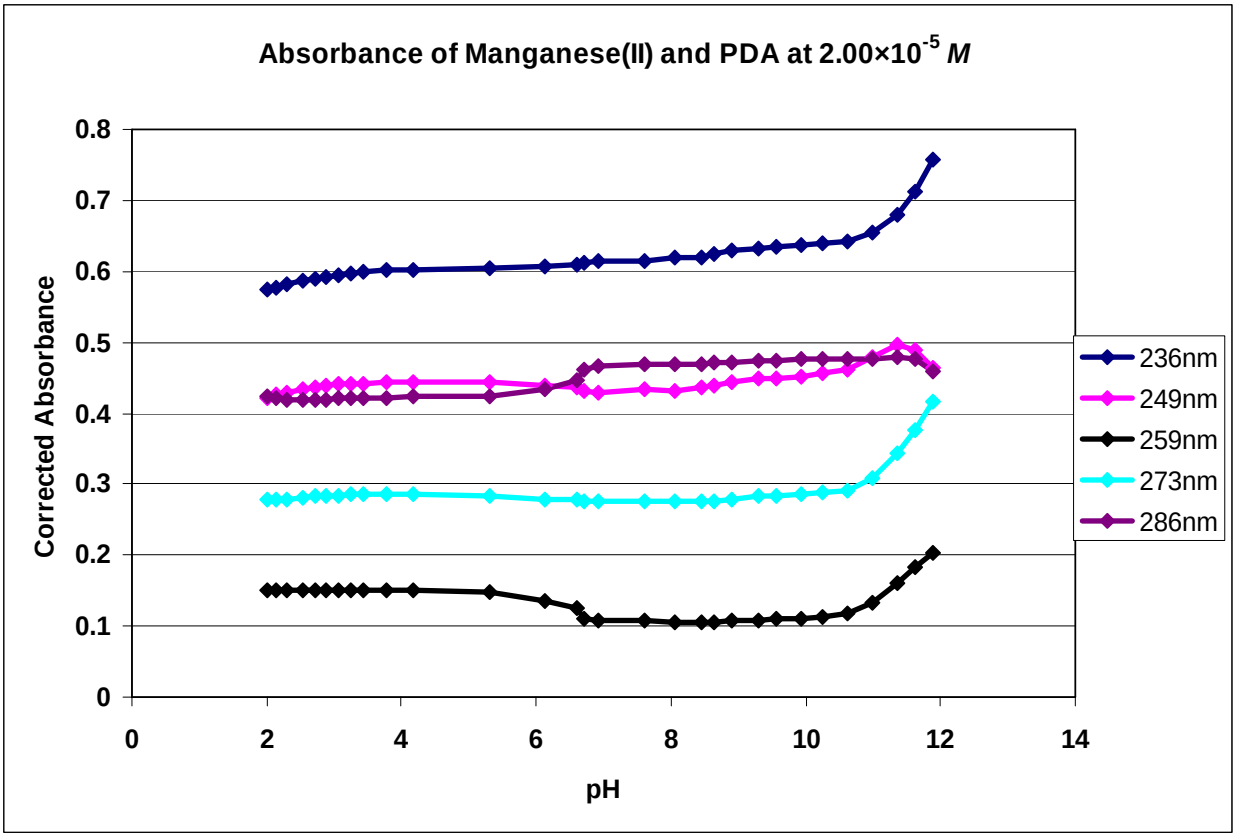

Figure 42. Plot of absorbance values corrected for dilution of the titration of manganese(II) and PDA at 2.00×10^{-5} *M*, in 0.10 *M* $NaClO_4$ at 25.0 ºC..

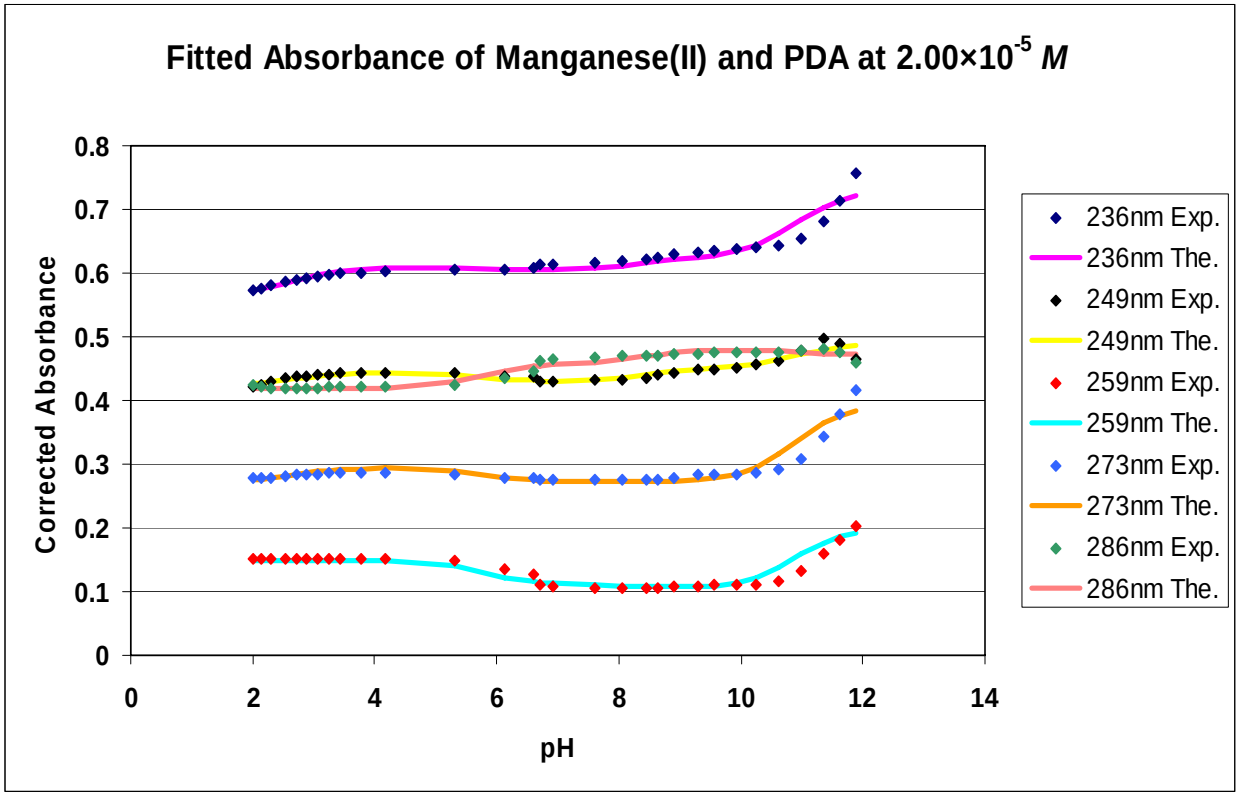

Figure 43. Experimental absorbance data (Exp.) fitted with calculated values (The.) to determine the protonation equilibria of the titration of manganese(II) and PDA at 2.00×10^{-5} *M*, in 0.10 *M* $NaClO_4$ at 25.0 ºC.

Thorium(IV)-PDA results

Thorium(IV) has an ionic radius of 0.94 Å which is very similar to the ideal 1.0 Å favored by PDA. Many titration experiments were performed with thorium and PDA. The UV absorbance spectrum for thorium(IV) and PDA complex at 2.00×10^{-5} *M* is shown in Figure 44. A plot of the corrected absorbance values versus pH is shown in Figure 45 and a plot of the theoretical absorbance values calculated to determine the protonation constants of the complex is shown alongside the experimental data in Figure 46. From the selected wavelengths of 236, 249, 260, 270and 283 nm, 5 successive pH-dependent equilibria were observed. The equilibria are described below at the pH they occured.

$$Th(PDA) + H^{+} \leftrightarrows Th(PDA)H \qquad (pH = 2.12)$$

$$Th(PDA) + OH^{-} \leftrightarrows Th(PDA)OH \qquad (pH = 4.52)$$

$$Th\,(PDA)(OH) + OH^{-} \leftrightarrows Th\,(PDA)(OH)_2 \qquad (pH = 8.39)$$

$$Th\,(PDA)(OH)_2 + OH^{-} \leftrightarrows Th\,(PDA)(OH)_3 \qquad (pH = 10.35)$$

$$Th\,(PDA)(OH)_3 + OH^{-} \leftrightarrows Th\,(OH)_4 + PDA^{2-} \qquad (pH = 12.60)$$

Using log K_w = 13.78, the log K_1 [OH^-] of the Th-PDA complex can be described as follows.

$$Th\,(PDA) + OH^{-} \leftrightarrows Th\,(PDA)OH \qquad (\log K_1\,[OH^-] = 9.26)$$

$$Th\,(PDA)(OH) + OH^{-} \leftrightarrows Th\,(PDA)(OH)_2 \qquad (\log K_2\,[OH^-] = 5.39)$$

$$Th\,(PDA)(OH)_2 + OH^{-} \leftrightarrows Th\,(PDA)(OH)_3 \qquad (\log K_3\,[OH^-] = 3.43)$$

$$Th\,(PDA)(OH)_3 + OH^{-} \leftrightarrows Th\,(OH)_4 + PDA^{2-} \qquad (\log K_4\,[OH^-] = 1.18)$$

The log β_4 [OH^-] for thorium(IV) is 40.2 and from this value[15] a log K_1 for PDA with thorium(IV) of 25.9 was calculated using Equation (9),

$$\log K_1 = 40.2–(1.18+3.43+5.39+9.26)+5.0 \qquad (9)$$

where the 5.0 takes into account the amount of free ligand at the isosbestic point. To further test the validity of this result, additional titration experiments were performed. The UV absorbance spectrum for thorium(IV) and PDA complex at 4.00×10^{-6} *M* is shown in Figure 47. A plot of the correlation between E (mV) and the calculated pH, which was used to calculate E^0, is shown in Figure 48. A plot of the corrected absorbance values versus pH is shown in Figure 49 and a plot of the theoretical absorbance values calculated to determine the protonation equilibriam of the complex is shown alongside the experimental data in Figure 50. This titration was done in order to prove that a 10 fold dilution would not effect the isosbestic points of the thorium(IV)-PDA complex significantly proving that the complex did not form any dimers. The UV absorbance spectrum for 2:1 PDA and thorium(IV) with PDA at 4.00×10^{-5} *M* and thorium(IV) at 2.00×10^{-5} *M* is shown in Figure 51. A plot of the corrected absorbance values versus pH is shown in Figure 52 and a plot of the theoretical absorbance values calculated to determine the protonation equilibria of the complex is shown alongside the experimental data in Figure 53. This titration was done because there was crystallographic evidence that thorium(IV) would coordinate to 2 PDA molecules. This scan showed that should this be the case, the isosbestic points did not change significantly. The UV absorbance spectrum for 1:1:1 thorium(IV), PDA and DTPA at 2.00×10^{-5} *M* is shown in Figure 54. A plot of the corrected absorbance values versus pH is shown in Figure 55 and a plot of the theoretical absorbance values calculated to determine the protonation equilibria of the complex is shown alongside the experimental data in Figure 56. The UV absorbance spectrum for 1:1:10 with thorium(IV) and PDA at 2.00×10^{-5} *M* and DTPA at 2.00×10^{-4} *M* is shown in Figure 57. A plot of the corrected absorbance values versus pH is shown in Figure 58 and a plot of the theoretical absorbance values calculated to determine the protonation equilibria of the complex is shown alongside the experimental data in Figure 59.

The UV absorbance spectrum for 1:1:100 with thorium(IV) and PDA at 2.00×10^{-5} *M* and DTPA at 2.00×10^{-3} *M* is shown in Figure 60. A plot of the corrected absorbance values versus pH is shown in Figure 61 and a plot of the theoretical absorbance values calculated to determine the protonation equilibria of the complex is shown alongside the experimental data in Figure 62. These scans were done in an attempt to find a competing ligand to remove the thorium(IV) from PDA at low pH. The DTPA was unable to remove the thorium from the PDA even at 100 fold excess. The free-ligand spectrum was only generated once the pH had risen to 8.5 in each scan showing that hydroxide was still the competing ligand responsible for the removal of the thorium. The UV absorbance spectrum for 1:1:10 thorium(IV), PDA and TTHA with thorium(IV) and PDA at 2.00×10^{-5} *M* and TTHA at 2.00×10^{-4} *M* is shown in Figure 63. A plot of the corrected absorbance values versus pH is shown in Figure 64 and a plot of the theoretical absorbance values calculated to determine the protonation equilibria of the complex is shown alongside the experimental data in Figure 65. The TTHA was also unable to remove the thorium from the PDA even at low pH and 100 fold excess. The free-ligand spectrum was only observed once the pH had risen to 9.5 showing that hydroxide was still the competing ligand responsible for the removal of the thorium. As a large metal ion absorbance band is seen between 200 and 250 nm in all of the titration involving thorium, a titration was done of thorium(IV) and DTPA at 2.00×10^{-5} *M* to show the absorbance of the metal ion without PDA. This plot is shown in Figure 66. The reported formation constant for EDDA with thorium(IV) was 13.9, estimated from log $K = 6.54$[17] for $Th^{4+} + LH^{-} \leftrightarrows ThLH^{3+}$ (L = EDDA) by combining with a typical value[15] of log $K = 2.2$ for $ML + H^{+} \leftrightarrows MLH^{+}$ for aminocarboxylate ligands. This value was drastically weaker when compared to the log K_1 for that of PDA with thorium(IV). A Δ log K_1 of 12.04 between the log K_1 values of PDA and EDDA with thorium(IV) was calculated and showed a drastic

increase in stability of the PDA complex of thorium(IV) relative to the EDDA complex of thorium(IV).

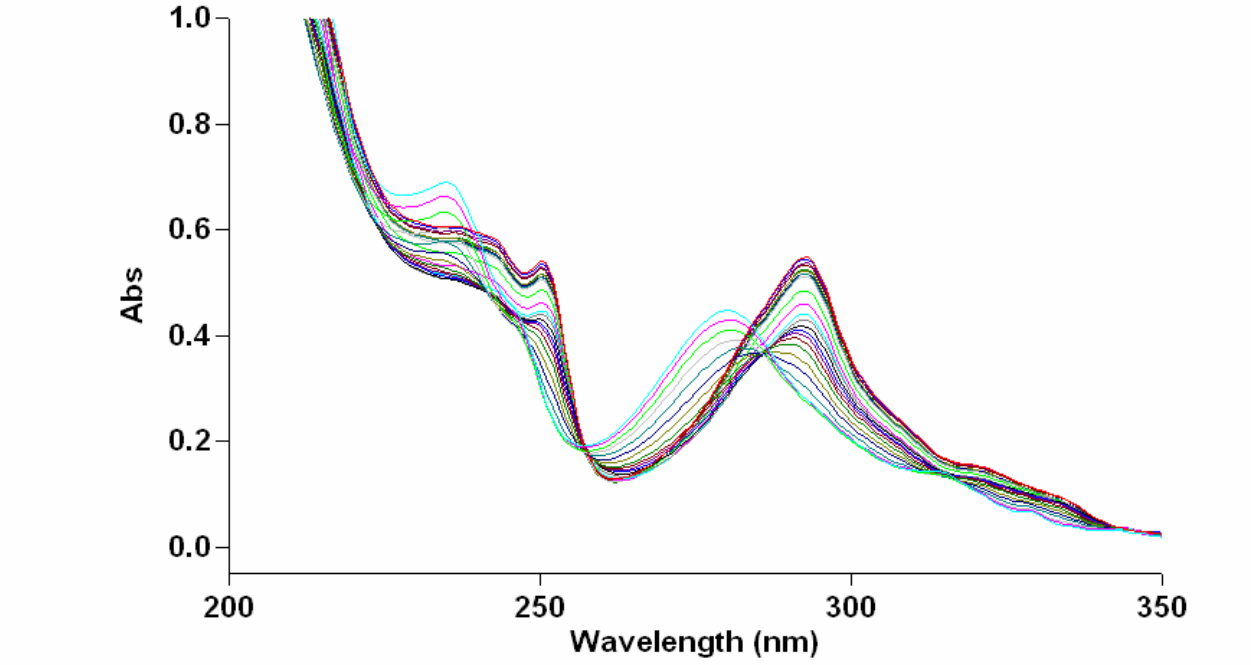

Figure 44. UV-Vis absorbance spectrum of the titration of thorium(IV) and PDA at 2.00×10^{-5} *M*, in 0.10 *M* $NaClO_4$ at 25.0 ºC.

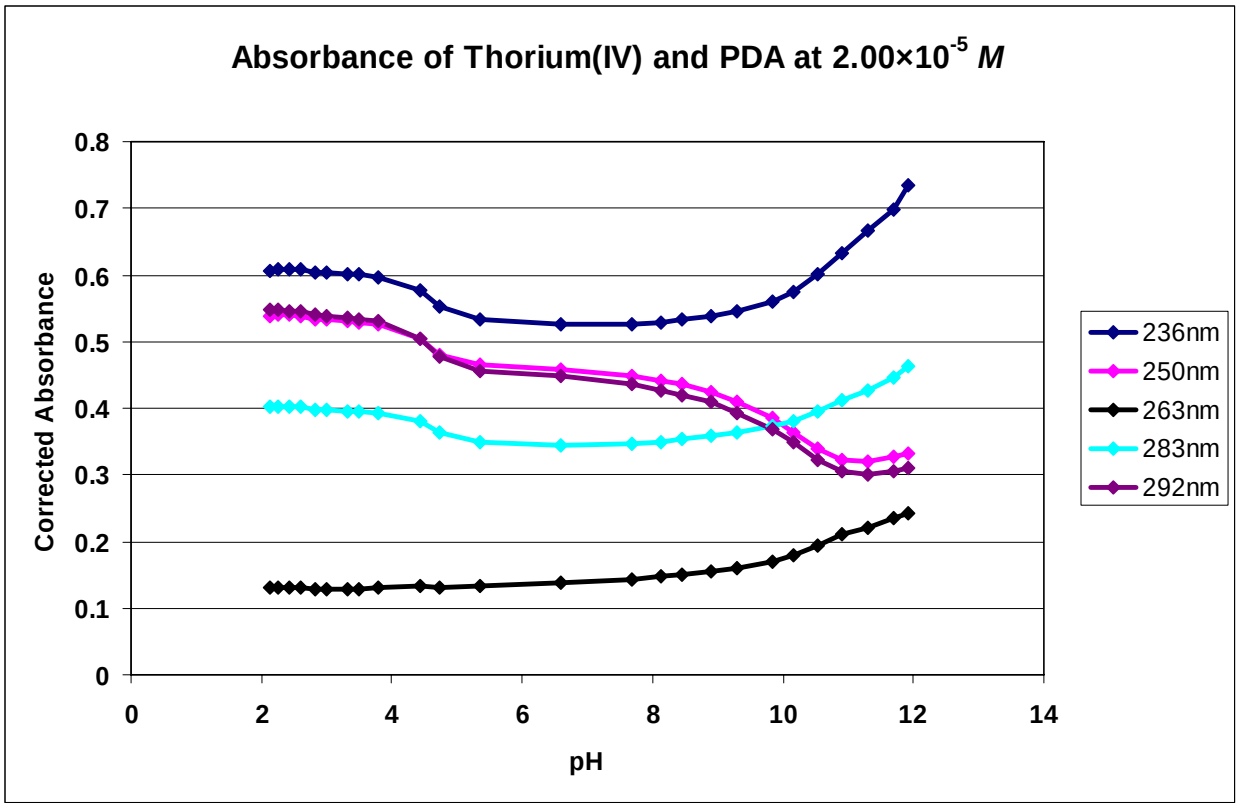

Figure 45. Plot of absorbance values corrected for dilution of the titration of thorium(IV) and PDA at 2.00×10^{-5} *M*, in 0.10 *M* $NaClO_4$ at 25.0 ºC.

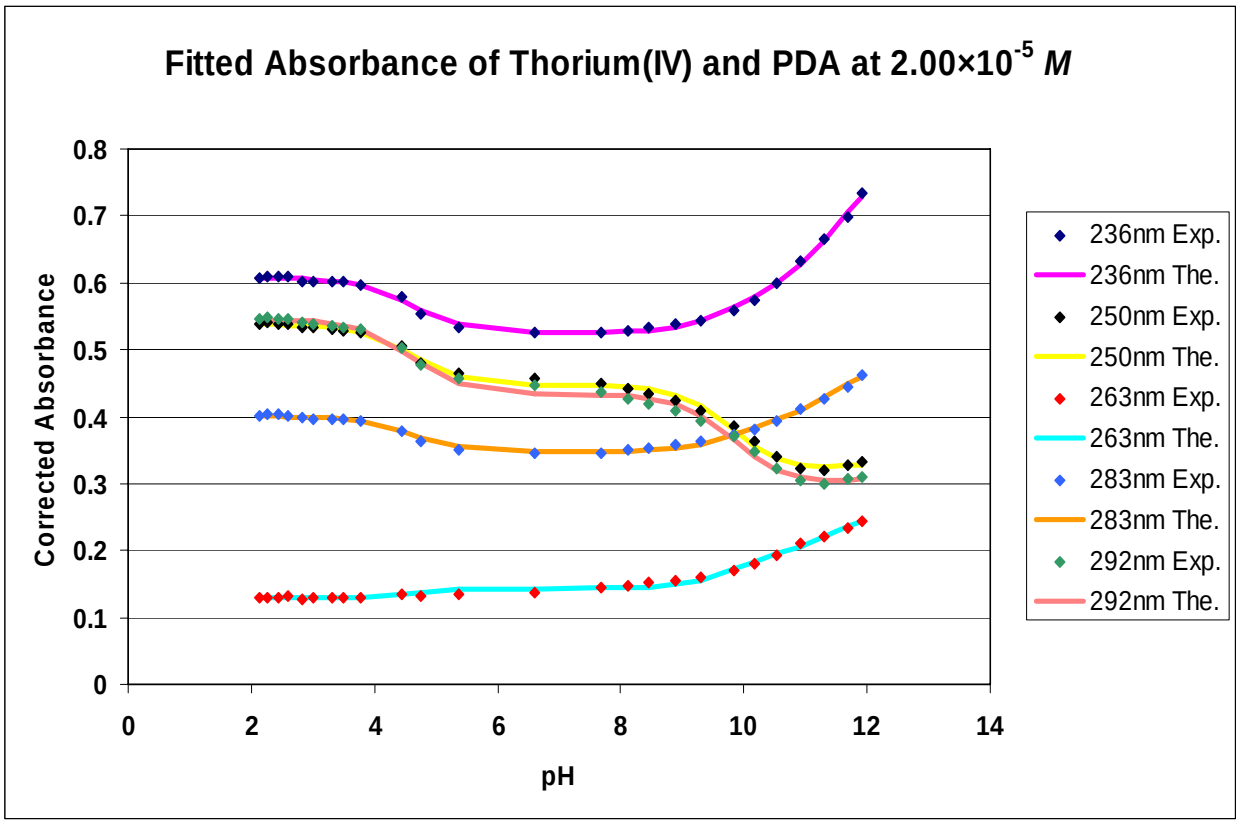

Figure 46(a). Experimental absorbance data (Exp.) fitted with calculated values (The.) to determine the protonation equilibria of the titration of thorium(IV) and PDA at 2.00×10^{-5} *M*, in 0.10 *M* $NaClO_4$ at 25.0 ºC.

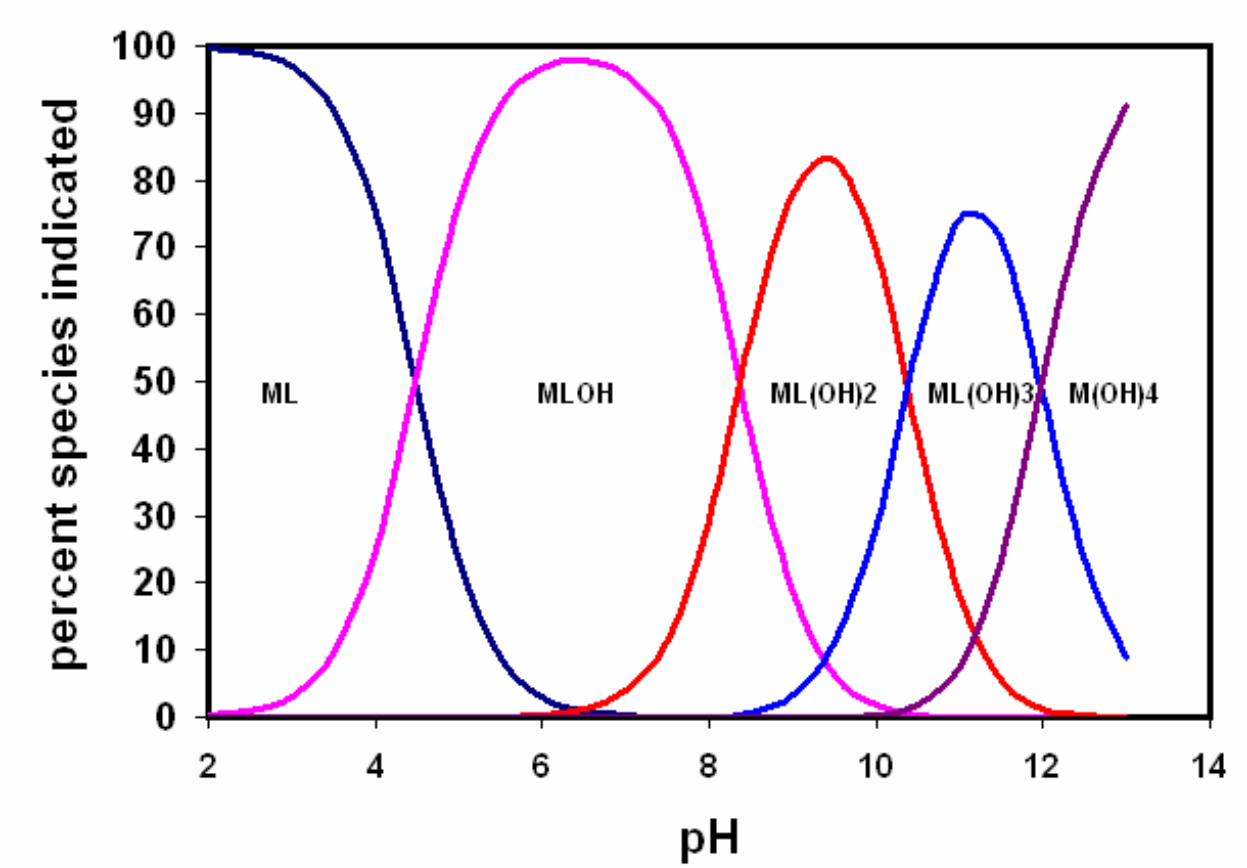

Figure 46(b). Species distribution diagram for the Th(IV)/PDA system at 2.00×10^{-5} *M* calculated using log K values determined here for Th(IV) and PDA. Diagram calculated using EXCEL. Abbreviation: L = PDA. Charges on species omitted for simplicity.

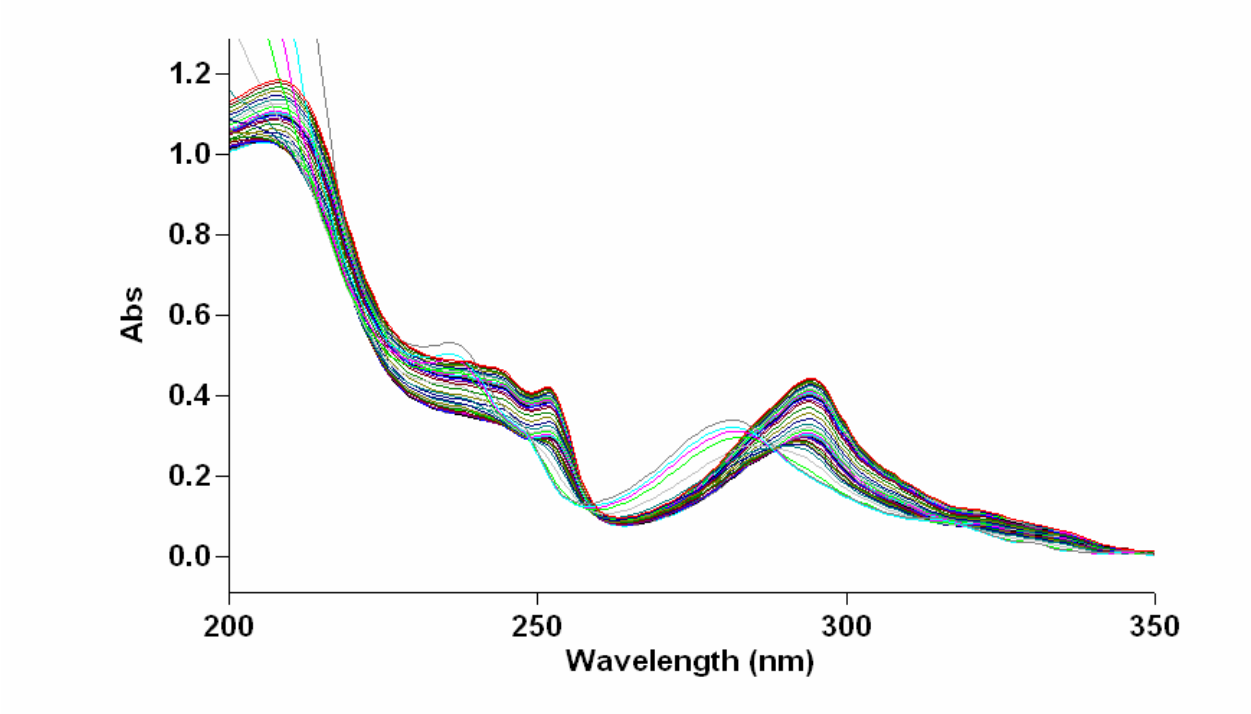

Figure 47. UV-Vis absorbance spectrum of the titration of thorium(IV) and PDA at 4.00×10^{-6} *M*, in 0.10 *M* $NaClO_4$ at 25.0 ºC.

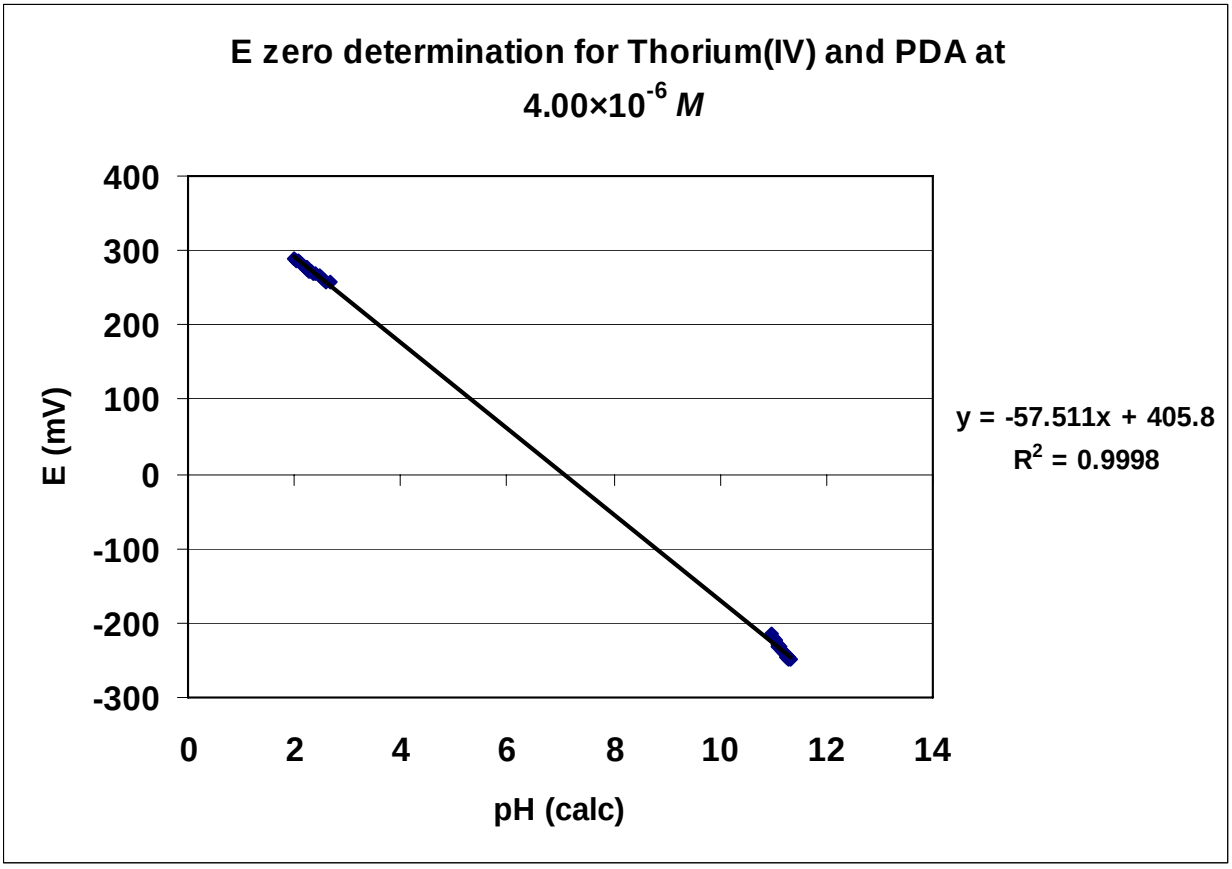

Figure 48. Plot of the correlation between E (mV) and the calculated pH used to calculate E^0 for the titration of thorium(IV) and PDA at 4.00×10^{-6} *M*, in 0.10 *M* $NaClO_4$ at 25.0 ºC.

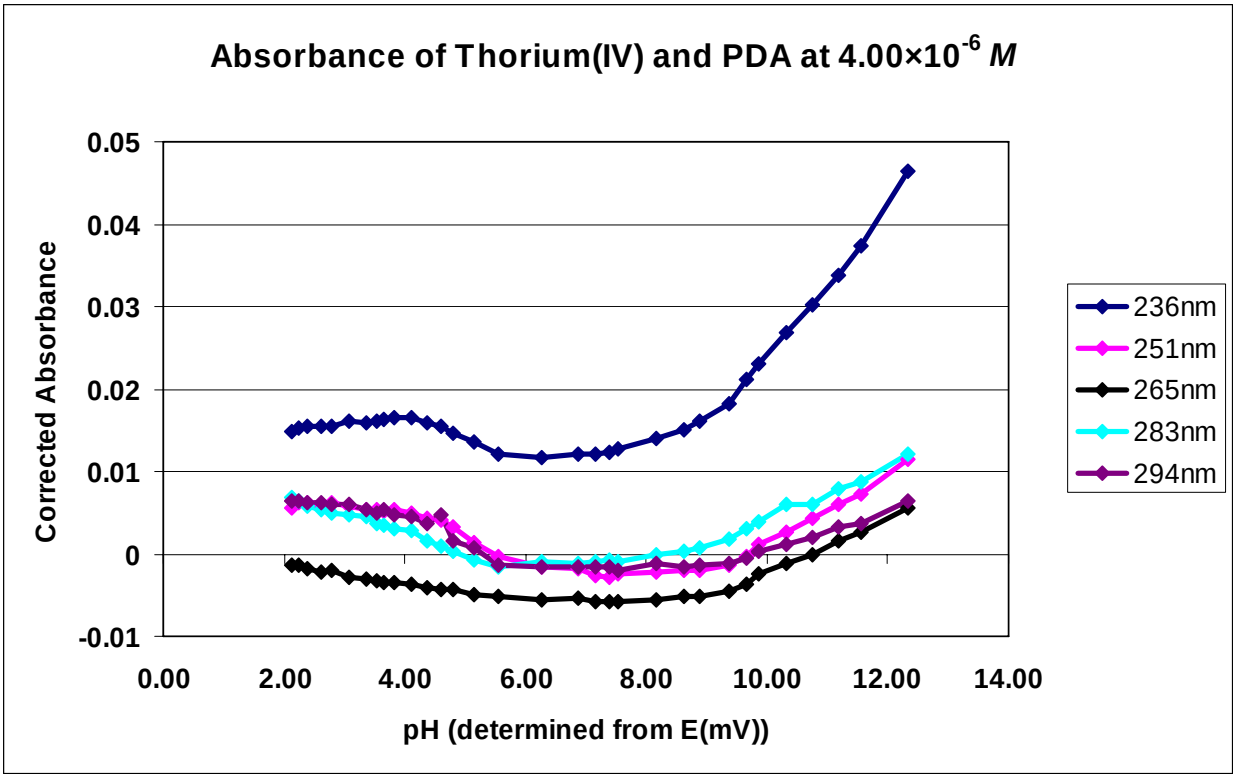

Figure 49. Plot of absorbance values corrected for dilution of the titration of thorium(IV) and PDA at 4.00×10^{-6} *M*, in 0.10 *M* $NaClO_4$ at 25.0 ºC.

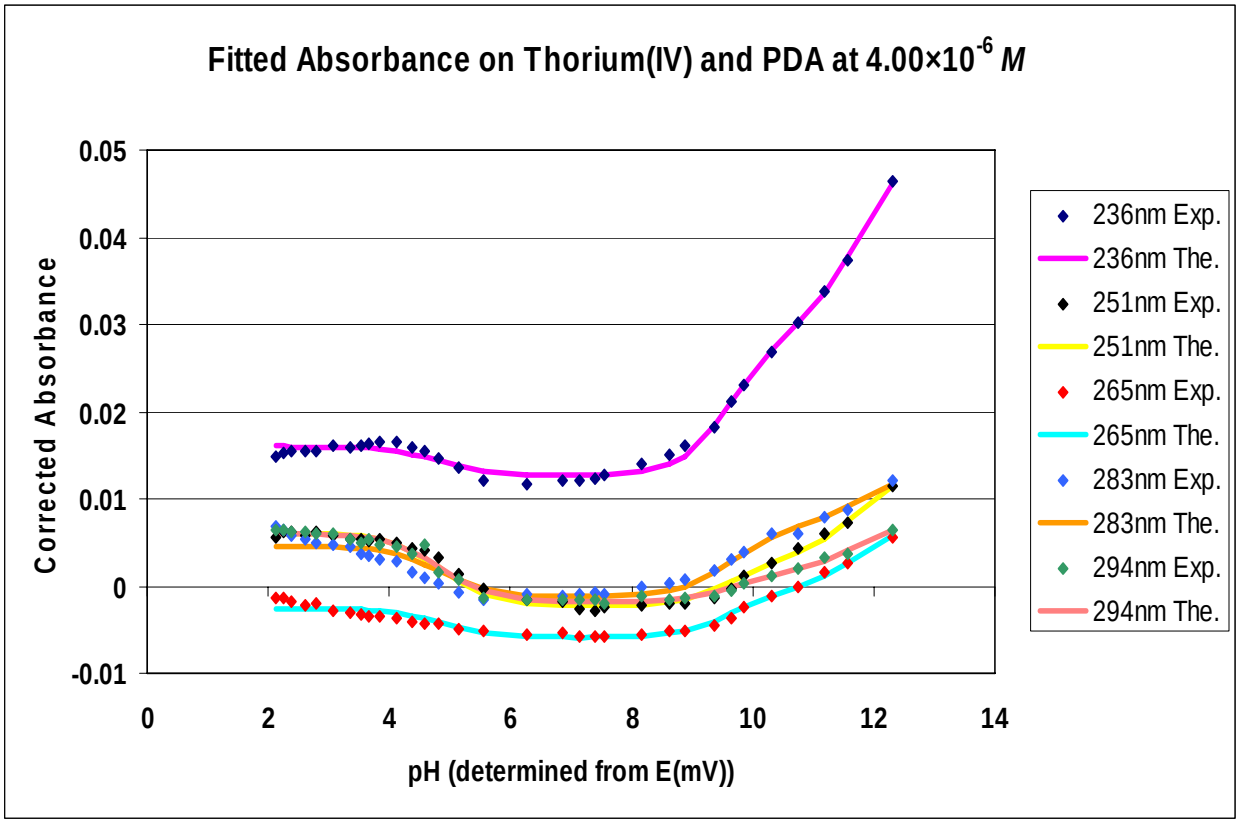

Figure 50. Experimental absorbance data (Exp.) fitted with calculated values (The.) to determine the protonation equilibria of the titration of thorium(IV) and PDA at 4.00×10^{-6} *M*, in 0.10 *M* $NaClO_4$ at 25.0 ºC.

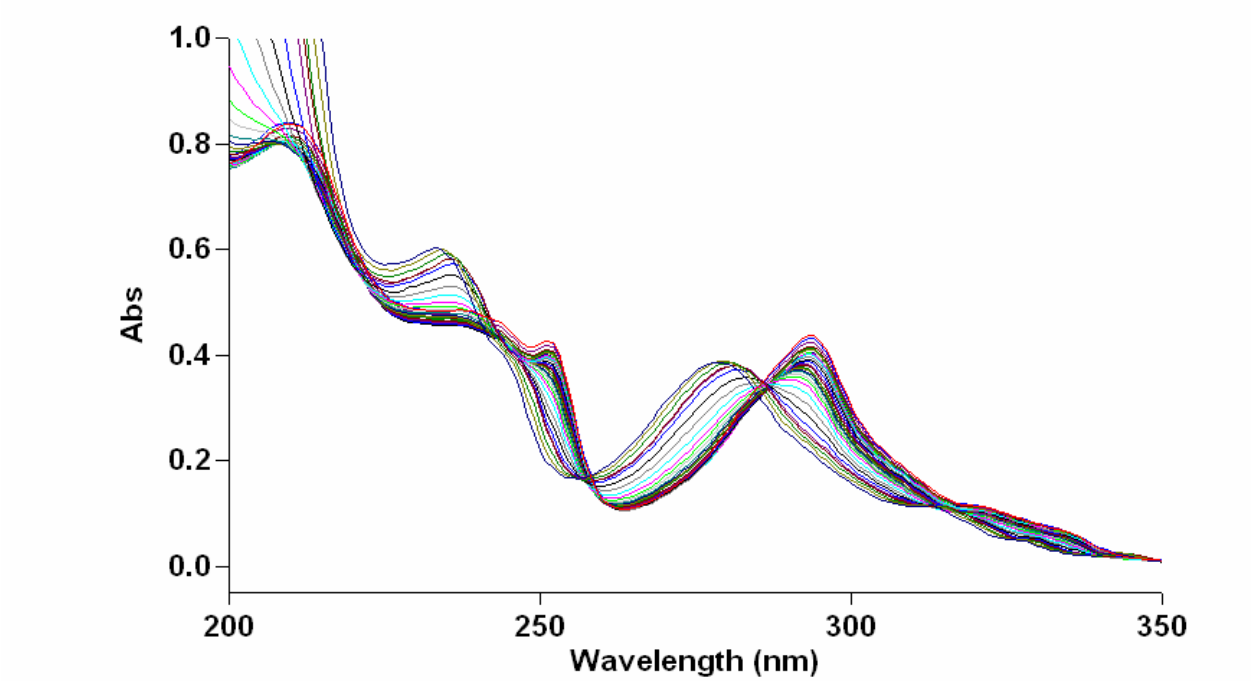

Figure 51. UV-Vis absorbance spectrum of the titration of 2:1 PDA and thorium(IV) with PDA at 4.00×10^{-5} *M* and thorium(IV) at 2.00×10^{-5} *M*, in 0.10 *M* $NaClO_4$ at 25.0 ºC.

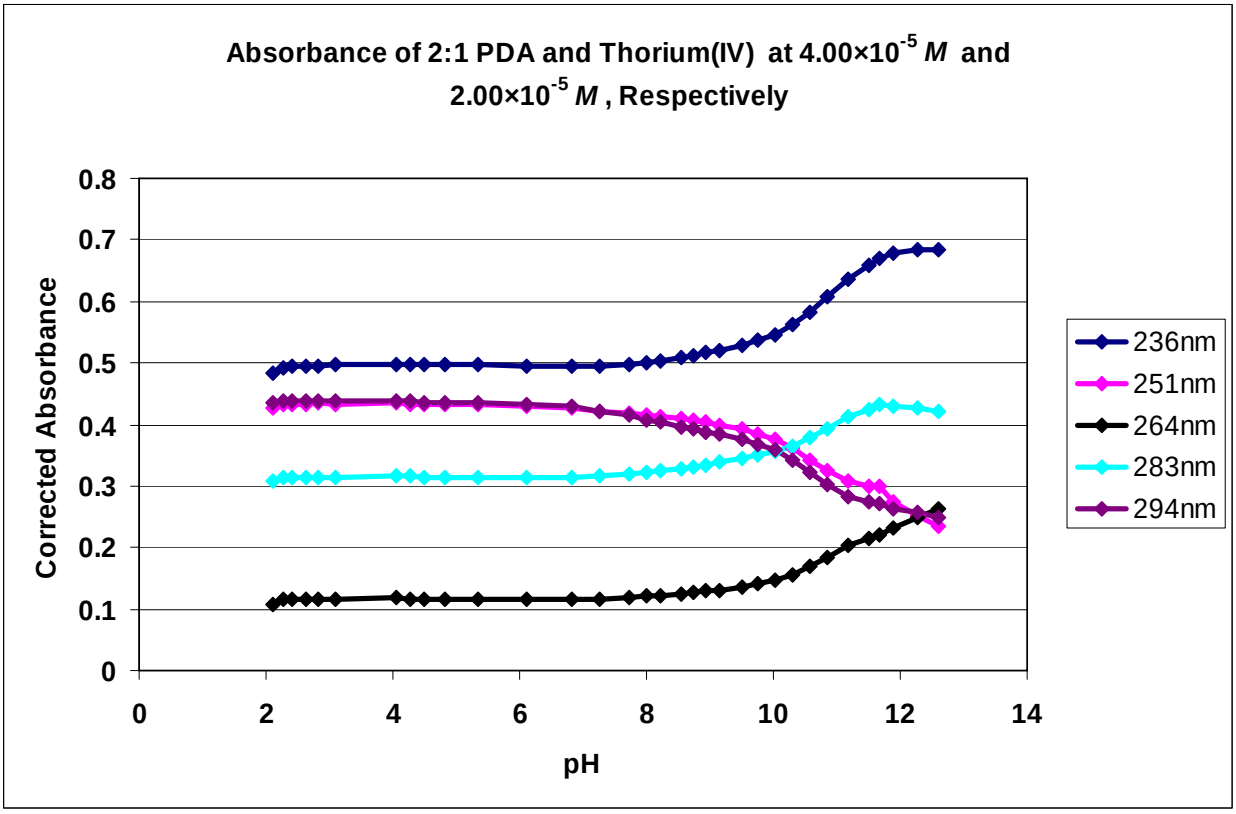

Figure 52. Plot of absorbance values corrected for dilution of the titration of 2:1 PDA and thorium(IV) with PDA at 4.00×10^{-5} *M* and thorium(IV) at 2.00×10^{-5} *M*, in 0.10 *M* $NaClO_4$ at 25.0 ºC.

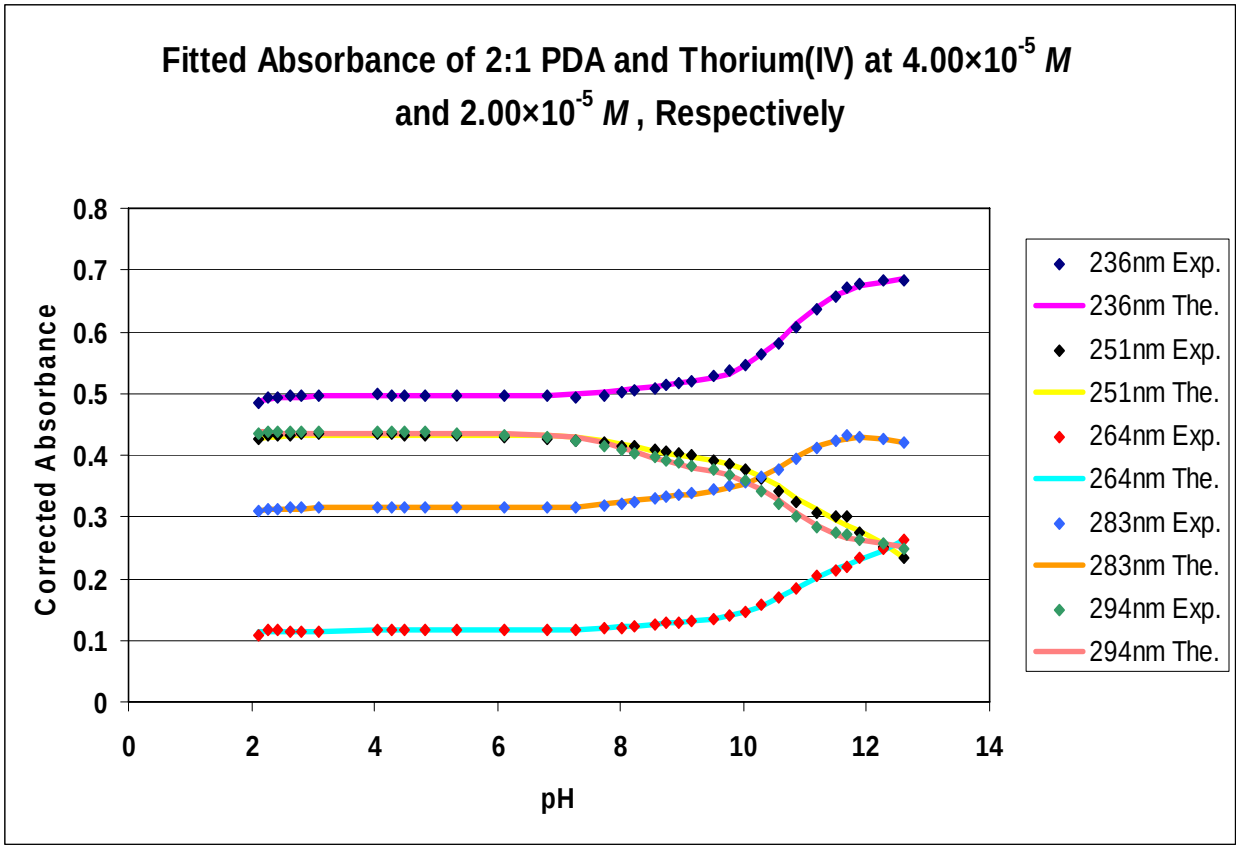

Figure 53. Experimental absorbance data (Exp.) fitted with calculated values (The.) to determine the protonation equilibria of the titration of 2:1 PDA and thorium(IV) with PDA at 4.00×10^{-5} *M* and thorium(IV) at 2.00×10^{-5} *M*, in 0.10 *M* $NaClO_4$ at 25.0 ºC.

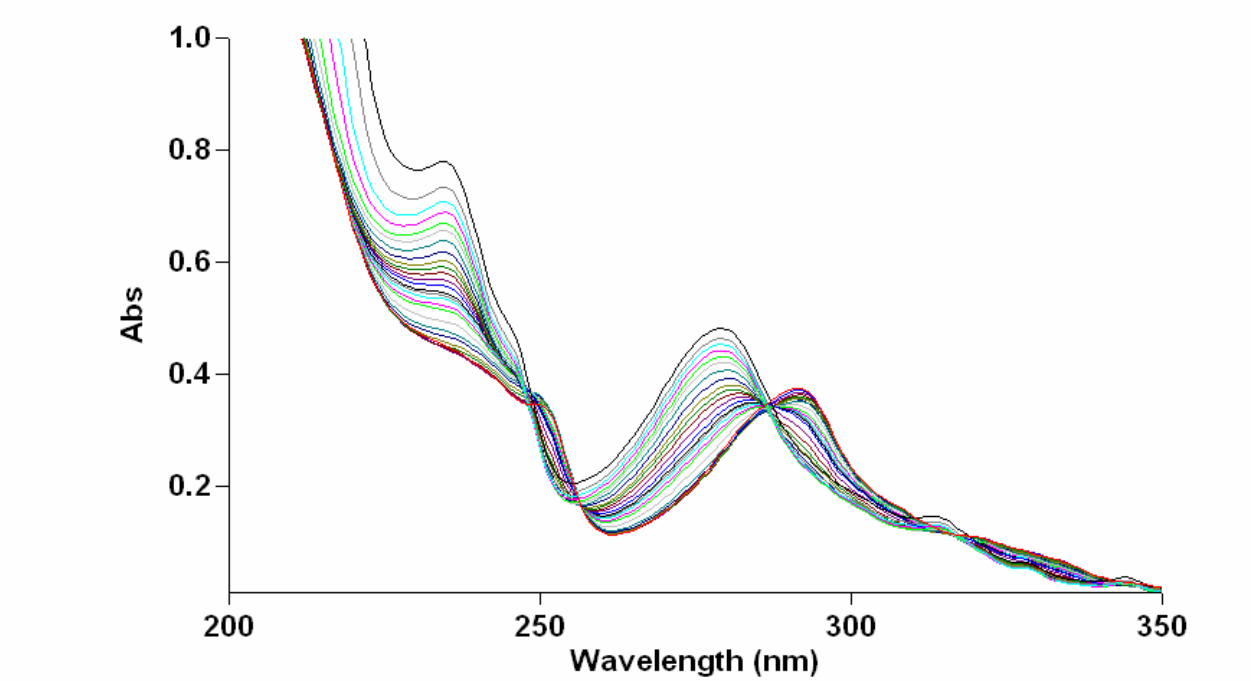

Figure 54. UV-Vis absorbance spectrum of the titration of 1:1:1 thorium(IV), PDA and DTPA at 2.00×10^{-5} *M*, in 0.10 *M* $NaClO_4$ at 25.0 ºC.

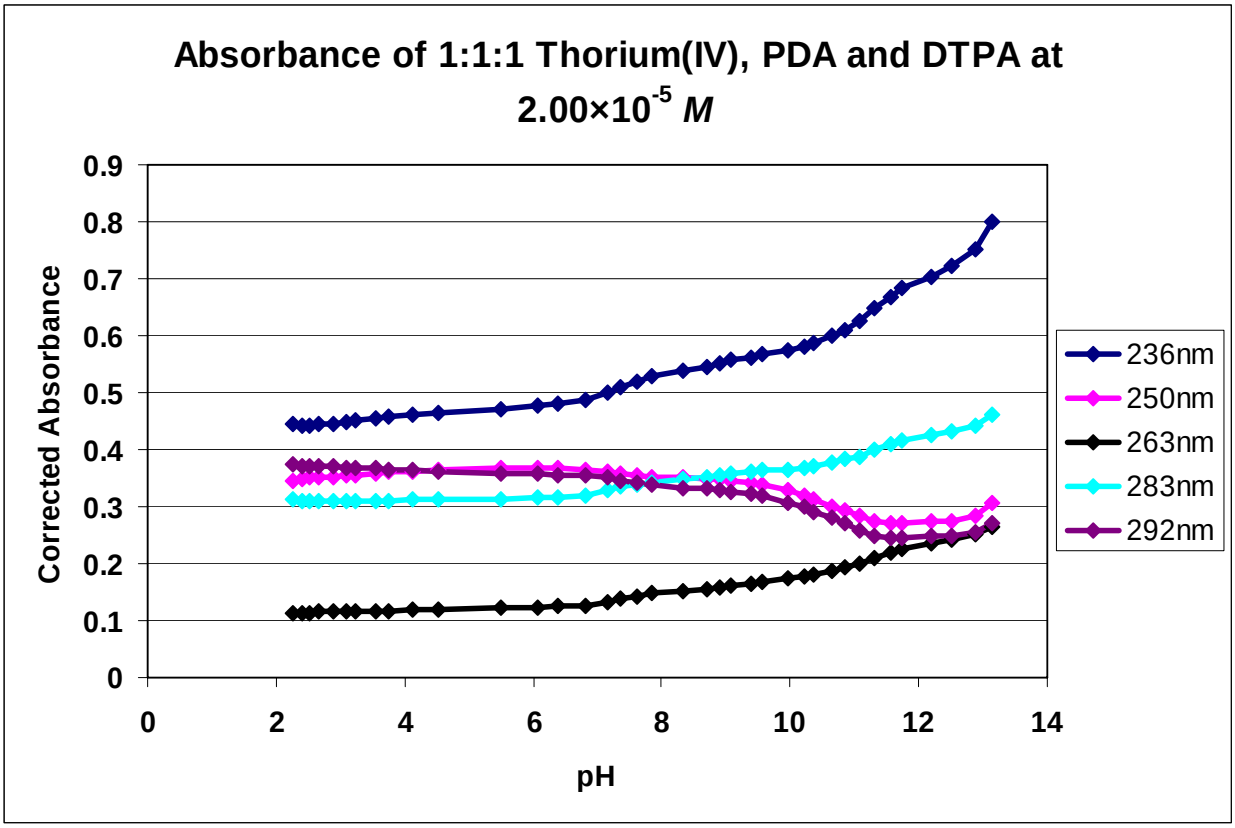

Figure 55. Plot of absorbance values corrected for dilution of the titration of 1:1:1 thorium(IV), PDA and DTPA at 2.00×10^{-5} *M*, in 0.10 *M* $NaClO_4$ at 25.0 ºC.

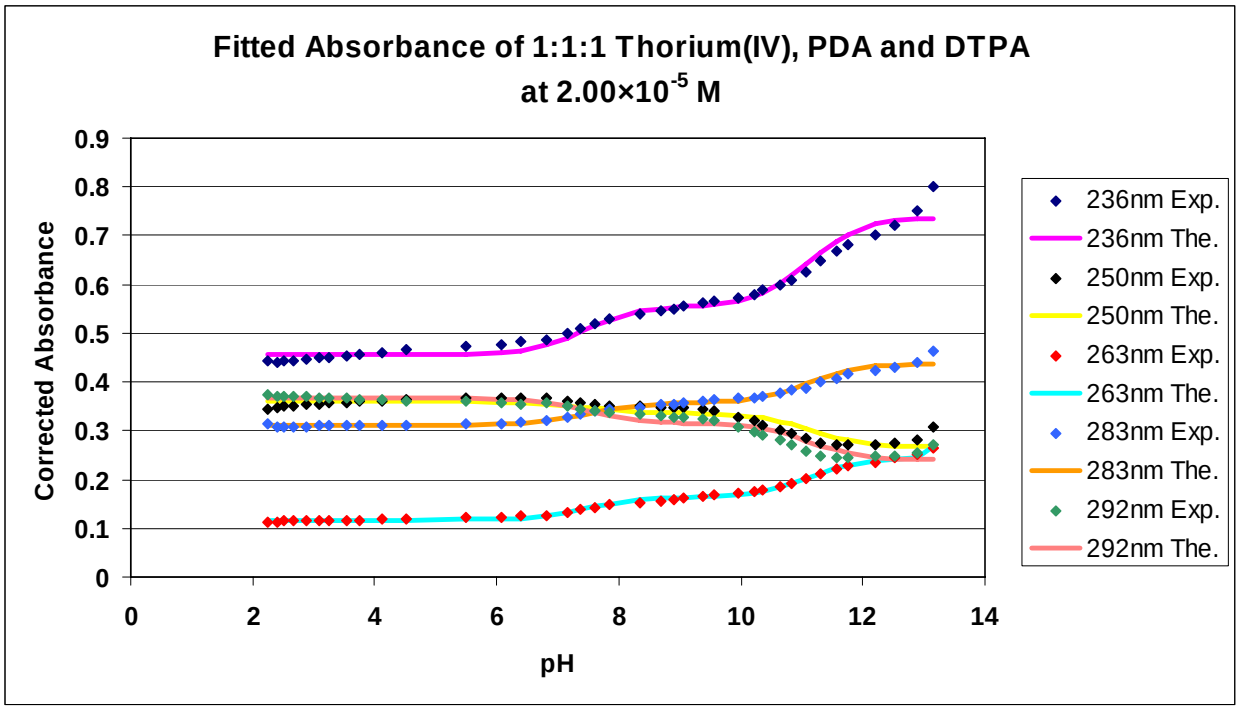

Figure 56. Experimental absorbance data (Exp.) fitted with calculated values (The.) to determine the protonation equilibria of the titration of 1:1:1 thorium(IV), PDA and DTPA at 2.00×10^{-5} *M*, in 0.10 *M* $NaClO_4$ at 25.0 ºC.

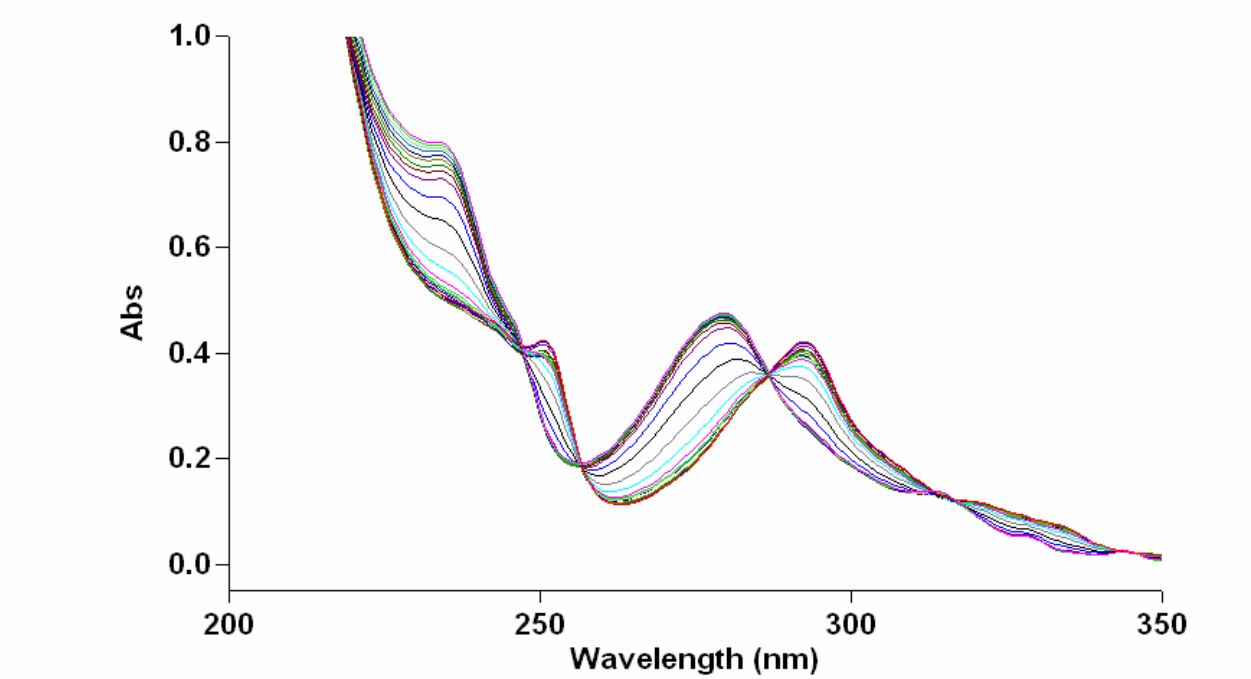

Figure 57. UV-Vis absorbance spectrum of the titration of 1:1:10 thorium(IV), PDA and DTPA with thorium(IV) and PDA at 2.00×10^{-5} *M* and DTPA at 2.00×10^{-4} *M*, in 0.10 *M* $NaClO_4$ at 25.0 ºC.

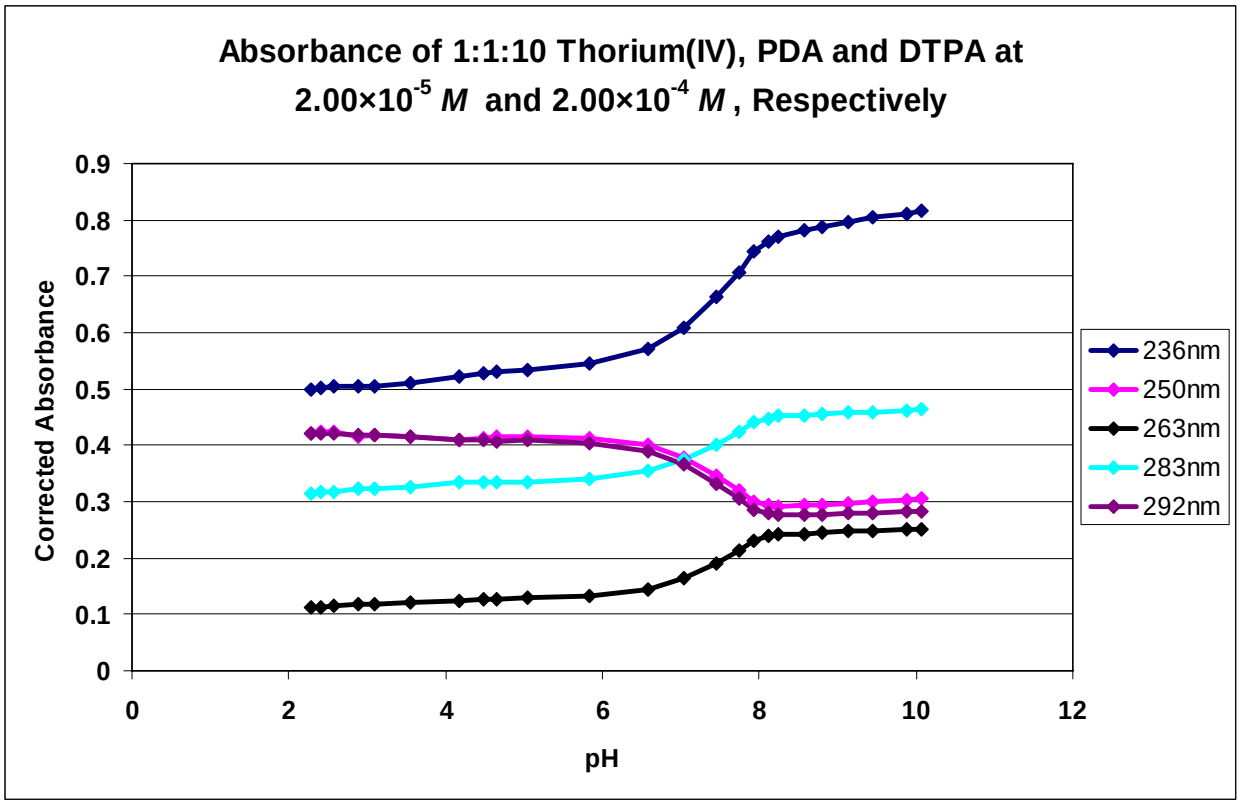

Figure 58. Plot of absorbance values corrected for dilution of the titration of 1:1:10 thorium(IV), PDA and DTPA with thorium(IV) and PDA at 2.00×10^{-5} *M* and DTPA at 2.00×10^{-4} *M*, in 0.10 *M* $NaClO_4$ at 25.0 ºC.

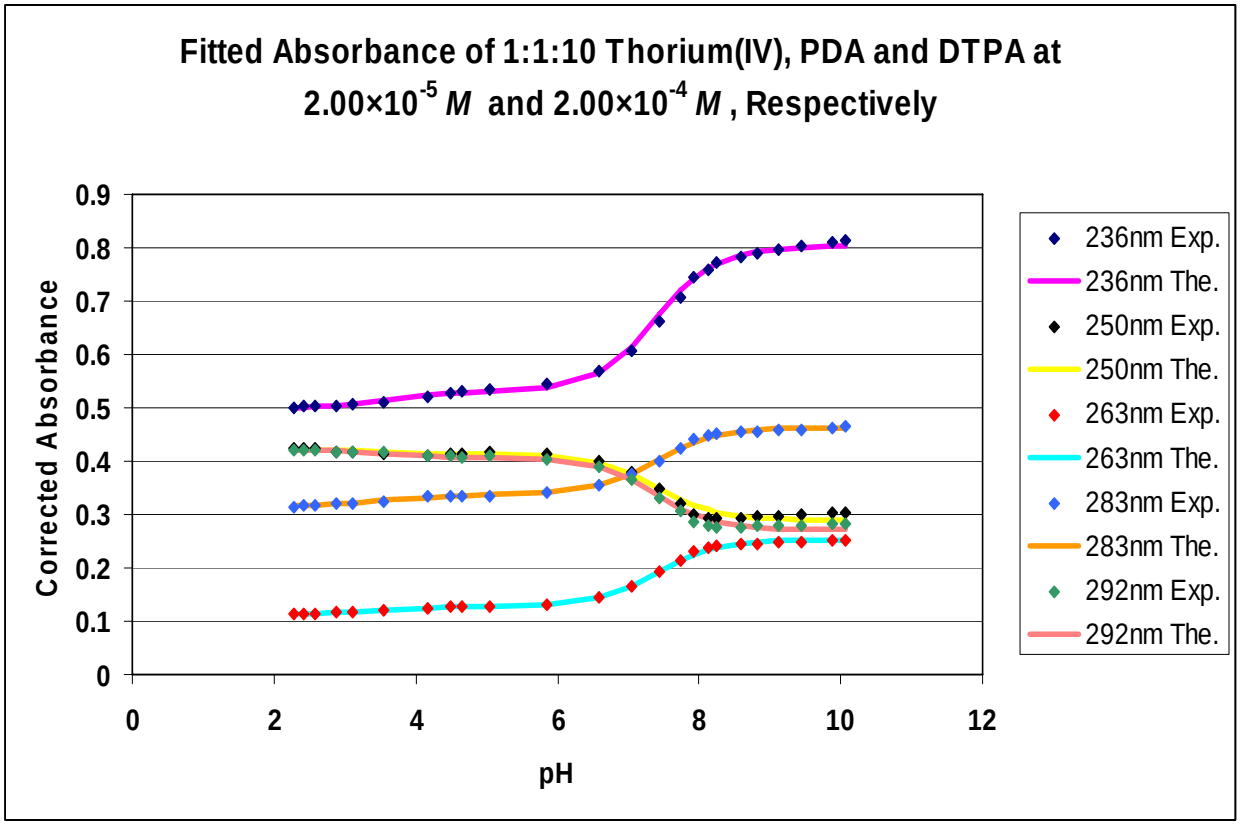

Figure 59. Experimental absorbance data (Exp.) fitted with calculated values (The.) to determine the protonation equilibria of the titration of 1:1:10 thorium(IV), PDA and DTPA with thorium(IV) and PDA at 2.00×10^{-5} *M* and DTPA at 2.00×10^{-4} *M*, in 0.10 *M* $NaClO_4$ at 25.0 ºC.

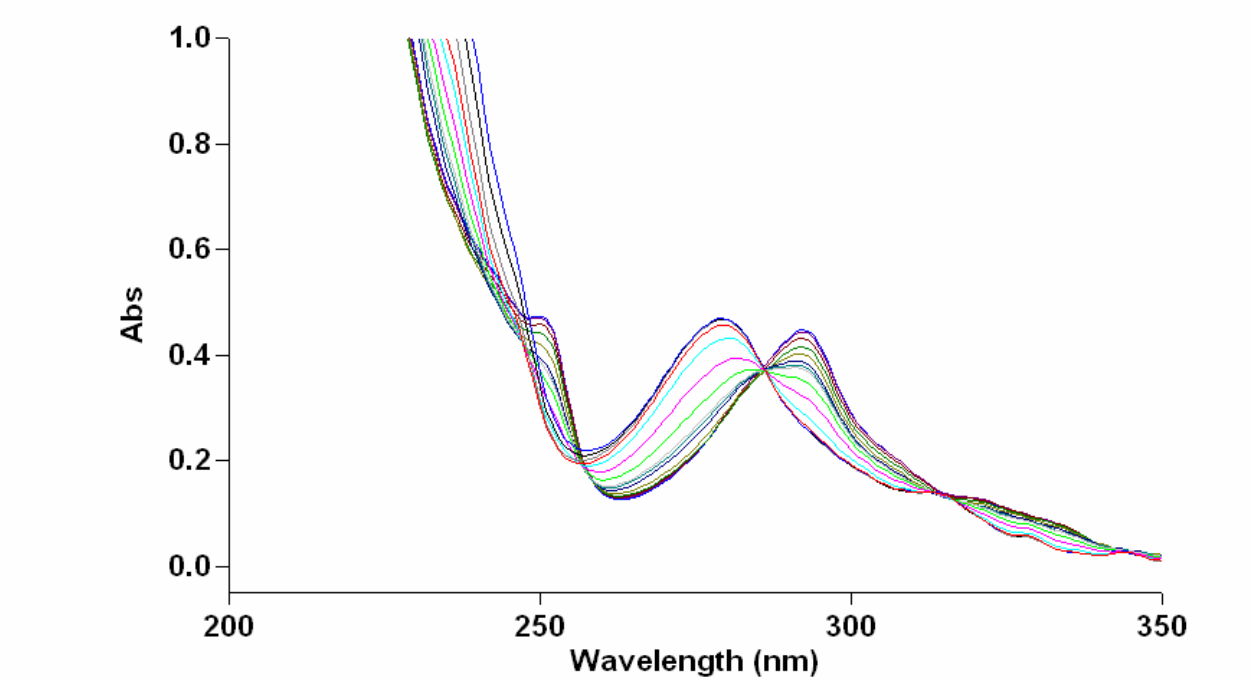

Figure 60. UV-Vis absorbance spectrum of the titration of 1:1:100 thorium(IV), PDA and DTPA with thorium(IV) and PDA at 2.00×10^{-5} *M* and DTPA at 2.00×10^{-3} *M*, in 0.10 *M* $NaClO_4$ at 25.0 ºC.

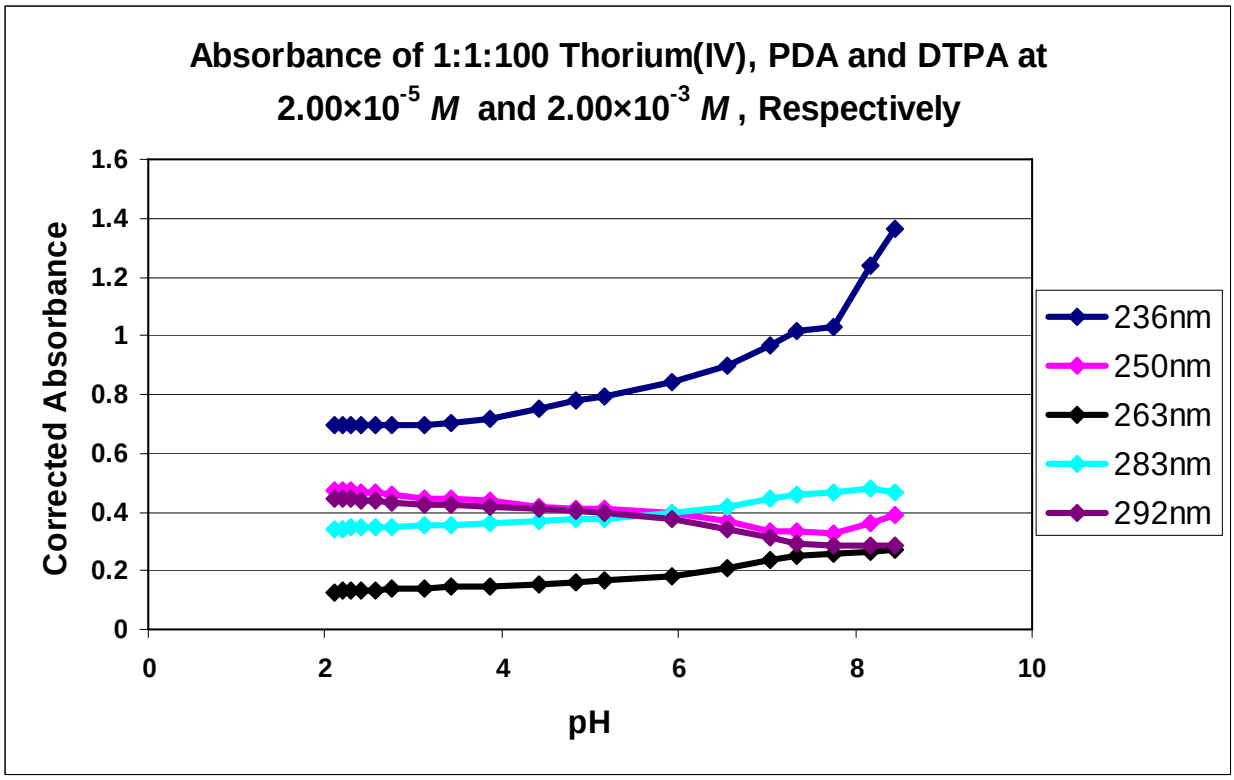

Figure 61. Plot of absorbance values corrected for dilution of the titration of 1:1:100 thorium(IV), PDA and DTPA with thorium(IV) and PDA at 2.00×10^{-5} *M* and DTPA at 2.00×10^{-3} *M*, in 0.10 *M* $NaClO_4$ at 25.0 ºC.

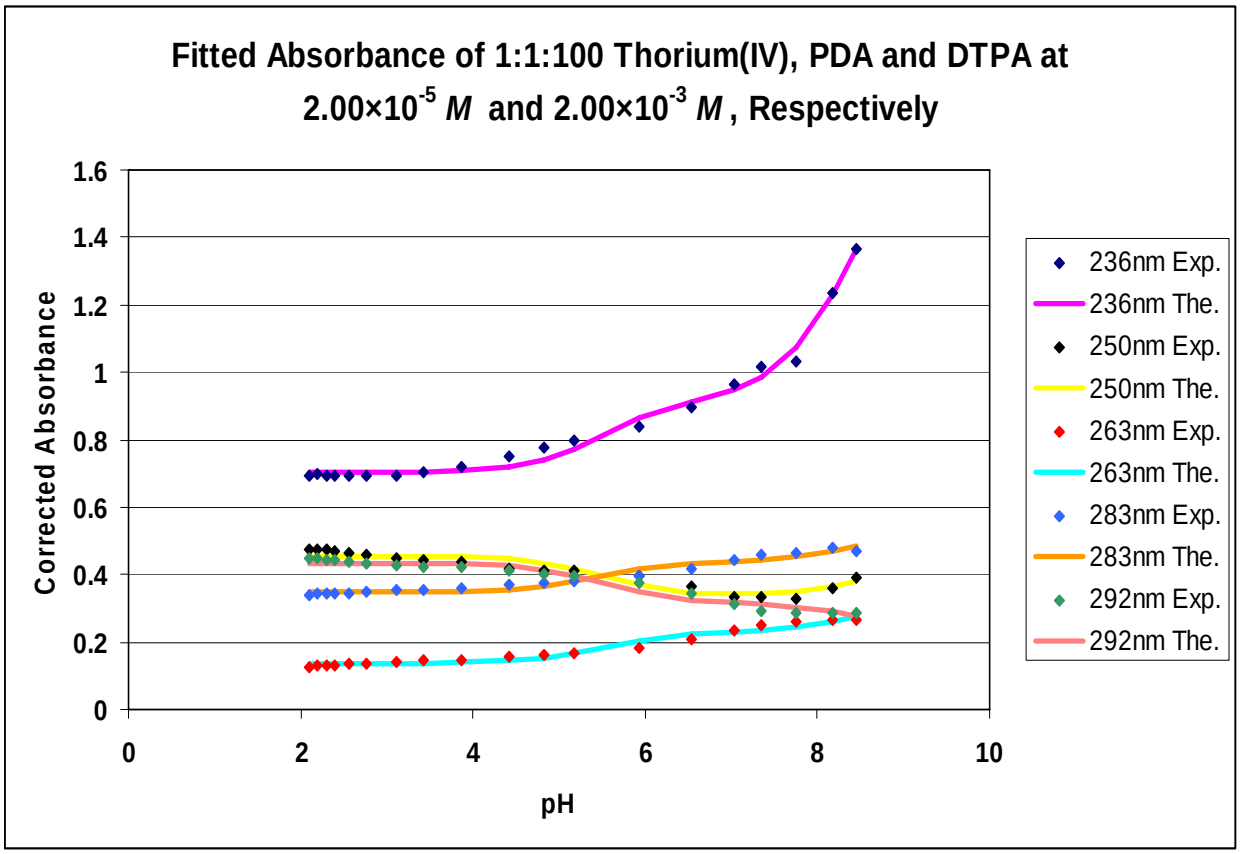

Figure 62. Experimental absorbance data (Exp.) fitted with calculated values (The.) to determine the protonation equilibria of the titration of 1:1:100 thorium(IV), PDA and DTPA with thorium(IV) and PDA at 2.00×10^{-5} *M* and DTPA at 2.00×10^{-3} *M*, in 0.10 *M* $NaClO_4$ at 25.0 ºC.

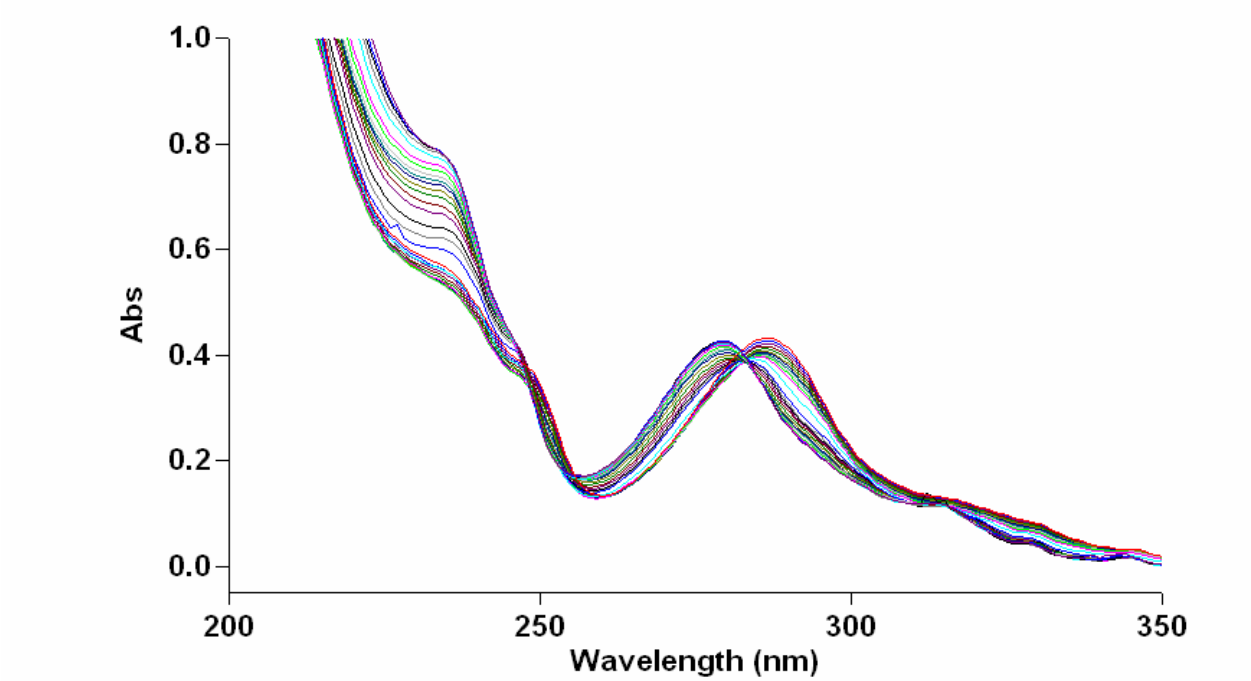

Figure 63. UV-Vis absorbance spectrum of the titration of 1:1:10 thorium(IV), PDA and TTHA with thorium(IV) and PDA at 2.00×10^{-5} *M* and TTHA at 2.00×10^{-4} *M*, in 0.10 *M* $NaClO_4$ at 25.0 ºC.

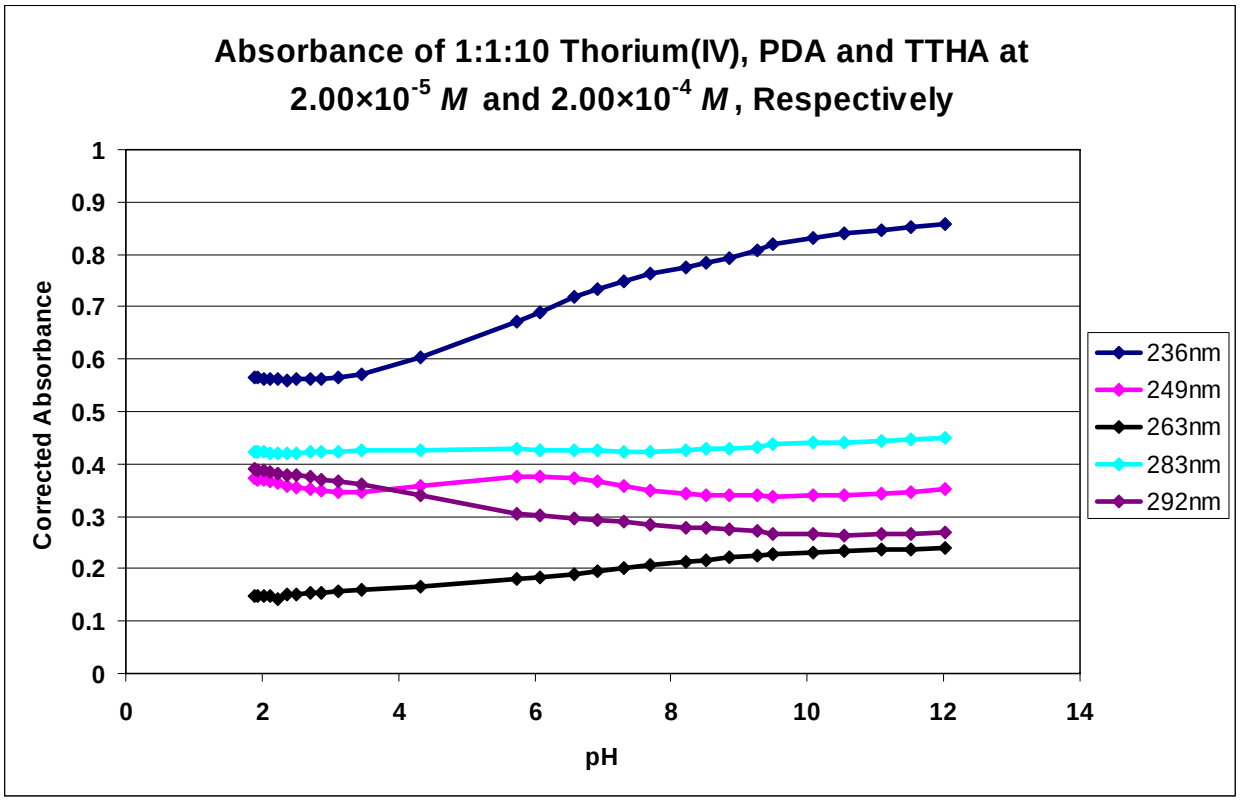

Figure 64. Plot of absorbance values corrected for dilution of the titration of 1:1:10 thorium(IV), PDA and TTHA with thorium(IV) and PDA at 2.00×10^{-5} *M* and TTHA at 2.00×10^{-4} *M*, in 0.10 *M* $NaClO_4$ at 25.0 ºC.

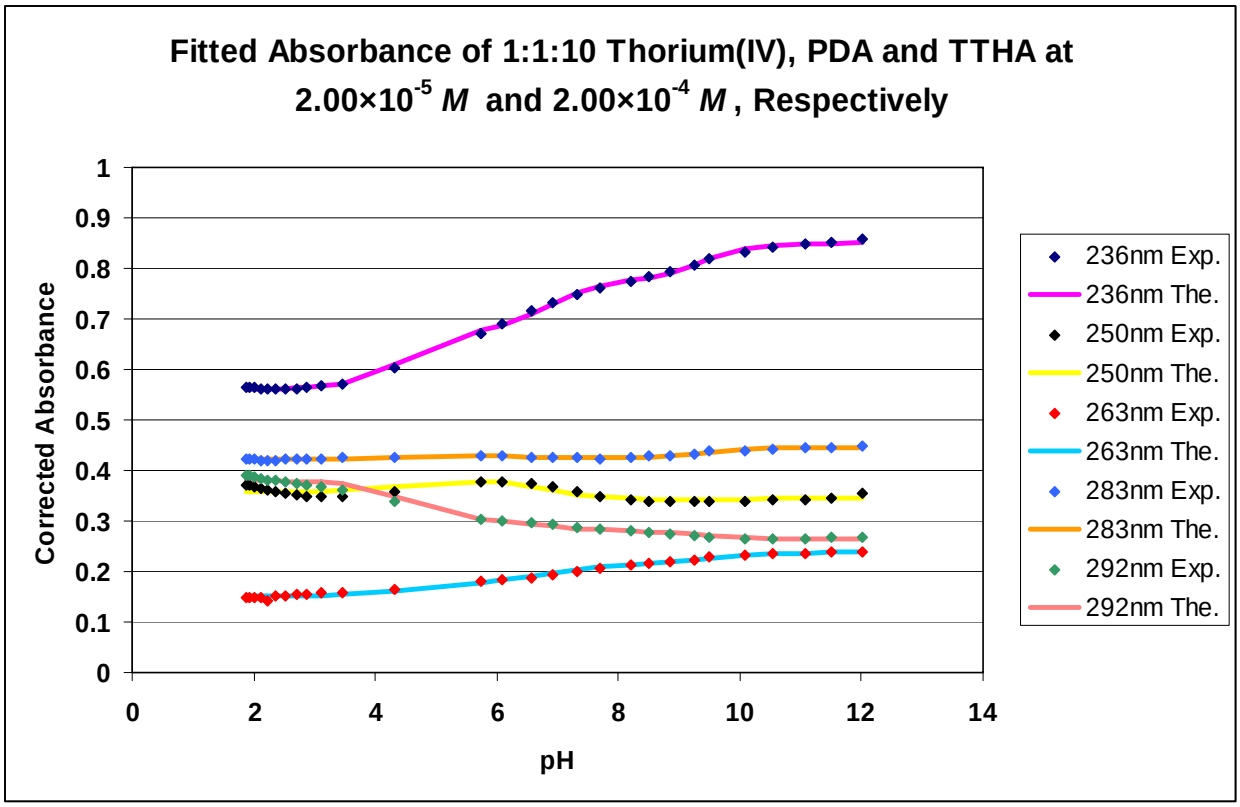

Figure 65. Experimental absorbance data (Exp.) fitted with calculated values (The.) to determine the protonation equilibria of the titration of 1:1:10 thorium(IV), PDA and TTHA with thorium(IV) and PDA at 2.00×10^{-5} *M* and TTHA at 2.00×10^{-4} *M*, in 0.10 *M* $NaClO_4$ at 25.0 ºC.

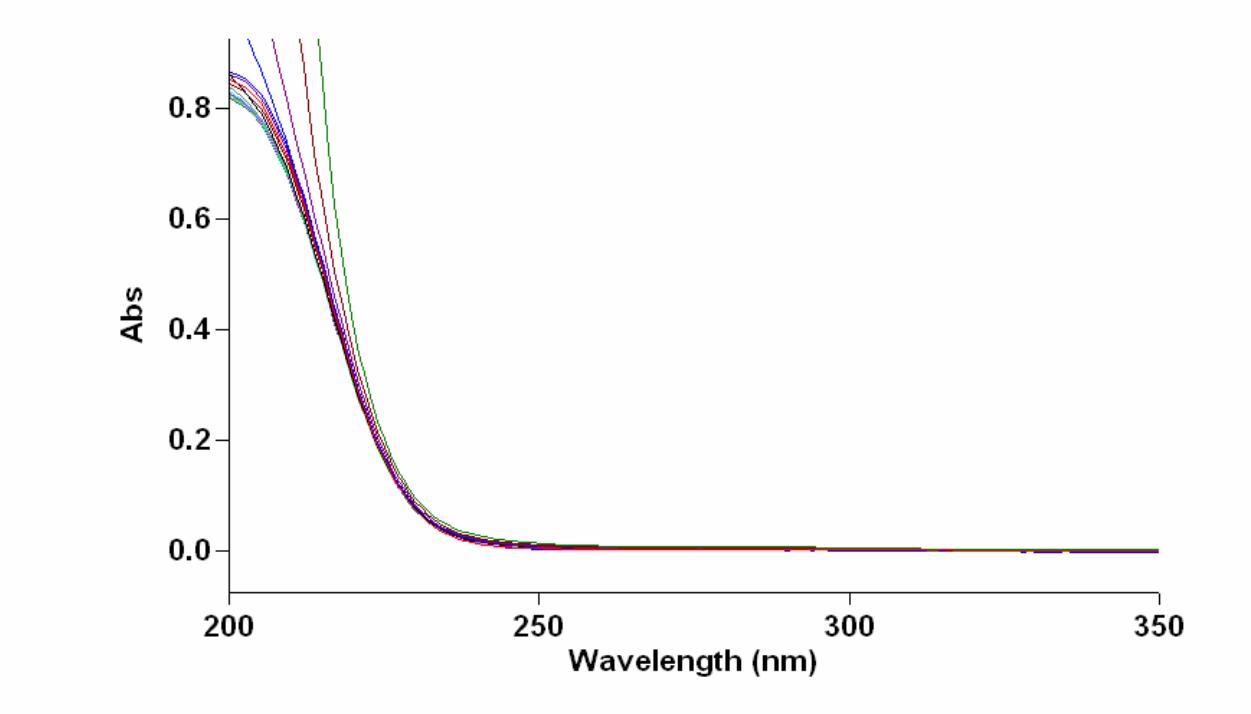

Figure 66. UV-Vis absorbance spectrum of the titration of thorium(IV) and DTPA at 2.00×10^{-5} *M*, in 0.10 *M* $NaClO_4$ at 25.0 ºC.

Uranyl(VI)-PDA results

Uranyl(VI) has an ionic radius of 0.86 Å which is slightly smaller than the ideal 1.0 Å favored by PDA. Two titration experiments were performed with uranyl and PDA. The UV absorbance spectrum for uranyl(VI) and PDA complex at 2.00×10^{-5} *M* is shown in Figure 67. A plot of the corrected absorbance values versus pH is shown in Figure 68 and a plot of the theoretical absorbance values calculated to determine the protonation constants of the complex is shown alongside the experimental data in Figure 69. From the selected wavelengths of 236, 249, 263, 283 and 293 nm, 4 successive pH-dependent equilibria were observed. The equilibria are described below at the pH they occured.

$$UO_2(PDA) + H^+ \leftrightarrows UO_2(PDA)H \qquad (pH = 1.50)$$

$$UO_2(PDA) + OH^- \leftrightarrows UO_2(PDA)OH \qquad (pH = 7.06)$$

$$UO_2(PDA)(OH) + OH^- \leftrightarrows UO_2(PDA)(OH)_2 \qquad (pH = 9.53)$$

$$UO_2(PDA)(OH)_2 + 2\,OH^- \leftrightarrows UO_2(OH)_4 + PDA^{2-} \qquad (pH = 11.90)$$

Using log K_w = 13.78, the log K_1 [OH^-] of the UO_2-PDA complex can be described as follows.

$$UO_2(PDA) + OH^- \leftrightarrows UO_2(PDA)OH \qquad (\log K_1\,[OH^-] = 6.72)$$

$$UO_2(PDA)(OH) + OH^- \leftrightarrows UO_2(PDA)(OH)_2 \qquad (\log K_2\,[OH^-] = 4.25)$$

$$UO_2(PDA)(OH)_2 + 2\,OH^- \leftrightarrows UO_2(OH)_4 + PDA^{2-} \qquad (\log K_3K_4\,[OH^-] = 1.88)$$

The log β_4 [OH^-] for uranyl(VI) is 23.43 and from this value[15] a log K_1 for PDA with uranyl(VI) of 13.7 was calculated using Equation (9),

$$\log K_1 = 23.43 - (2\times(1.88) + 4.25 + 6.72) + 5.0 \qquad (9)$$

where the 5.0 takes into account the amount of free ligand at the isosbestic point. The UV absorbance spectrum for uranyl(VI) and PDA complex at 2.00×10^{-6} *M* is shown in Figure 70. A plot of the correlation between E (mV) and the calculated pH, which was used to calculate E^0, is

shown in Figure 71. A plot of the corrected absorbance values versus pH is shown in Figure 72 and a plot of the theoretical absorbance values calculated to determine the protonation constants of the complex is shown alongside the experimental data in Figure 73. This scan was conducted to show that a 10-fold dilution did not affect the isosbestic points of the uranyl(VI)-PDA complex significantly proving that the complex does not form any dimers. The reported formation constant for EDDA with uranyl(VI)[15] was 11.41, which was weaker when compared to the log K_1 for that of PDA with uranyl(VI). A Δ log K_1 of 2.29 between the log K_1 values of PDA and EDDA with uranyl(VI) was calculated and showed a slight increase in stability of the PDA complex of uranyl(VI) relative to the EDDA complex of uranyl(VI).

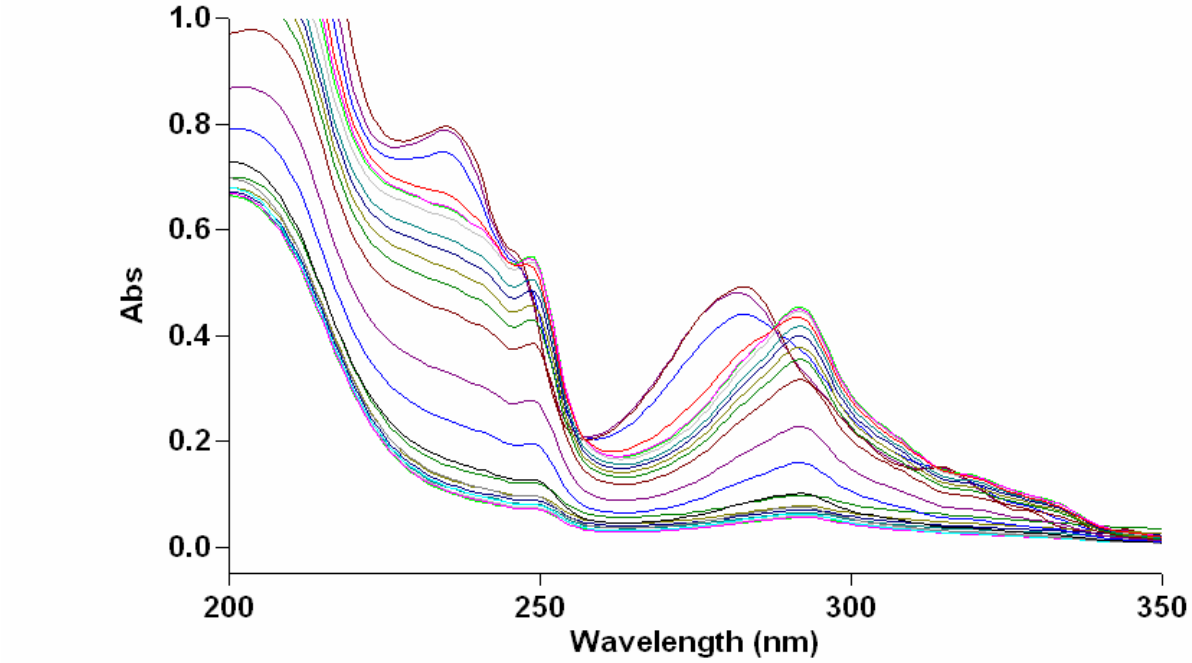

Figure 67. UV-Vis absorbance spectrum of the titration of uranyl(VI) and PDA at 2.00×10^{-5} *M*, in 0.10 *M* $NaClO_4$ at 25.0 ºC.

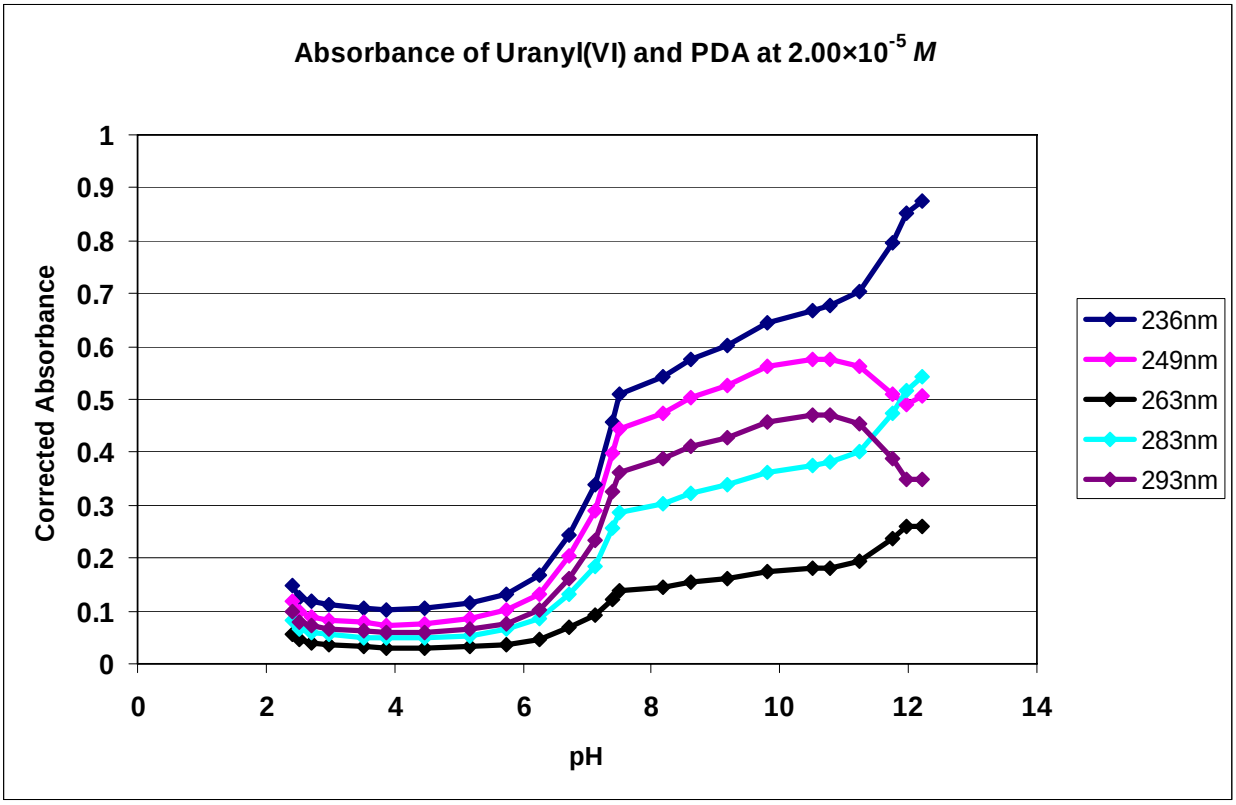

Figure 68. Plot of absorbance values corrected for dilution of the titration of uranyl(VI) and PDA at 2.00×10^{-5} *M*, in 0.10 *M* $NaClO_4$ at 25.0 ºC.

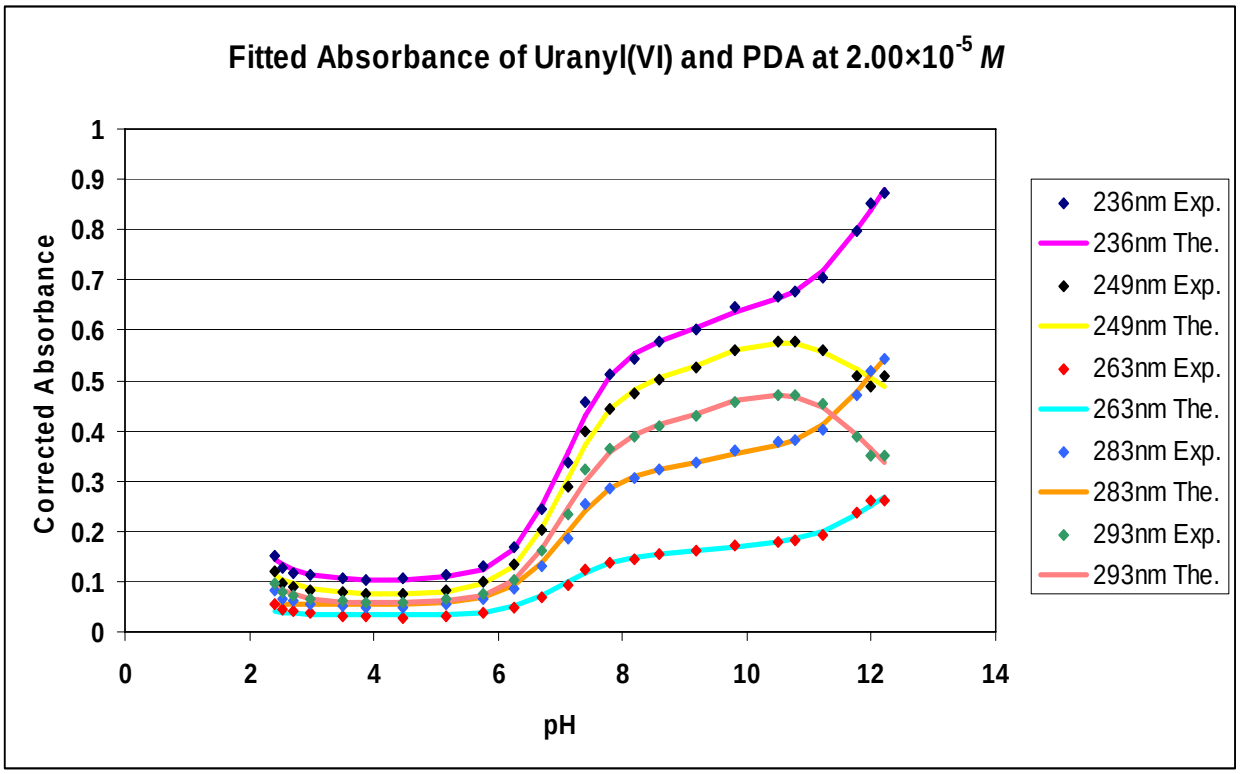

Figure 69. Experimental absorbance data (Exp.) fitted with calculated values (The.) to determine the protonation equilibria of the titration of uranyl(VI) and PDA at 2.00×10^{-5} *M*, in 0.10 *M* $NaClO_4$ at 25.0 ºC.

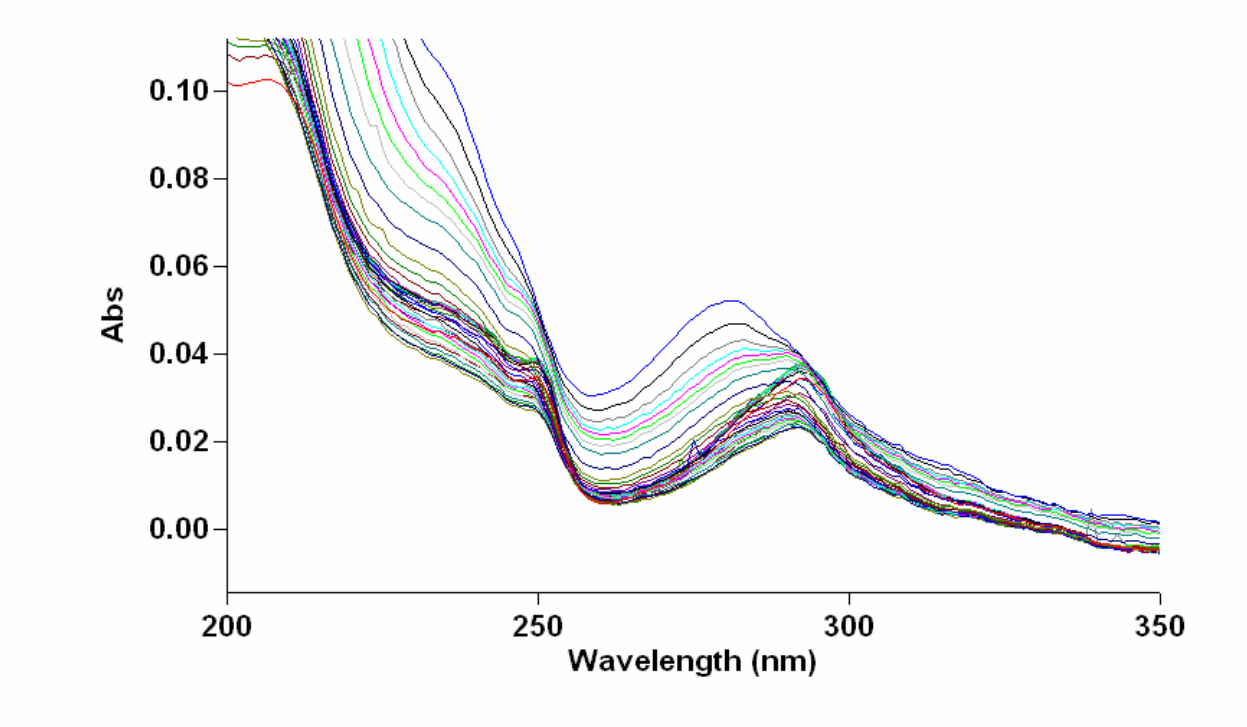

Figure 70. UV-Vis absorbance spectrum of the titration of uranyl(VI) and PDA at 2.00×10^{-6} *M*, in 0.10 *M* $NaClO_4$ at 25.0 ºC.

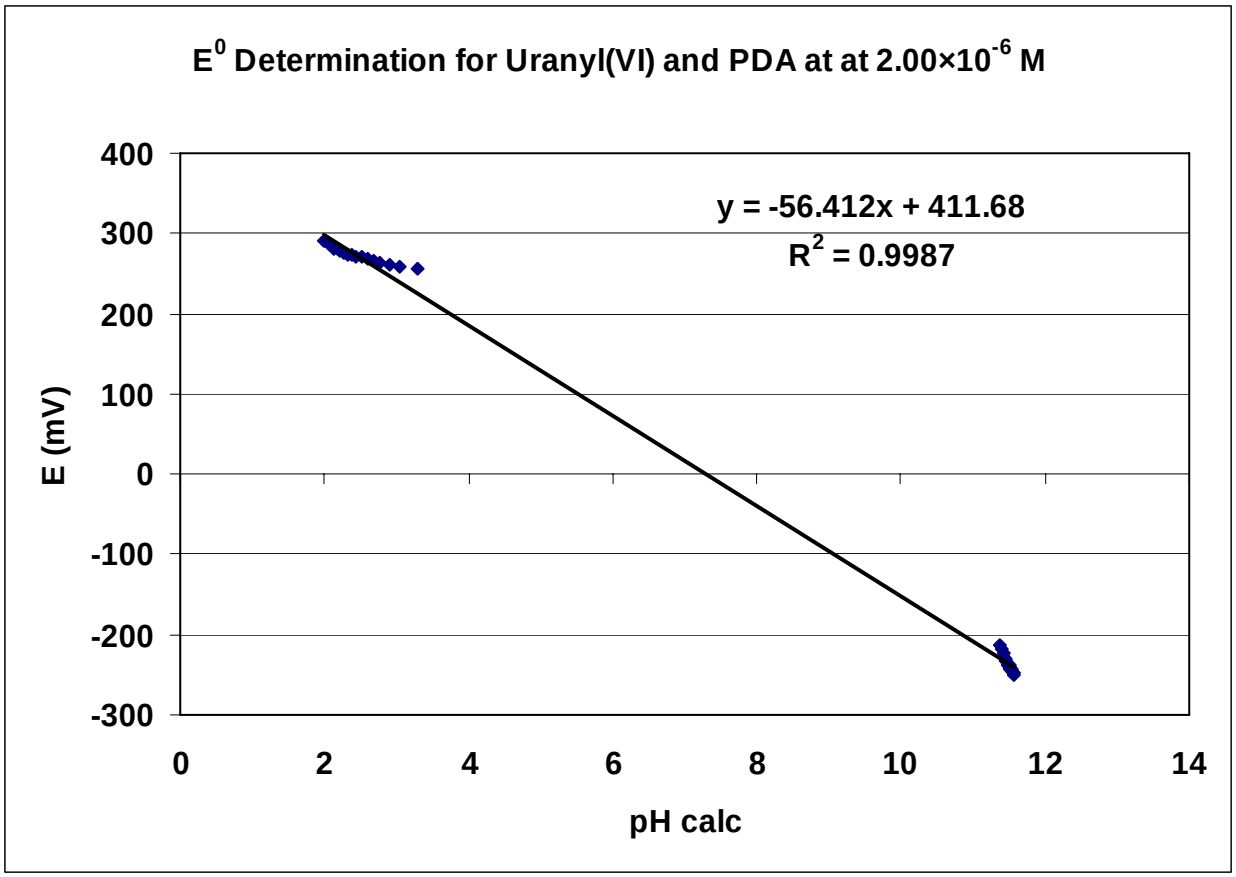

Figure 71. Plot of the correlation between E (mV) and the calculated pH used to calculate E^0 for the titration of uranyl(VI) and PDA at 2.00×10^{-6} *M*, in 0.10 *M* $NaClO_4$ at 25.0 ºC..

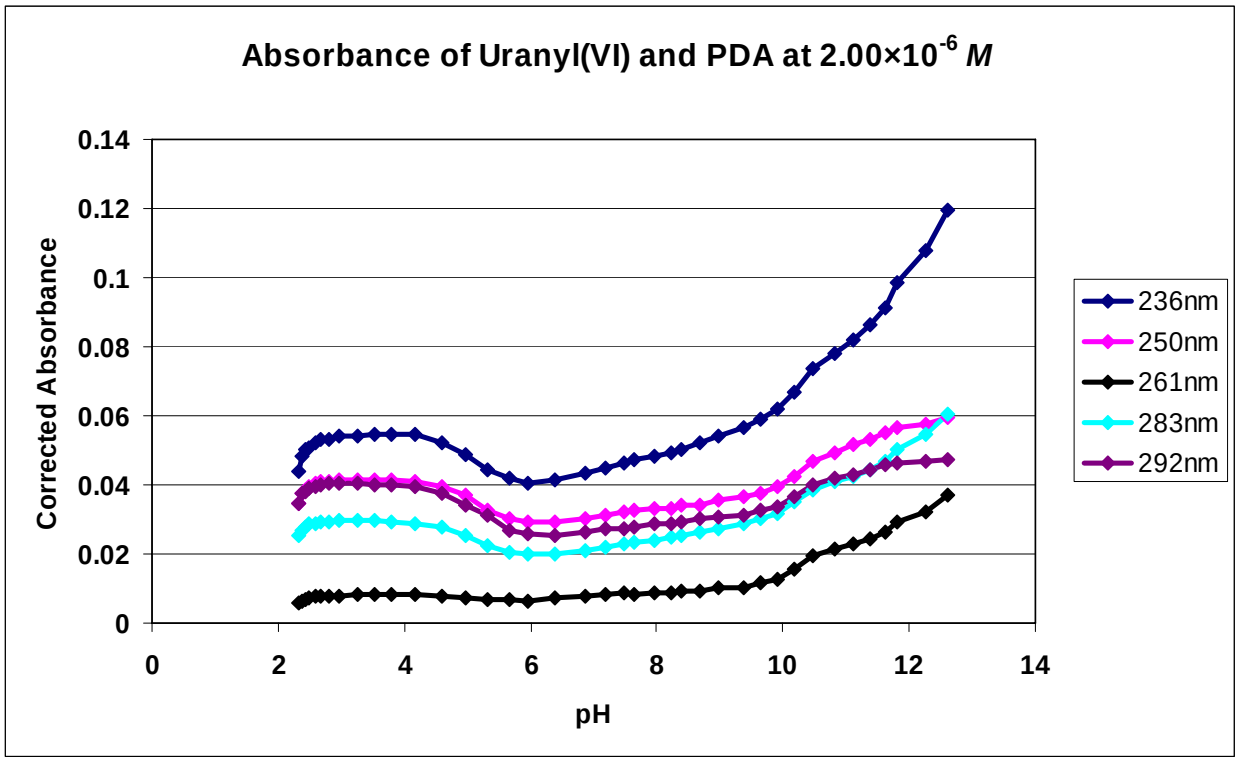

Figure 72. Plot of absorbance values corrected for dilution of the titration of uranyl(VI) and PDA at 2.00×10^{-6} *M*, in 0.10 *M* $NaClO_4$ at 25.0 ºC.

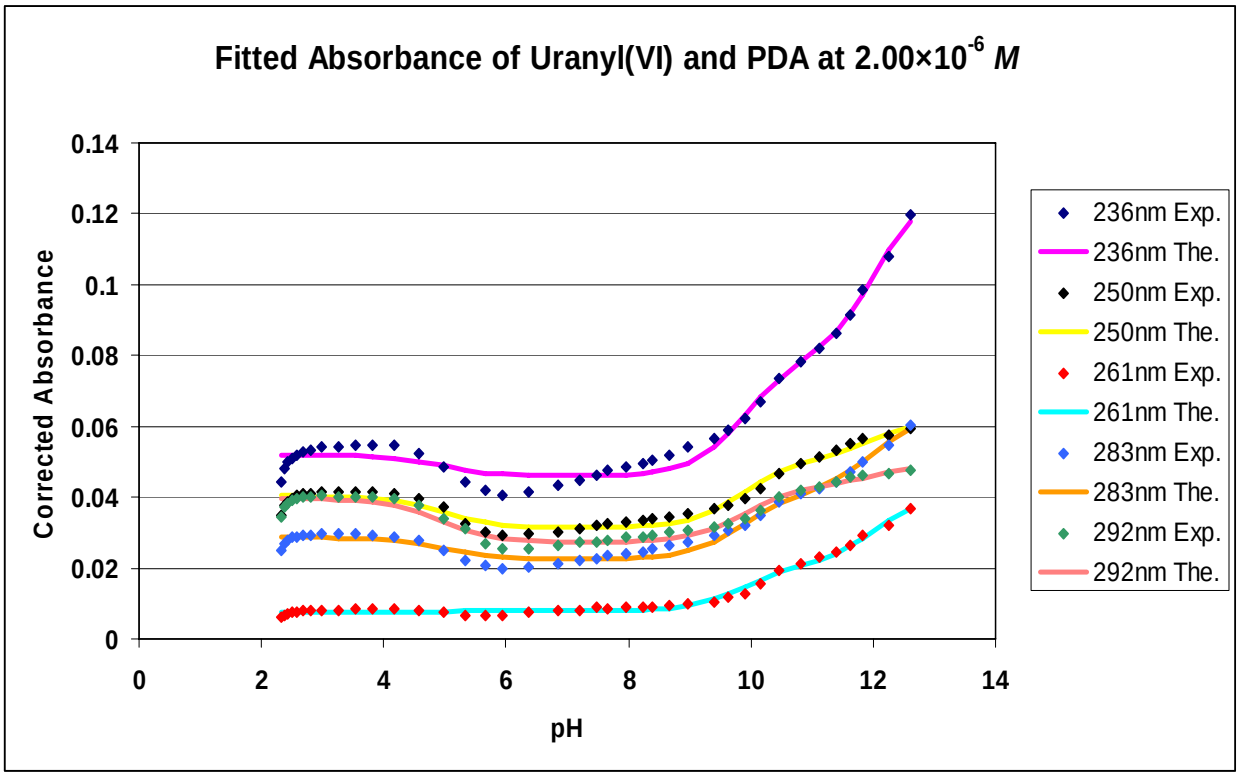

Figure 73. Experimental absorbance data (Exp.) fitted with calculated values (The.) to determine the protonation equilibria of the titration of uranyl(VI) and PDA at 2.00×10^{-6} *M*, in 0.10 *M* $NaClO_4$ at 25.0 ºC.

X-Ray Crystallography Results

X-Ray Crystallography was done on metal-PDA complexes of barium(II), thorium(IV) and uranyl(VI). The crystal structures of $(UO_2)(PDA)$ and $Th(PDA)_2(H_2O)_2 \cdot H_2O$ were determined via single crystal X-ray diffraction. A representative crystal from both compounds was mounted on a glass fiber using epoxy gel. Intensity data were collected on a Bruker SMART diffractometer equipped with an APEX II CCD detector. Data processing was performed using SAINT[9]. The structures were solved using direct methods while the refinement was carried out using SHELXL-97[10] within the WINGX software suite[11]. Powder X-ray diffraction data were collected on a Rigaku MiniFlex II Desktop X-ray Diffractometer (Cu-Kα, 3-60˚, 0.05˚ step, 1.0 s step^{-1}) and manipulated utilizing the JADE[12] software package. Crystallographic data for both thorium(IV) and uranyl(VI) metal ions is given in Table 2.

Barium(II)-PDA Results

The crystal structure of $[Ba_2(PDA)_2(NO_2)_2] \cdot 2H_2O$ is shown in Figure 74. At this time no further refinement of the crystal structure has been completed in order to receive reliable data. The structure consists of a 2 barium-PDA complexes bridged by a nitrate group coordinated to the barium atoms. Both PDA molecules remain planar and two water molecules are also coordinated to each barium atom. This crystal also has a very unique barium coordination number of 9 for one of the barium atoms and a coordination number of 8 for the other.

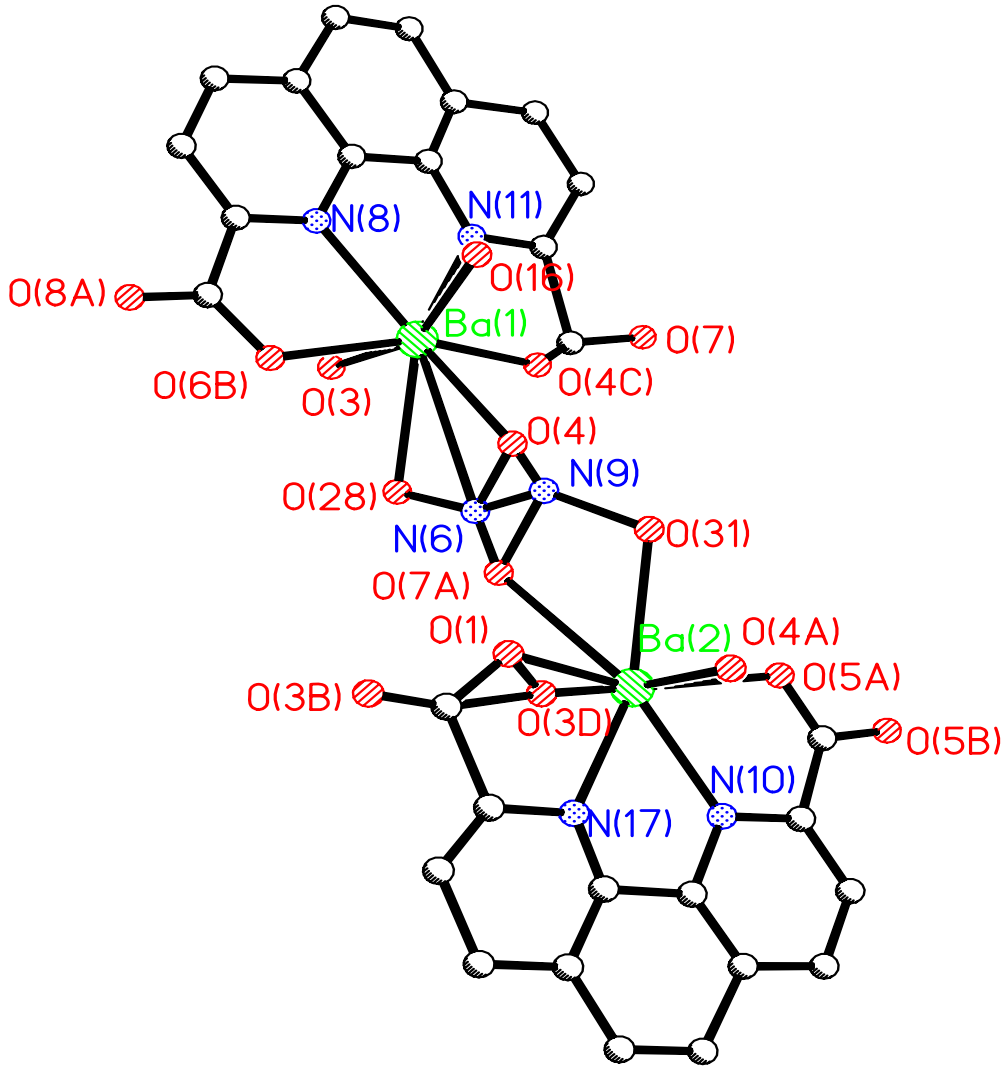

Figure 74. ORTEP[18] drawing of the complex $[Ba_2(PDA)_2(NO_2)_2]\cdot 2H_2O$ with thermal ellipsoids shown at the 50% probability level.

Table 1. Crystallographic data for $[UO_2(PDA)]$ (**1**) and $[Th(PDA)_2(H_2O)_2].H_2O$ (**2**).

	1	**2**
Empirical formula:	$C_{14}H_6N_2O_6U$	$C_{28}H_{18}N_4O_{11}Th$
M	536.24	812.46
T/K	298(2)	298(2)
Crystal system:	orthorhombic	triclinic
Space group:	*Pnma*	$P\bar{1}$
a/(Å)	11.1318(7)	7.6190(15)
b/(Å)	6.6926(4)	10.423(2)
c/(Å)	17.3114(12)	17.367(4)
α/º	90	94.93(3)
β/º	90	97.57(3)
γ/º	90	109.26(3)
V/Å^3	1289.71(14)	1278.3(4)
Z	4	2
μ/mm^{-1}	12.623	5.909
reflections collected:	20119	9412
R_{int}(Independent reflections):	0.0972 (1453)	0.1122 (4474)
Final *R* indices [I≥2σ(I)]	0.0313	0.0654
R indices (all data)	0.0654	0.0955

Thorium(IV)-PDA Results

The structure of $Th(PDA)_2(H_2O)_2 \cdot H_2O$ is seen in Figure 75, and a selection of bond angles and lengths for $Th(PDA)_2(H_2O)_2 \cdot H_2O$ are given in Table 3. The structure of $Th(PDA)_2(H_2O)_2 \cdot H_2O$ consists of a central Th(IV) metal center coordinated to two distinct PDA anions, each bound in a tetradentate fashion. Each PDA is bound to the Th(IV) through both nitrogen atoms along with two carboxylate oxygen atoms at an average distance of 2.694 and 2.430 Å, respectively. Completing the 10-coordinate local geometry, two water molecules are additionally bound to the Th metal centers at distances of 2.473 and 2.532 Å to create the corresponding Ow(1)-Th(1)-Ow(2) angle of 147.6(3)˚. Around each molecular unit, there is one unbound water molecule, Ow(3), located 2.751 Å away from Ow(2). The PDA ligands are not planar, but are bowed, and the Th atom lies well out of the plane of the PDA ligands, as shown in Figure 76. It can be shown using MM (molecular mechanics)[19] calculations that this distortion of the PDA ligands is brought about by steric crowding. If the two water molecules coordinated to the Th are removed, and MM calculations are used to generate a structure for $[Th(PDA)_2]$, completely planar PDA ligands result. If the water molecules are replaced on the Th to give $[Th(PDA)_2(H_2O)_2]$, the bowing of the PDA ligands is restored in the MM energy-minimized structure. Inspection of the structure shows that each coordinated water molecule presses on the center of the adjacent PDA ligand, causing it to bow. Work in progress on other ligands related to PDA has shown that bowing of the ligand is quite common, and does not seem to be accompanied by any major loss in complex stability.

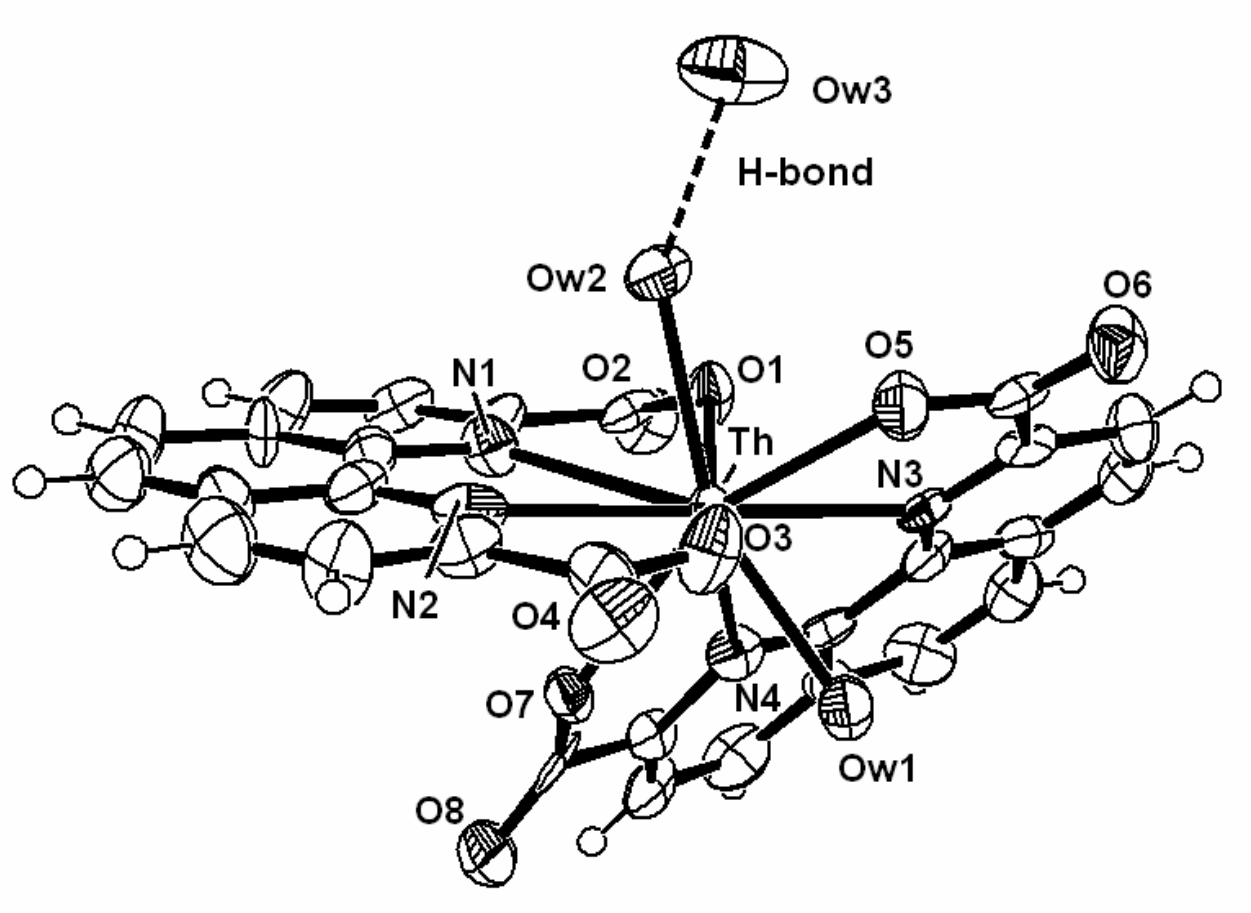

Figure 75. ORTEP[18] drawing of the complex $[Th(PDA)_2(H_2O)_2].H_2O$ with thermal ellipsoids shown at the 50% probability level. The structure shows how the Th atom lies out of the plane of the bowed PDA ligands. Ow1 and Ow2 are waters coordinated to the Th, and Ow3 is a lattice water H-bonded to Ow2.

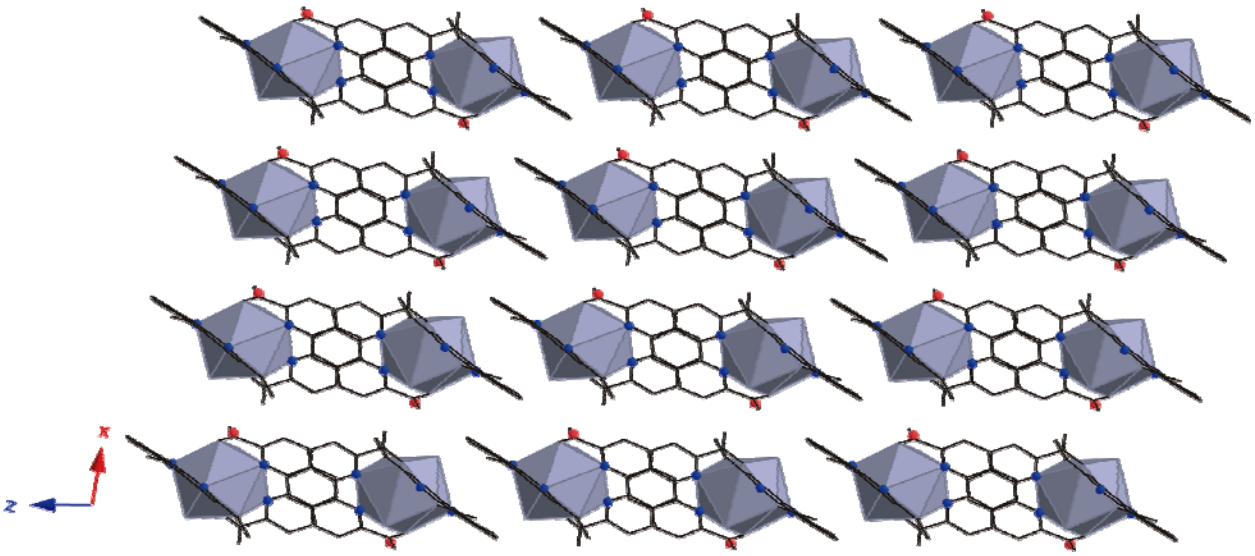

Figure 76. A view of $[Th(PDA)_2(H_2O)_2].H_2O$ down the [010] direction. The polyhedra are the thorium metal centers whereas the black lines are the PDA ligands. The spheres are the nitrogen atoms from the PDA. The red spheres are the unbound water molecules. Hydrogen atoms have been omitted for clarity. The diagram shows the π-stacking that typically is involved in the packing of complexes of this type in the unit cell. Some π–stacking is taking place between pairs of PDA ligands almost in the plane of the page, while the other π-stacking is at right angles to the plane of the page.

Table 2. A selection of bond lengths (Å) and angles (deg) in $[Th(PDA)_2(H_2O)_2].H_2O$.

Th1-O5	2.399(10)	Th1-O7	2.405(9)	Th1-O3	2.443(9)
Th1-Ow1	2.473(9)	Th1-O1	2.474(8)	Th1-Ow2	2.532(9)
Th1-N4	2.652(11)	Th1-N3	2.658(12)	Th1-N1	2.718(11)
Th1-N2	2.744(13)				
O5-Th1-O7	152.0(3)	O5-Th1-O3	70.8(3)	O7-Th1-O3	90.3(3)
O5-Th1-Ow1	80.1(3)	O7-Th1-Ow1	74.2(3)	O3-Th1-Ow1	71.4(3)
Ow1-Th1-O1	125.6(3)	O5-Th1-Ow2	70.0(3)	Ow1-Th1-Ow2	147.6(3)
O7-Th1-N4	60.7(4)	Ow1-Th1-N4	68.9(3)	Ow2-Th1-N4	137.3(3)
O5-Th1-N3	60.5(3)	O1-Th1-N3	63.8(3)	N4-Th1-N3	60.1(4)
O1-Th1-N1	59.0(3)	O7-Th1-N2	63.2(3)	O3-Th1-N2	60.4(3)
N3-Th1-N2	178.9(4)	N1-Th1-N2	58.8(3)		

Uranyl(VI)-PDA Results

The structure of (UO_2)(PDA) is seen in Figure77 and a selection of bond angles and lengths are given in Table 4. The structure of (UO_2)(PDA) consists of a central uranium (VI) metal center bound to two symmetry equivalent oxygen atoms, O1, at a distance of 1.767(4) Å resulting in an O1-U1-O1 angle of 176.4(3)˚ to form the familiar uranyl cation (UO_2^{2+}). One PDA anion is bound to the uranyl cation in a tetradentate fashion through both nitrogen atoms at an average distance of 2.558 Å and through two carboxylate oxygen atoms at an average distance of 2.351 Å. Completing the pentagonal bipyramidal local geometry of the uranium metal centers, an additional carboxylate oxygen atom, O3', from a second PDA anion is bound at a distance of 2.345(6) Å resulting in one-dimensional chains as can be viewed down [010] as shown in Figure 78. The question of interest here is the evidence that the structure provides on whether the PDA is coordinated to the uranyl group in a low-strain fashion, and what bearing this might have on the slightly lower than expected log K_1(PDA) measured here for the UO_2^{2+} cation. The PDA ligand is almost exactly planar, with the U atom lying in the plane of the ligand, as was also found for the Ca(II)/PDA complex,[20] which suggests that it is coordinated to the uranyl group in a fairly low-strain manner. Complexes of UO_2^{2+} with simple bidentate ligands such as 1,10-phen and picolinic acid (2-carboxypyridine) should have more nearly ideal geometry involving the donor atoms and the U atom than is true for the more sterically demanding tetradentate PDA ligand. A search of the CSD shows 5 structures of uranyl 1,10-phen complexes, and 13 structures of uranyl complexes with picolinate-type ligands. A comparison of bond angles and lengths involving the UO_2 group and the N and O donors shows that the structural features are effectively identical to the corresponding structural features in the 1,10-phen and picolinate complexes, and that the coordination of UO_2^{2+} in its PDA complex is

probably quite low-strain. This is summarized in Table 5, which shows that the structural features are very similar to the corresponding structural features in the UO_2^{2+} complexes of phen and picolinic acids, and that the more preorganized structure of the PDA ligand imposes no more steric penalties on its UO_2^{2+} complex than do the sterically much less demanding phen and picolinate ligands.

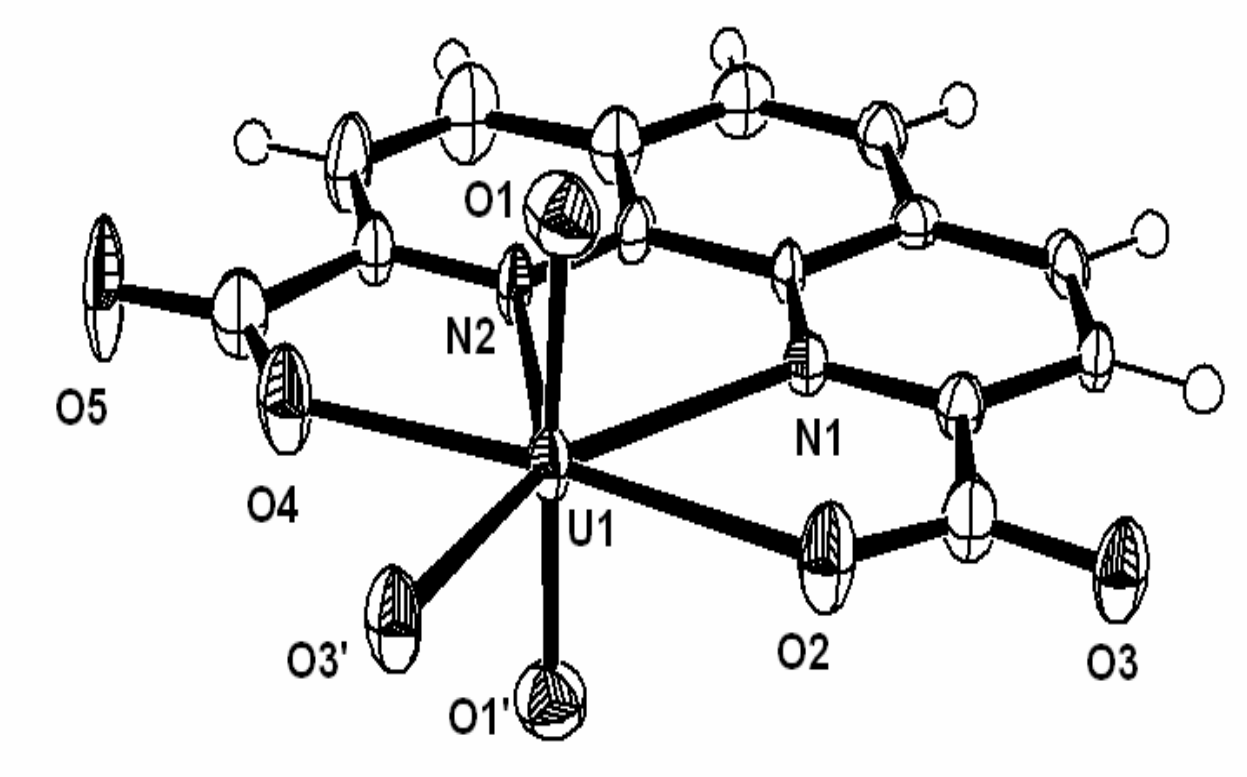

Figure 77. ORTEP[18] drawing of the complex [UO_2(PDA)]. Ellipsoids are shown at the 50% level. Symmetry equivalents: (i) x, -y + ½, z; (ii) x + ½, -y + ½, -z + ½. The atom O(3)' is a bridging carboxylate oxygen from a neighboring UO_2/PDA individual.

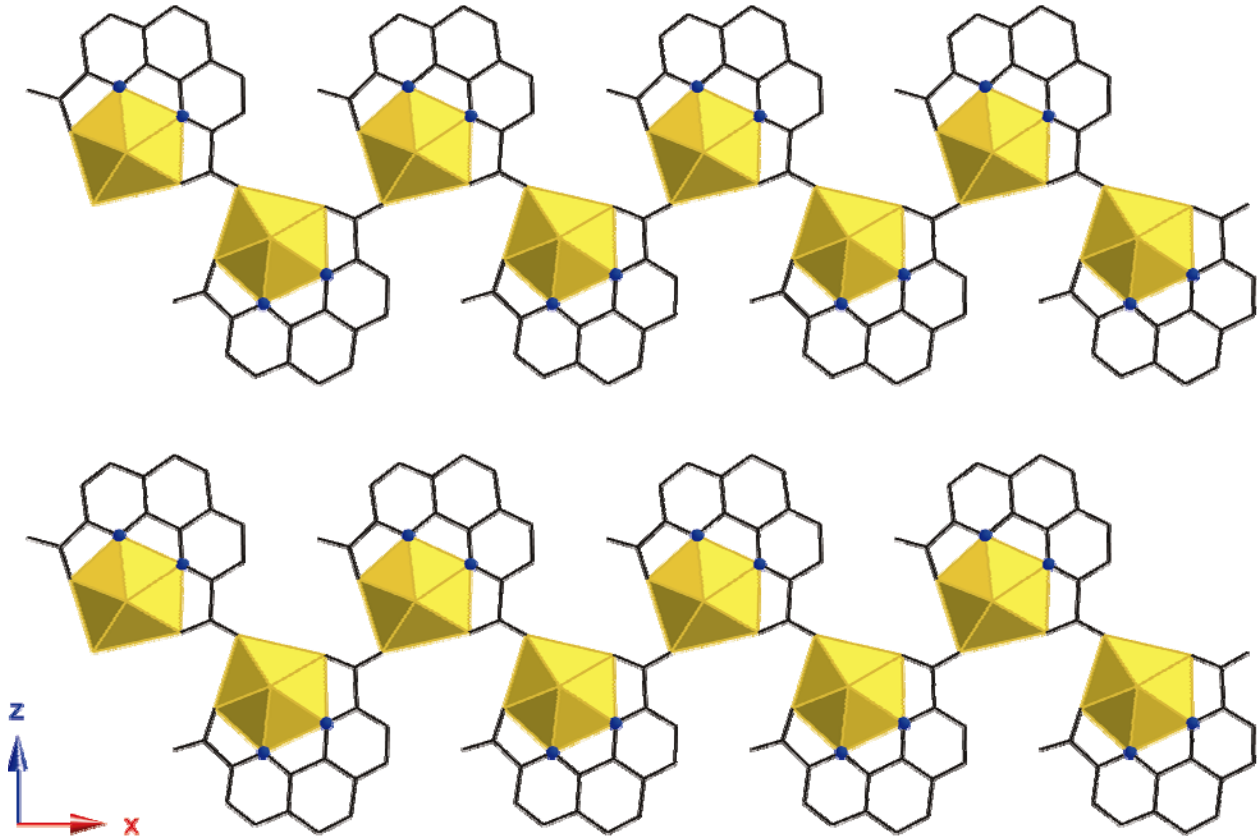

Figure 78. A view of [UO_2(PDA)] down the [010] direction. The polyhedra are the uranium pentagonal bipyramids whereas the black lines are the organic linkers. The spheres are the nitrogen atoms from the PDA. The hydrogen atoms have been omitted for clarity. This sheet of [UO_2(PDA)] complexes π–stacks on similar sheets above and below it.

Table 3. A selection of bond lengths (Å) and angles (deg) in [UO_2(PDA)].

U1-O1	1.767(4)	U1-O1’	1.767(4)	U1-O4	2.279(6)
U1-O3’	2.345(6)	U1-O2	2.423(6)	U1-N2	2.543(7)
U1-N1	2.572(7)				
O1-U1-O1’	176.4(3)	O1-U1-O4	91.80(14)	O1-U1-O3	90.54(13)
O4-U1-O3	79.7(2)	O1-U1-O2	88.25(14)	O4-U1-O2	171.6(2)
O3-U1-O2	91.9(2)	O1-U1-N2	90.60(13)	O4-U1-N2	63.8(2)
O3-U1-N2	143.49(19)	O4-U1-N1	125.8(2)	O3-U1-N1	154.5(2)
O2-U1-N1	62.58(19)	N2-U1-N1	62.0(2)		

Table 4. Bond lengths and angles involving the coordination around U in $[UO_2(PDA)]$ compared with the corresponding structural features in the complexes of UO_2^{2+} with the much less sterically demanding phen and picolinate-type ligands found in the CSD[19].

	U-O(Å)	N-U-O(º)	U-O-C(º)	U-N(Å)	N-U-N(º)	U-N-C(º)
Structural features of **1** ($[UO_2(PDA)]$):	2.36	62.9	128.9	2.56	62.62	122.3
Corresponding values in UO_2/1,10-phen complexes:[21]				2.60(3)	62.4(7)	120.4(9)
Corresponding values in UO_2/ picolinate type complexes:[18]	2.41(5)	62.2(1.7)	128.5(1.4)	2.58(5)		

CONCLUSIONS

Chemists have been using preorganization as a means of creating highly selective ligands for years. The ability of a ligand to selectively bind a specific metal ion in solution is of great importance in many areas of chemistry including the bioinorganic, nuclear, and metallurgy fields. 1,10-phenanthroline-2,9-dicarboxylate (PDA) has been shown to be a highly preorganized ligand drawing in aspects of denticity, chelate ring size, donor atoms selection, and rigidity in order to design a ligand which will form complexes with metal ions of higher charge and larger ionic radius.

PDA was synthesized according to the literature method with changes in overall reaction times and the product was characterized by IR and UV spectroscopy as well as X-Ray Crystallography. UV/Vis absorption spectroscopy was also used to detect metallation and demetallation in solution as a function of pH and was concluded to be a very successful method.

PDA was shown to exhibit higher formation constants, log K_1, with metal ions of large size and higher charge and was also shown to have higher formation constants than its non-preorganized precursor EDDA. Further, PDA-metal complexes were shown to exhibit such thermodynamic stability, that a 10 to 100 fold excess of a competing ligand was unable to remove the metal-ion from PDA. This remarkable ability for the tetra-dentate ligand is a result of the very rigid hemi-cyclic backbone of PDA which keeps the donor atoms locked in position necessary for metallation.

It is also of importance to note the variability of the PDA-metal ion complex as a function of pH. Since the complex has been shown to be very strong at low and even neutral pH ranges for most metal ions, yet subject to demetallation at higher pH ranges, 7.5-12 depending on the metal ion present, PDA has enormous potential as a filter material for expensive and dangerous

aqueous metal ions. For example, a molecular sieve could be constructed with PDA as the active molecule and be used to filter acidified metal ion solutions. The metal ions could then be removed from the filter as hydroxide salts by running a basic aqueous solution through.

LITERATURE CITED

1. Housecroft, Catherine E. and Sharpe, Alan G. Inorganic Chemistry. **2008.**

2. Guo, Zijian and Peter Sadler. *Angew. Chem. Int. Ed.*, **1999**. *38*. 1512-1531.

3. Cram, D.J., "The design of molecular hosts, guests, and their complexes." Nobel Lecture, **1987**.

4. Pedersen, C.J., *J. Am. Chem. Soc.,* **1967**. *89*, 2495-2496.

5. Pedersen, C.J., *J. Am. Chem. Soc.*, **1967**. *89*, 7017-7036.

6. Dietrich, B. and J. M. Lehn, *Tetrahedron Lett.*, **1969**. 2885-2888.

7. Dietrich, B. and J. M. Lehn, *Tetrahedron Lett.*, **1969**. 2889-2892.

8. Chandler, C.J., Leslie W. Deady, and James A. Reiss. *J. Heterocyclic Chem.*, **1981**. *18*. 599-601.

9. Saint - SAINT, V 5.053. *Area-Detector Integration Software*, Seimens Industrial Automation, Inc., Madison, WI, 1998

10. Shelxl-97 - G.M. Sheldrick, SHELX97, Programs for Crystal Structure Analysis (Release 97–2) University of Gottingen, Germany, Institüt für Anorganische Chemie der Universität, Tammanstrasse 4, D-3400 Göttingen, Germany, 1998.

11. WingX - L.J. Farrugia, J. *Appl. Crystallogr.* **1999**, *32*, 837.

12. JADE - JADE, V6.1, Materials Data Inc., Livermore, CA, 2002.

13. Cambridge Crystallographic Data Centre,12 Union Road, Cambridge CB2 1EZ, United Kingdom.

14 E. J. Billo, *EXCEL for Chemists*, Wiley-VCH, New York, 2001.

15. Martell, A. E.; Smith, R. M. *Critical Stability Constant Database, 46*; National Institute of Science and Technology (NIST): Gaithersburg, MD, USA, 2003.

16. Martell, A. E.; Motekaitis, R. J. *The Determination and Use of Stability Constants*, VCH Publishers: New York, 1989.

17. Hancock, R. D. *Acc. Chem. Res*. **1990**, *26*, 875.

18. ORTEP-3 for Windows, Version 1.08, Farrugia, L. J., *J. Appl. Cryst.*, **1997**, *30*, 565.

19. Hyperchem program, version 7.5, Hypercube, Inc., 419 Philip Street, Waterloo, Ontario, N2L 3X2, Canada

20. Melton, D. L.; VanDerveer, D. G.; Hancock, R. D. *Inorg. Chem.*, **2006**, *45*, 9306.

21. Kinard, W. F.; Grant, P. M.; Baisden, P. A. *Polyhedron* **1989**, *8*, 2385.